The effect of molecular composition on the properties of polyolefin-wood composites

by

Nicolaas Christiaan Basson

Dissertation presented for the degree of *Doctor of Philosophy (Polymer Science) in the Faculty of Science Stellenbosch University*

Promotor: Prof Albert Johannes van Reenen
Copromotor: Dr Martina Meincken

March 2013

Declaration

By submitting this thesis/dissertation electronically, I declare that the entirety of the work contained therein is my own, original work, that I am the sole author thereof (save to the extent explicitly otherwise stated), that reproduction and publication thereof by Stellenbosch University will not infringe any third party rights and that I have not previously in its entirety or in part submitted it for obtaining any qualification.

_____

March 2013

Dedication:

My family and friends, thank you for your continued support over these long years, and encouragement to pursue my dream. By the grace of God, I am one step closer to His purpose for my life and may the dream He has given me, become a reality, not just for me as His instrument, but for the community, my country, for whom it is intended to prosper, I will continue to exercise my faith and believe in God and His promises. God is faithful, always, and He will provide both the open doors and the means for His purpose. Amen.

Rev 3:8 ESV

"I know your works. Behold, I have set before you an open door, which no one is able to shut. I know that you have but little power(strength), and yet you have kept my word and have not denied my name."

Acknowledgements

I would like to thank the All Mighty God and the Lord Jesus for helping me, I am thankful for the opportunity I had to come to university, and through many trials and tribulations I have come to this point in my studies, I want to acknowledge you here God, that whomever reads this page, may serve as a witness, that all of this, every single thing that led me to this point in my life, has been due to You, God. If not by the hand of God, none of this would have taken place.

I know that nothing I can do, can add to or please God in any manner, for the way He feels about me will remain as loving as He always was, is and will be, all I can do, is but to direct His glory in my life, back to Him, where it rightfully came from and belongs to.

I'd also like to thank you, Prof. Albert van Reenen, thank you for being my mentor and support, at the University of Stellenbosch, I have great respect for you, you have played a large role in training me and encouraging me to pursue my studies here at university and have given me the opportunity to acquire precious skills.

I'd also like to thank my co-promoter, Dr. Martina Meincken, thank you for all of your support, I appreciated it.

I would like to thank the following people for their contributions:

1. The Olefins research group
2. Dr. Gareth Harding
3. Technical assistants and financial staff at the Polymer Science division.
4. Dr. Ben Loos, for his wonderful assistance in the fluorescence work.
5. Roediger Agencies for your tensile tester, and the several hours and days I was kindly given to use it, thank you Andy.
6. Dr. M. J. Hurndall (Student Liaison Officer)
7. All my family, friends and colleagues.

Abstract

Polymer composites, and in particular wood-polymer composites have become commercially and environmentally important materials. Studies in polyolefin-wood composites have mostly focused on polypropylene (PP) and polyethylene (PE). To our knowledge, no study has been undertaken on advancing impact polypropylene copolymer (IPPC)-wood composites as a suitable alternative to using PP and PE. IPPC have proven to be a suitable alternative to PP at low temperatures to improve impact resistance for manufactured polymer products, and could be a great addition to improved properties for wood polymer composites.

This study shows that the physical properties of IPPC-wood composites can be markedly improved when compatibilizer(s) are used to improve the distribution of the wood within the matrix, as well as improving the interaction between the wood and the polymer matrix.. The use of different compatibilizers, vi polypropylene-graft-maleic anhydride (PPgMA) and poly(ethylene-co-vinyl alcohol) (EvOH) results in different physical properties. Using simple admixtures of the PPgMA and EvOH in IPPC-wood composites result in a large spread of results, while pre-reacting the PPgMA and EvOH to form a joint compatibilizer gives reproducible results w.r.t the physical testing.

A study of the fundamental interactions of the compatibilizer(s) with the molecular components of the IPPCs was undertaken. The IPPCs used were fractionated by preparative temperature rising elution fractionation, and the fractions were mixed with the compatibilizers. To this end, fluorescence microscopy was utilized to study the interaction. The results clearly indicate that the interaction of the PPgMA with the fractions differ from that of the EvOH. These differences can be explained in terms of the chemical composition distribution within the IPPC fractions.

Atomic force microscopy (AFM) was used to study adhesive forces between compatibilizer, polymer and cellulose and lignin. Successful coating of AFM tips with PPgMA and EvOH was achieved. Whilst interactions based on chemical force microscopy (CFM) could not be quantified, the AFM results in conjunction with fluorescence spectroscopy provided meaningful insight in the way that compatibilizers interact with both the wood and the impact copolymers used in this study..

Opsomming

Polimeer saamgestelde material, en meer spesifiek hout-polimeer saamgestelde material het die afgelope tyd belangrike produkte geword, beide kommersieel en in verband met omgewingvriendelikheid. Navorsing op die gebied van poli(olefien)-hout komposiete het tot op hede meestal gefokus op die grbruik van poli(propileen) (PP) en poli(etileen) (PE). Sover dit on kennis strek is daar nog geen studie gedoen om die gebied van impak polipropileen kopolimere (IPPK)-hout komposiete uit te bou nie. IPPKs is ‘n geskikte alternatief vir PP in veral lae-temperatuur aanwendings. Die gebruik van IPPKs as matriks vir die hout komposiete kan ‘n groot staqp vorentoe beteken.

Hierdie studie wys dat die fisiese eienskappe van iPPK-hout komposiete merkwaardig verbeter kan word waneer versoeningmateriale gebruik word om die verspreiding van die hout in die polimeer-matriks sowel as die interaksie tussen die hout en polimeer te verbeter. Die gebruik van verskillende versoenings material, t.w poli(propileen-ent-maleinsuur anhidried) (PPeMA) en pol(etlieen-ko-viniel alkohol) (EVOH). Deur gebruik te maak van eenvoudige mengsels van PPeMA en EVOH in IPPK-hout composite het ‘n geweldige wye verpreiding van resultate tot gevolg gehad, terwyl ‘n voorafgaande reaksie tussen die PPeMA en die EVOH om ‘n saamgestelde versoeningmateriaal te maak tot gevolg gehad het dat reproduseerbare resultate verkry kon word.

‘n Studie van die fundamentele interaksies van die versoeningsmateriale met die molkulêre komponente van die IPPKs is uitgevoer. Die IPPKs is gefraksioneer deur preparatiewe temperatuur-stygende uitloog frakasionering en die fraksies is gemeng met die versoeningmateriale. Fluoressensie mikroskopie is gebruik om hierdie interaksies te bestudeer. Die resultate dui duidelik daarop dat die interaksie van die PPeMA met die fraksies verskil met die van die EVOH. Die verskille kan verduidelik word aan die hand van die chemiese samestelling verspreiding van die IPPK fraksies.

Atoomkrag mikroskopie (AKM) is gebruik om die adhesive-kragte tussen die versoeningmateriale, polimere, sellulose en lignien. AKM tippe is suksesvol bedek met PPeMA en EVOH, onderskeidelik. Alhoewel interaksies gebaseer op chemiese krag mikroskopie (CKM) nie gekwantifiseer kon word nie, lewer hierdie resultate tesame met die fluoressensie spektroskopie unieke insig in die manier wat versoeningmateriale met beide die hout en die polimeer reageer.

Contents

List of Contents

Chapter 4 Determination of physical properties

Chapter 5 Interaction of the compatibilizers with the polymer matrix

List of Figures

Chapter 3

Chapter 4

Chapter 5

List of Tables

List of Schemes

Chapter 3

List of Abbreviations

PP	Polypropylene
PE	Polyethylene
IPPC	Impact polypropylene copolymer
PPgMA	Polypropylene-graft-maleic anhydride
EvOH	Poly(ethylene-co-vinyl alcohol)
TREF	Temperature rising elution fractionation
AFM	Atomic force microscopy
SEC	Size exclusion chromatography
FTIR	Fourier transform infra-red spectroscopy
EPR	Ethylene propylene rubber
MAH	Maleic anhydride
CFM	Chemical force microscopy
m_p	Melt point
M_n	Number average molecular weight
M_w	Weight average molecular weight
GPC	Gel permeation chromatography
Tg	Glass transition temperature
DMAP	Dimethyl amino pyridine
wt %	Weight percentage
DMSO	Dimethyl sulfoxide
SEM	Scanning electron microscopy
FE SEM	Field emission scanning electron microscopy
DSC	Differential scanning calorimetry
HV	Hardness value
iPP	Isotacticpolypropylene
TGA	Thermo gravimetric analysis
pTREF	Preparative temperature rising elution fractionation
PD	Polydispersity
ATR	Attenuated total reflectance
WPCs	Wood-polymer composites

CHAPTER 1 INTRODUCTION AND OBJECTIVES

1.1 Introduction

Polymer composites have become very important materials in our everyday life, since they give improved properties over using pure polymers alone. The advantages of these materials lie in the combination of properties between the polymer and filler material.

Since wood polymer composites (WPC) with a thermoplastic matrix and wood as filler are recyclable,[1-3] they can be melted down, processed and re-used. WPC applications are mostly in the building industry; and WPCs are used for decking, paneling, flooring, window frames etc.[4] Wood is also a renewable resource as filler, and as such wood polymer composites have become an attractive proposition.

Due to the hydrophobic and hydrophilic character of the polymer and wood components, respectively, they do not interact easily. This often results in poor mechanical properties. This drawback can be overcome by the incorporation of compatibilizers able to bridge this interface between wood and polymer.[5-15] Impact polypropylene has improved impact resistance over its parent polymer, polypropylene, and, due to its complex morphology, could provide improved properties in this field of composites, depending on the compatibilization between wood and the different fractions/ major components of this polymer matrix.

Impact polypropylene is a semi-crystalline copolymer, consisting of a crystalline isotactic polypropylene matrix, a rubbery part (random ethylene-propylene copolymer, (EPR)), and a range of ethylene-propylene copolymers; with long crystallizable sequences of both propylene and ethylene units.[16-18]

This study will focus on the understanding of the effect of compatibilizers for the impact PP copolymers (IPPCs), taking into consideration the complex, heterogeneous nature of the polymer. Several previous studies have taken into account aspects like the wood species used, wood geometry, and chemical modification of the wood species.[19-27] These aspects will not be covered during this study.

Impact polypropylene copolymer as polymer matrix was selected as this family of polymers has improved impact properties (compared to polypropylene). Thus his polymer should yield composite materials with improved impact compared to polypropylene. Most of the research in the field of polyolefin-wood composites has focused on composites prepared

with polyethylene (all three types) and polypropylene. To our knowledge, there is no available literature that describes fundamental aspects of IPPC-wood composites..

As already mentioned, impact polypropylene has a very complex chemical structure. Due to its chemical heterogeneity, we would expect the chemically different parts of the polymer to interact differently with wood particles. This interaction could be enhanced or changed by the introduction of compatibilizers. This would be dependent on the type of compatibilizer used. While the physical properties of the wood polymer composites will undoubtedly be influenced by the polymer matrix upon compatibilization with different specific compatibilizers, the challenge will lie in being able to gain a fundamental understanding of why these changes take place.

Improving the physical properties of wood polymer composites have remained an important subject of continued research in this field, since its early development. A proper understanding of compatibilizer, polymer and wood interactions is however still very vague and not yet fully understood.

1.2 Objectives

The main objective is to gain an understanding of the role of the molecular composition of a complex copolymer like impact polypropylene on the interaction with compatibilizers and wood fillers.

Under the main objective, the aims were:

1. To use two chemically dissimilar compatibilizers, polypropylene-graft-maleic anhydride (PPgMA) and pol(ethylene-co-vinyl alcohol) (EvOH) and to study aspects of the interaction of these materials with the polymeric components that make up the impact PP copolymers.

2. Following on from this, the effect of using more than one compatibilizer at the same time would be investigated. This would initially be done by observing the macroscopic properties of the composites produced.

3. A fundamental study regarding the interaction of the compatibilizers with the main constituents of wood (lignin and cellulose) will also be attempted, as well as the interaction of the compatibilizers with the individual molecular components of the impact copolymers.

4. Relating the fundamental understanding of these interactions to the macroscopic properties of WPCs.

Under the aims, goals emerged during the course of the study. These were:

- Developing a methodology, or methodologies, to study the interaction between the compatibilizer and the polymer components in the solid state, after melt processing. Here fluorescence microscopy and atomic force microscopy emerged as techniques.
- To fractionate the impact copolymers used in this study and to use these individual fractions in the interaction studies. To this effect, preparative temperature rising elution fractionation (pTREF) emerged as the principle technique.

1.3 Layout of the thesis

The following is a summary of the thesis layout.

Chapter 1 introduces the problem and formulates the aims and objectives of the research and presents the layout of the thesis.

Chapter 2 gives an overview of the relevant historical information and theoretical concepts that pertains to this research.

Chapter 3 gives an overview of the experimental techniques used during and developed for the research.

Chapter 4 gives the results of the initial physical tests conducted on composites prepared with no compatibilizer. This is then contrasted with the use of (a) PPgMA as compatibilizer, and (b) EvOH as compatibilizer. The use of these compatibilizers in combination (simple admixture) is then discussed, as well as the use of pre-reaction techniques to produce a "joint" compatibilizer.

Chapter 5 presents the results of fundamental studies concerning the interaction of the compatibilizers with the individual components of the impact copolymers. Here the use of fluorescence microscopy and fluorescence spectroscopy is illustrated as a means of studying these interactions. In addition the use of AFM (in the chemical force mode) for the study of interactions between wood components, compatibilizers and components of the impact copolymers is discussed.

Chapter 6 presents a brief overview of the thermal characteristics of the composites in the presence and absence of compatibilizers.

Chapter 7 gives an overview of the morphology of the composites in the absence and presence of the compatibilizers. The results presented in Chapters 4 – 6 are used to illustrate the differences in morphology that are presented.

Chapter 8 presents a summary of the conclusions reached during this study, as well as some recommendations for further work.

1.4 References

1. X. Xu, K. Jayaraman, C. Morin, N. Pecqueux, Life cycle assessment of wood-fiber-reinforced polypropylene composites, Journal of Materials Processing Technology, 198 (1-3), p 168 (2008).
2. S. E. Selke, I. Wichman, Wood fiber/ polyolefins composites, Composites: Part A, 35, p 321 (2004).
3. A. Viksne, L. Rence, Effect of re-compounding on the properties of polypropylene/ wood flour composites, Progress in Rubber, Plastics and Recycling Technology, 24 (3), p 153 (2008).
4. V. K. Mathur, Composite materials from local sources, Construction and Building Materials, 20, p 470 (2006).
5. S. B. Elvy, Gary R. Denis, L.-T. Ng, Effects of coupling agent on the physical properties of wood-polymer composites, Journal of Materials Processing Technology, 48, p 365 (1995).
6. K. Oksman, Improved interaction between wood and synthetic polymers in wood/ polymer composites, Wood Science and Technology, 30, p 197 (1996).
7. Y. X Pang, D. M Jia, H. J. Hu, D. J. Hourston, M. Song, Effects of a compatibilizing agent on the morphology, interface and mechanical behavior of polypropylene/ poly(ethylene terephthalate) blends, Polymer, 41, p 357 (2000).
8. A. Karmarkar, S. S. Chauhan, J. M. Modak, M. Chanda, Mechanical properties of wood–fiber reinforced polypropylene composites: Effect of a novel compatibilizer with isocyanate functional group, Composites: Part A, 38, p 227 (2007).
9. K. Oksman, Craig Clemons, Mechanical properties and morphology of impact modified polypropylene-wood flour composites, Journal of Applied Polymer Science, 67, p 1503 (1998).
10. S. Nenkova, Cv. Dobrilova, M. Natov, St. Vasileva, P. Velev, Modification of wood flour with maleic anhydride for manufacture of polymer-wood composites, Polymers and Polymer composites, 14 (2), p 185 (2006).
11. L. Danyadi, K. Renner, J. Moczo, B. Pukanszky, Wood flour filled polypropylene composites: interfacial adhesion and micromechanical deformations, Polymer Engineering and Science, p 1246 (2007).
12. T. J. Keener, R. K. Stuart, T. K. Brown, Maleated coupling agents for natural fiber composites, Composites: Part A, 35, p 357 (2004).

13. M. Tasdemir, H. Biltekin, G. T. Caneba, Preparation and characterization of LDPE and PP-wood fiber composites, Journal of Applied Polymer Science, 112, p 3095 (2009).
14. N. Sombatsompop, C. Yotinwattanakumtorn, C. Thongpin, Influence of type and concentration of maleic anhydride grafted polypropylene and impact modifiers on mechanical properties of PP/ wood sawdust composites, Journal of Applied Polymer Science, 97, p 475 (2005).
15. P. W. Balasuriya, L. Ye, Y.-W. Mai, J. Wu, Mechanical properties of wood flake–polyethylene composites. II. Interface modification, Journal of Applied Polymer Science, 83, p 2505 (2002).
16. C. Zhang, Y. Shangguan, R. Chen, Q. Zheng, Study on thermal behavior of impact polypropylene copolymer and its fractions, Journal of Applied Polymer Science, 119, p 1560 (2011).
17. H. N. Cheng, M. Kakugo, 13C NMR analysis of compositional heterogeneity in ethylene-propylene copolymers, Macromolecules, 24, p 1724 (1991).
18. A. J. van Reenen, N. C. Basson, Molecular composition and properties of impact propylene copolymers, eXPRESS Polymer Letters, 6 (5), p 427 (2012).
19. Y. Cui, S. Lee, B. Noruziaan, M. Cheung, J. Tao, Fabrication and interfacial modification of wood/ recycled plastic composite materials, Composites: Part A, 39, p 655 (2008).
20. N. M. Stark, R. E. Rowlands, Effects of wood fiber characteristics on mechanical properties of wood/ polypropylene composites, Wood and Fiber Science, 35 (2), p 167 (2003).
21. A. K. Bledzki, O. Faruk, Wood Fibre Reinforced Polypropylene Composites: Effect of fibre geometry and coupling agent on physico-mechanical properties, Applied Composite Materials, 10, p 365 (2003).
22. J. Prachayawarakorn, K. Anggulalat, Influence of meranti sawdust aspect ratios and amount of loadings on mechanical and morphological properties of composites from polypropylene and meranti sawdust, Songklanakarin Journal of Science and Technology, 25 (5), p 595 (2003).
23. D. G. Dikobe, A. S. Luyt, Effect of filler content and size on the properties of ethylene vinyl acetate copolymer–wood fiber composites, Journal of Applied Polymer Science, 103, p 3645 (2007).
24. S. Migneault, A. Koubaa, F. Erchiqui, A. Chaala, K. Englund, M. P. Wolcott, Effects of processing method and fiber size on the structure and properties of wood–plastic composites, Composites: Part A, 40, p 80 (2009).

25. V. Hristov, J. Vlachopoulos, Effects of polymer molecular weight and filler particle size on flow behavior of wood polymer composites, Polymer Composites, p 831 (2008).
26. A. V Spiglazov, V. P Stavrov, Influence of the size of the wood particles and the degree of filling on the flow of polypropylene composites, International Polymer Science and Technology, 32 (9), p T8 (2005).
27. A. N. Shebani, A. J. van Reenen, M. Meincken, The effect of wood species on the mechanical and thermal properties of wood-LLDPE composites, Journal of Composite Materials, 43 (11), p 1305 (2009).

CHAPTER 2 RELEVANT THEORETICAL BACKGROUND

The following is a brief overview of certain aspects that we regard as being useful with respect to the body of the thesis. Within the literature cited there are many excellent papers that discuss in some detail the concepts that are summarized in the following sections.

2.1 Basic factors to consider in polymer composites

F. R Jones said "composite technology utilizes the high stiffness and strength of filamentary materials".[1] The strength of polymer composite materials and other physical properties are greatly influenced by the chemistry (functionality) of these filamentary materials, and several other aspects such as; their size, size distribution and aspect ratio, to mention but a few.[2-4]

According to Xanthos[2] the boundary between the polymer matrix and the filler is a crucial factor with respect to the adhesion between the polymer and the filler. This will affect the efficiency of the stress transfer between the polymer and the filler or filament. This interaction, in conjunction with the method of mixing or incorporation, also affects the distribution and orientation of the filler in the polymer matrix.

The orientation of fibres in the polymer matrix is an important factor to consider when making composite materials, as discussed by Holister and Thomas.[5] Stark and Rowlands[6] discuss the effect of wood fibre characteristics on mechanical properties in wood polypropylene composites. They found a high fibre aspect ratio including coupling agents between polymer and wood is necessary for good composite properties.

The source or type of fibres used in polymer composites also varies considerably; they can be assigned to two classes, inorganic or organic. The most common inorganic fibre used is glass fibre[7], which can be manipulated to control a whole array of fibre properties, such as length, size, and thickness. Being able to control the fibre properties also enables better control over the influence of the filler material on the polymer composite properties.

Natural fibres are a renewable source and they contribute to the recyclability and environmental aspects of polymer composite materials. Natural fibres have become more attractive for the consumer market, as the concern for the effect of materials on the environment has increased. The appeal of natural fibres has led to the development of composite materials using natural fibres as reinforcing materials.

The use of natural fibres have led to the exploration of an array of plant sources, as pointed out by Mohanty et al.[8] in a review on natural fibres and their contribution to bio composites. Natural fibres can be sourced from the stem, leaf or fruit of a plant.

Wood as a plant source has been extensively used in polymer composites, since the unique combination of cellulose and lignin makes for a strong fibrous material which may reinforce the polymer matrix. Depending on availability, the wood species can also be changed. This will affect the morphology and chemical composition of the wood fibres and therefore the physical properties of the composite. Some of the wood species used in WPCs are listed below:

Table 2.1: Some wood species used in wood polymer composites.

Bamboo[9-10]
Coconut[11]
Aspen[12]
Eucalyptus[13]
Oak, Maple and Pine[2]

As WPCs undergo degradation at high processing temperatures, it is important to select a suitable polymer matrix which can be melted and processed at relatively low temperatures. Thermoplastic polymers are preferred, since they allow easy processing and reuse of WPCs. The most general polymer matrices used are the polyoefins; mostly PE and PP.[2,14] Three types of PE used in WPCs.[2,15-18] High density polyethylene (HDPE), gives a strong composite due to high crystallinity. Low-density polyethylene (LDPE) gives a composite with good impact resistance/ toughness, due to high degree of branching in the polymer chains. Linear low density polyethylene (LLDPE) combines the properties of both HDPE and LDPE. A few other polymer matrices used in WPCs are listed below:

Table 2.2: Polymers other than polyolefins used in wood-polymer composites.

Polyurethane[19]
Polybutene succinate[20]
Polybutene[21]
Polystyrene[22]
Polyesters, Polyepoxide and Polymethylmethacrylate[23]
Polyvinyl chloride[24]

2.2 General aspects in polyolefin-wood composites

In the field of wood-polymer composite materials, several studies have been performed on polypropylene - (PP) and polyethylene - (PE) wood composites. This aspect will be briefly

discussed in the following sections. There are several aspects to consider when making a successful wood polymer composite material.

First, as with all composites, the effect of fibre geometry[25] and size[26], as well as fibre distribution[27] and content[28] affects the physical properties of the composite.

Some examples are referred to here: The type of wood could play a role; for example, Bledzki and Faruk[25] found that composites with hard wood fibres have better impact strength than soft wood fibres. Similarly it was claimed that impact strength also increased as the fibre length (for a specific type of wood) was increased. In the same vein, Ashori and Nourbakhsh[26] found that composites containing oak fibres had inferior strength compared to pine composites. In this case, however, the oak fibres they evaluated had a lower aspect ratio than the pine fibres, so here the difference in properties might be due to either the type of wood or the aspect ratio. The same authors reported that the higher the amount of extractables in the wood, the lower water absorption of the wood fibres is. This was explained in terms of the extractables interacting with the hydroxyl groups of the cellulose and lignin, making these inaccessible for interaction with water molecules. The same authors showed that wood fillers as fibres or flour could be used to prepare WPCs.

Second, the type of polymer matrix also influences the properties of the composite (as discussed in Section 2.1). In addition to the first two aspects, the amount of wood that can be loaded and the processing ability of the composite material (and the ability to recycle and reprocess) plays a significant role in determining the physical properties and longevity of the material. Beg and Pickering[29] showed that reprocessing of wood polymer composites with a polypropylene matrix, pine wood fibres, and a maleic anhydride modified polypropylene as compatibilizer at 4 wt % are possible, with major loss in physical properties after 8 cycles. They mentioned that reprocessing also improved interfacial adhesion between wood and polymer, believed to be due to reduction in molecular weight. Along with a reduction in molecular weight, reprocessing creates polymer chains that have some functional groups present due to degradation setting in, the influence of degraded species of the olefin polymer chains and wood particles, enhances the compatibility between polymer matrix and wood.[30]

One of the most important questions to consider is the compatibility between the fibres and the polymer matrix, which will greatly influence properties, such as strength and rigidity, and the stress to strain relationship of the composite, or transfer of stress from the polymer matrix to the wood particles.

In a composite comprised of a polyolefin matrix such as PP and wood fibres, the interface chemistry at the polymer wood boundary becomes quite important. Danyadi et al.[31] pointed out that

a polypropylene maleic anhydride modified polymer with a large molecular weight and lower functionality, has better improvement on the strength of a composite material. As explained in Chapter 1, these materials are incompatible, with poor adhesion properties[32]and poor mechanical properties as a result. Since the interaction between the polymer and the wood is only due to polymer penetration into the "vessels and cracks of a fibre"[33] or particle in the absence of chemical interactions, a suitable compatibilizer is necessary in order to bridge the two components.

2.3 Compatibilization

Compatibilizers are crucial in wood polymer composites and are essentially polymeric materials comprised of two functional parts. A good example is polypropylene-graft-maleic anhydride (PPgMA), which is essentially a polypropylene (PP) chain containing pendant groups of maleic anhydride.[34-37] The PP section is able to interact well with the PP matrix while the maleic anhydride is responsible for interaction with the wood, which results in improved adhesion between wood and polymer matrix.

PPgMA has proved to be the compatibilizer of choice with PP-wood composites. It was found to improve the strength of the composites (tensile strength, impact strength, and elongation at break), the processing ability, distribution of the wood particles/ fibres, the interfacial adhesion and the moisture resistance.[31, 38-48]

A similar compatibilizer for PE composites is polyethylene-graft-maleic anhydride.[49-53]

Some studies concentrated on compatibilizers with isocyanate as a functional group[54-57] and Karmarkar et al.[58] reported significant increases in the tensile strength and flexural modulus, but a decrease in impact strength and elongation at break. Another compatibilizer is poly(ethylene-co-vinyl alcohol) (EvOH).[59] EvOH has the ability to bind with wood particles through its hydroxyl group and interact with PE through its ethylene sequences.

2.4 Impact polypropylene

Impact polypropylene (impact PP) was developed to overcome the restrictions of PP; primarily its poor impact resistance at low temperatures. Impact PP is a complex copolymer of propylene and ethylene, consisting of ethylene propylene rubber (EPR), which is a random copolymer of ethylene, and propylene units, crystallizable copolymer sections of longer ethylene and propylene segments within the same polymer chains, some crystalline polyethylene and the major proportion of the material, isotactic PP. There have been several studies that focussed on the development of the morphology of the impact PP particles during gas-phase polymerization, and the development of the final morphology of the material during melt processing.[60-61]

An extensive amount of work has been done to increase our understanding of impact PP. This remains a challenging topic.[62-69] As with other polyolefins the technique of temperature rising elution fractionation or TREF has been employed to fractionate impact PP according to crystallizatbility.[70-74] These fractions can then be characterized to gain an understanding of the structure/ property relationships with these complex materials.[75-79] In the last few years, characterization of impact polypropylene by coupling of two or more techniques has also been performed, and has proven quite valuable; specifically in combining TREF, size exclusion chromatography (SEC) and Fourier transform infra-red spectroscopy (FTIR) analysis.[80-82] In this way chemical composition distribution across different crystallisable components as well as a function of molecular weight distribution can be established.

Yong Chen et al.[83] also performed a study on the complex phase morphology of impact PP with interesting results; yielding a "multi-layered core-shell structure of the dispersed phase"[83] in the isotactic PP matrix and they concluded that this structure was responsible for the high rigidity and impact toughness of the polymer. Similar results were also found in a study previously done in our group, where we studied the effect on properties and morphology, of the removal of specific fractions of impact PP, on the recombined material.[79, 84]

The introduction of TEM as a suitable technique to study morphology of impact polypropylene is useful, but the scale on which the morphology is studied makes the technique very subjective.

The staining chemistry used in TEM is also quite dangerous for the chemist, and great care has to be taken. From these aspects it has become important to use or develop a technique that could give morphological information on a more appropriate scale, specifically in the micro meter range in order to relate it to the macro properties observed for these materials.

2.5 Fluorescence microscopy

Fluorescence microscopy has mostly been applied in the medical and biological sciences and is not as yet widely used in polymer characterization as an established analysis technique. It is perhaps important to just highlight the basics of this technique, and to briefly discuss some polymer related applications already performed with this technique.

Fluorescence is essentially the luminescent light that a substance emits (fluorescence), after it has been excited by a light source with a specific wavelength. The emitted light has a slightly longer wavelength, at lower energy, than that of the incident light source and thus enables the recording of an excitation and emission wavelength spectrum.[85]

Allen et al.[86] carried out a study to monitor fluorescence/ luminescence as a characterization technique for commercial polymers that is able to give a strong fluorescence signal (due to the

presence of a chromophoric species) and proved it to be a fast and easy method, with little sample preparation required. In addition this is a non-destructive technique. These authors also mention that it could be possible to combine this technique with infra-red spectroscopy.

Zhang et al.[87] investigated the distribution of maleic anhydride (MA) grafting, on random ethylene-propylene copolymers, and was able to monitor the microstructure of this polymer and its effect on the properties of these polymers in a non-polar solvent system by attaching fluorescent dye molecules to the MA functional groups along the polymer chains. Fluorescence analysis is a fast-growing technique, continually being improved, specifically in its instrumentation capabilities and decreased acquisition time to make it a more sensitive technique. Muretta et al.[88] discussed the advantage of time-resolved (TR) fluorescence over the conventional steady-state (SS) method that is uniquely "sensitive to non-radiative decay processes that originate from variations in molecular structure, dynamics and environment of the fluorophore"[88] and should thus make fluorescence spectroscopy a valuable technique to monitor changes in fluorescence with regards to changes in polymer morphology.

Some fluorescence work has also been done on nano-particles, dissolved polymer solutions and cellulose[89-95] but not, to our knowledge, on polyolefin systems. Among many other uses, the development of fluorescence for solid state analysis appears quite rewarding.[96-100] Fluorescent dyes in the solid state give increased fluorescence enhancement as a result of the constrained media around the dye, which makes fluorescence detection more sensitive, yet also allows the possibility to explore changes in the solid state media of the polymer, with this technique.

2.6 Atomic force microscopy

Atomic force microscopy (AFM) is a relatively new technique that was developed by Binnig et al.[101]and is fast becoming a valuable analysis tool, since it is a technique which is able to analyze surface morphology on the nanometre scale and provides hardness information and physical interaction forces, such as adhesive forces between sample and tip.

Improvements of AFM led to further development in this field, for example chemical force microscopy (CFM). Here the AFM tip is chemically modified in order to detect special functional groups and their distribution on the surface of a sample via adhesive force measurements.[102-104]

CFM involves the coating of a silicon nitride tip with a fine gold layer and then attaching alkane-thiols onto the tip. These alkane-thiols form a self-assembled monolayer on the gold surface. The thiols can be tailored with specific functional groups, for example methyl (CH_3), hydroxyl (OH) or carboxylic acid (C(O)OH) groups.[105] These functional groups of the modified tip can be used to

detect certain functionalities on the sample. Only a few studies have used CFM on polymers[106]and wood polymer composites.[107]

Klash[108] successfully used CFM to monitor the distribution of specific chemical functional groups on wood and pulp fibres, to determine the lignin and cellulose content and distribution on these fibres and proved this technique feasible to describe the surface structure of wood/ pulp fibres.

AFM is therefore a valuable technique to study chemical interactions, and provides a means of quantitatively defining adhesive forces between different components, such as polymer and a filler material, and provides the ability to measure the strength of adhesion (via force distance curves) between different materials on the molecular scale, which helps to explain physical properties of a composite material and its fracture properties.

2.7 References

1. Handbook of Polymer-Fibre Composites, Polymer Science & Technology Series, F. R. Jones, Pearson Higher Education & Professional Group (1994), Chapter 1.
2. Functional Fillers for Plastics, Marino Xanthos, 1st edition, Wiley-VCH Verlag, Germany (2005).
3. A. N. Shebani, A. J. van Reenen, M. Meincken, The effect of wood species on the mechanical and thermal properties of wood-LLDPE composites, Journal of Composite Materials, 43 (11), p 1305 (2009).
4. A. N. Shebani, The effect of wood composition and compatibilizers on polyethylene/ wood fibre composites, PhD thesis, University of Stellenbosch, South Africa, 2010.
5. Fibre Reinforced Materials, G. S. Holister and C. Thomas, Elsevier, London (1966), Chapter 5.
6. N. M. Stark, R. E. Rowlands, Effects of wood fiber characteristics on mechanical properties of wood/ polypropylene composites, Wood and Fiber Science, 35(2), p 167 (2003).
7. T. Mohan, K Kanny, Influence of nanoclay on rheological and mechanical properties of short glass fibre-reinforced polypropylene composites, Journal of Reinforced Plastics and Composites, 30(2), p 152 (2011).
8. A. K. Mohanty, M. Misra, L. T. Drzal, Surface modifications of natural fibres and performance of the resulting biocomposites: An overview, Composite interfaces, 8(5), p 313 (2001).
9. M. Thwe, K. Liao, Effects of environmental aging on the mechanical properties of bamboo-glass fiber reinforced polymer matrix hybrid composites, Composites: Part A, 33, p 43 (2002).
10. K. Okubo, T. Fujii, N. Jamashita, Improvement of interfacial adhesion in bamboo polymer composite enhanced with micro-fibrillated cellulose, JSME International Journal Series A, 48(4), p 199 (2005).
11. M. Brahmakumar, C. Pavithran, R. Pillai, Coconut fibre reinforced polyethylene composites: effect of natural waxy surface layer of the fibre on fibre/ matrix interfacial bonding and strength of composites, Composites Science and Technology, 65, p 563 (2005).
12. X. Cai, B. Riedl, S. Zhang, H. Wan, The impact of the nature of nanofillers on the performance of wood polymer nanocomposites, Composites: Part A, 39, p 727 (2008).

13. A. Karmarkar, S. Chauhan, J. Modak, M. Chanda, Mechanical properties of wood-fiber reinforced polypropylene composites: Effect of a novel compatibilizer with isocyanate functional group, Composites: Part A, 38, p 227 (2007).
14. A. Ashori, Wood-plastic composites as promising green-composites for automotive industries!, Bioresource Technology, 99, p 4661 (2008).
15. M. Chanda, S. Roy, Plastics Technology Handbook, Chapter 5, 4th edition, CRC Press, USA, p 146 (2007).
16. H.-S. Kim, S. Kim, H. Kim, H. Yang, Thermal properties of bio-flour-filled polyolefin composites with different compatibilizing agent type and content, Thermochimica Acta, 451, p 181 (2006).
17. J. Kim, T. Yoon, S. Mun, J. Rhee, J. Lee, Wood-polyethylene composites using ethylene-vinyl alcohol copolymer as adhesion promoter, Bioresource Technology, 97(3), p 494 (2006).
18. B. Li, J. He, Investigation of mechanical property, flame retardancy and thermal degradation of LLDPE-wood-fibre composites, Polymer Degradation and Stability, 83, p 241 (2004).
19. R. Araujo, V. Pasa, New Eucalyptus tar-derived polyurethane coatings, Progress in Organic Coatings, 51, p 6 (2004).
20. H. Kim, H. Yang, H. Kim, B. Lee, T. Hwang, Thermal properties of agro-flour-filled biodegradable polymer bio-composites, Journal of Thermal Analysis and Calorimetry, 81, p 299 (2005).
21. A. Afrifah, R Hickok, L. Matuana, Polybutene as a matrix for wood plastic composites, Composites Science and Technology, 70, p 167 (2010).
22. T. Handa, I. Seo, H. Akimoto, M. Saito, Y. Ikeda, Physical properties of wood-polymer composites materials prepared by I.C.T-type electron accelerator, Proceedings of the 15th Japan Congress on Materials Research, Japan, (1972).
23. R. Gauthier, C. Joly, A. C. Coupas, H. Gauthier, M. Escoubes, C. Bernard, Interfaces in polyolefin/ cellulosic fibre composites: Chemical coupling, morphology, correlation with adhesion and ageing in moisture, Polymer Composites, 19, p 287 (1998).
24. C. Bloyaeart, New PVC resin for wood-polymer composites, Plastics Rubber and Composites, 37 (9/10), p 383 (2008).
25. A. K. Bledzki, O. Faruk, Wood Fiber reinforced polypropylene composites: effect of fibre geometry and coupling agent on physic-mechanical properties, Applied Composite Materials, 10, p 365 (2003).
26. A. Ashori, A. Nourbakhsh, Reinforced polypropylene composites: Effects of chemical compositions and particle size, Bioresource Technology, 101, p 2515 (2010).

27. C. Xing, S. Y. Zhang, J. Deng, B. Riedl, A. Cloutier, Medium-density fibreboard performance as affected by wood fiber acidity, bulk density, and size distribution, Wood Science and Technology, 40, p 637 (2006).
28. A. K. Bledzki, J. Gassan, S. Theis, Wood-filled thermoplastic composites, Mechanics of Composite Materials, 34 (6), p 563 (1998).
29. M. D. H. Beg, K. L. Pickering, Reprocessing of wood fibre reinforced polypropylene composites. Part I: Effects on physical and mechanical properties, Composites: Part A, 39(7), p 1091 (2008).
30. M. D. H. Beg, K. L. Pickering, Reprocessing of wood fibre reinforced polypropylene composites. Part II: Hygrothermal ageing and its effects, Composites: Part A, 39(9), p 1565 (2008).
31. L. Danyadi, T. Janecska, Z. Szabo, G. Nagy, J. Moczo, B. Pukanszky, Wood flour filled PP composites: Compatibilization and adhesion, Composites Science and Technology, 67(13), p 2838 (2009).
32. S. E. Selke, I. Wichman, Wood fibre/polyolefin composites, Composites: Part A, 35, p 321 (2004).
33. Q. Yuan, D. Wu, J. Gotama, S. Bateman, Wood fiber reinforced polyethylene and polypropylene composites with high modulus and impact strength, Journal of Thermoplastic Composite Materials, 21, p 195 (2008).
34. United States patent no. US 6,437,049 B1, August 20, 2002, Bortolon et al., Process for modifying polypropylene with maleic anhydride.
35. United States patent no. US 7,605,197 B2, October 20, 2009, Matuana et al., Process for the preparation of maleated polyolefin modified wood particles in composites and products.
36. M. Schlavons, M. Laurent, J. Devaux, V. Carlier, Maleic anhydride-grafted polypropylene: FTIR study of a model polymer grafted by ene-reaction, Polymer, 46, p 8062 (2005).
37. S. H. P. Bettini, J. A. M. Agnelli, Grafting of maleic anhydride onto polypropylene by reactive processing. II. Effect of rotor speed and reaction time, Journal of Applied Polymer Science, 74, p 256 (1999).
38. F. Michaud, B. Riedl, P. Castera, Improving wood/ polypropylene fibreboards properties with an original MAPP coating process, HolzalsRoh-und Werkstoff, 63, p 380 (2005).
39. N. Sombatsompop, C. Yotinwattanakumtorn, C. Thongpin, Influence of type and concentration of maleic anhydride grafted polypropylene and impact modifiers on mechanical properties of PP/ wood sawdust composites, Journal of Applied Polymer Science, 97, p 475 (2005).

40. P. Wang, J. Liu, W. Yu, C. Zhou, Dynamic rheological properties of wood polymer composites: from linear behaviours, Polymer Bulletin, 66, p 683 (2011).
41. R. A. Garcia, A. Cloutier, B. Riedl, Dimensional stability of MDF panels produced from fibres treated with maleated polypropylene wax, Wood Science and Technology, 39, p 630 (2005).
42. V. N. Hristov, M. Krumova, St. Vasileva, G. H. Michler, Modified polypropylene wood flour composites. II. Fracture, deformation, and mechanical properties, Journal of Applied Polymer Science, 92, p 1286 (2004).
43. J.-M. Park, S. T.Quang, B.-S. Hwang, K. L. DeVries, Interfacial evaluation of modified jute and hemp fibers/ polypropylene (PP)-maleic anhydride polypropylene copolymers (PP-MAPP) composites using micromechanical technique and non-destructive acoustic emission, Composites Science and Technology, 66, p 2686 (2006).
44. A. K. Bledzki, O. Faruk, Creep and impact properties of wood fibre-polypropylene composites: influence of temperature and moisture content, Composite Science and Technology, 64, p 693 (2004).
45. A. Ashori, A. Nourbakhsh, Characteristics of wood-fiber plastic composites made of recycled materials, Waste Management, 29, p 1291 (2009).
46. A. Ashori, A. Nourbakhsh, Performance properties of microcrystalline cellulose as a reinforcing agent in wood plastic composites, Composites: Part B, 41, p 578 (2010).
47. M. N. Ichazo, C. Albano, J. Gonzalez, R. Perera, M. V. Candal, Polypropylene/ wood flour composites: treatments and properties, Composite Structures, 54, p 207 (2001).
48. D. Ndiaye, E. Fanton, S. Morlat-Therias, L. Vidal, A. Tidjani, J.-L. Gardette, Durability of wood polymer composites: Part 1. Influence of wood on the photochemical properties, Composites Science and Technology, 68, p 2779 (2008).
49. M. Behzad, M. Tajvidi, G. Ehrahimi, R. H. Falk, Dynamic mechanical analysis of compatibilizer effect on the mechanical properties of wood flour – High density polyethylene composites, IJE Transaction B : Applications, 17 (1), p 95 (2004).
50. J. Z. Lu, I. I. Negulescu, Q. Wu, Maleated wood-fiber/high-density-polyethylene composites: Coupling mechanisms and interfacial characterization, Composite Interfaces, 12 (1-2), p 125 (2005).
51. K. Carlborn, L. M. Mutuana, Influence of processing conditions and material compositions on the performance of formaldehyde-free wood-based composites, Polymer Composites, p 601 (2006).
52. J. Z. Lu, Q. Wu, I. I. Negulescu, Wood-fiber/ High-density-polyethylene composites: Coupling agent performance, Journal of Applied Polymer Science, 96, p 93 (2005).

53. M. Tasdemir, H. Biltekin, G. T. Caneba, Preparation and characterization of LDPE and PP-Wood fiber composites, Journal of Applied Polymer Science, 112, p 3095 (2009).
54. Y. Lei, Q. Wu, F. Yao, Y. Xu, Preparation and properties of recycled HDPE/natural fiber composites, Composites: Part A, 38, p 1664 (2007).
55. N. E. Marcovich, M. A. Villar, Thermal and mechanical characterization of linear low-density polyethylene/ wood flour composites, Journal of Applied Polymer Science, 90, p 2775 (2003).
56. The effect of Poly(methylene(polyphenylisocyanate)) and maleated polypropylene coupling agents on New Zealand Radiata Pine fiber-polypropylene composites, Journal of Reinforced Plastics and Composites, 23 (18), p 2011 (2004).
57. D. Georgieva, S. Nenkova, G. Behrendt, Wood polymer composites using binder based on polyurethane recycling products, Journal of the University of Chemical Technology and Metallurgy, 42 (4), p 345 (2007).
58. A. Karmarkar, S. S. Chauhan, J. M. Modak, M. Chanda, Mechanical properties of wood-fiber reinforced polypropylene composites: Effect of a novel compatibilizer with isocyanate functional group, Composites: Part A, 38, p 227 (2007).
59. J.-P. Kim, T.-H. Yoon, S.-P. Mun, J.-M. Rhee, J.-S. Lee, Wood-polyethylene composites using ethylene-vinyl alcohol copolymer as adhesion promoter, Bioresource Technology, 97, p 494 (2006).
60. Y. Chen, Y. Chen, W. Chen, D. Yang, Morphology of high impact polypropylene particles, Polymer, 47, p 6808 (2006).
61. Y. Chen, Y. Chen, W. Chen, D. Yang, Evolution of phase morphology of high impact polypropylene particles upon thermal treatment, European Polymer Journal, 43, p 2999 (2007).
62. C. Hongjun, L. Xiaolie, M. Dezhu, W. Jianmin, T. Hongsheng, Structure and properties of impact copolymer polypropylene. I. Chain structure, Journal of Applied Polymer Science, 71, p 93 (1999).
63. C. Hongjun, L. Xiaolie, C. Xiangxu, M. Dezhu, W. Jianmin, T. Hongsheng, Structure and properties of impact copolymer polypropylene. II. Phase structure and crystalline morphology, Journal of Applied Polymer Science, 71, p 103 (1999).
64. T. Hongsheng, L. Li, C. Zhineng, S. Yihu, Z. Qiang, Phase morphology and impact toughness of impact polypropylene copolymer, Polymer, 46, p 3522 (2005).
65. N. Tortorella, C. L. Beatty, Morphology and crystalline properties of impact-modified polypropylene blends, Polymer Engineering and Science, 48,p 1476(2008).

66. G. C. Pandey, A. Kumar, R. K. Garg, Nondestructive evaluation of physico-mechanical properties of polypropylene copolymer by infra-red spectroscopy, European Polymer Journal, 38, p 745 (2002).

67. Y. Tanaka, K. Hatada, Carbon-13 Nuclear magnetic resonance of ethylene-propylene copolymer and the determination of sequence distribution of monomeric units, Journal of Polymer Science: Polymer Chemistry Edition, 11 (8), p 2057 (1973).

68. H. N. Cheng, M. Kakugo, ^{13}C NMR Analysis of compositional heterogeneity in ethylene-propylene copolymers, Macromolecules, 24, p 1724 (1991).

69. Carbon-13 Nuclear Magnetic resonance determination of monomer composition and sequence distribution in ethylene-propylene copolymers prepared with a stereo regular catalyst system, Macromolecules, 10 (4), p 773 (1977).

70. J. Xu, L. Feng, Application of temperature rising elution fractionation in polyolefins, European Polymer Journal, 36, p 867 (2000).

71. J. Xu, L. Feng, S. Yang, Y. Yang, X. Kong, Temperature rising elution fractionation of polypropylene produced by heterogeneous Ziegler-Natta catalysts, European Polymer Journal, 34 (3/4), p 431 (1998).

72. B. Monrabal, P. del Hierro, Characterization of polypropylene-polyethylene blends by temperature rising elution fractionation and crystallization analysis fractionation, Analytical and Bioanalytical Chemistry, 399,p 1557 (2011).

73. L. Wild, G. Glockner, Temperature rising elution fractionation, Advances in Polymer Science, 98, p 1(1991).

74. J. B. P. Soares, A. E. Hamielec, Temperature rising elution fractionation of linear polyolefins, Polymer, 36 (8), p 1639 (1995).

75. F. M. Mirabella Jr., Impact polypropylene copolymers: fractionation and structural characterization, Polymer, 34 (8), p 1729 (1993).

76. R. Zacur, G. Goizueta, N. Capiati, Dispersed phase morphology of impact PP copolymers. Effects of blend composition as determined by TREF, Polymer Engineering and Science, 40 (8), p 1921 (2000).

77. L. Gilet, M.-F. Grenier-Loustalot, Quantitative analysis of mixtures of ethylene- and propylene-based polymers by temperature-rising elution fractionation and ^{13}C nuclear magnetic resonance, Polymer, 33 (21), p 4605 (1992).

78. G. Harding, The fractionation and characterisation of propylene-ethylene random copolymers, MSc thesis, University of Stellenbosch, South Africa, 2005.

79. A. J. van Reenen, N. C. Basson, Molecular composition and properties of impact propylene copolymers, eXPRESS Polymer Letters, 6 (5), p 427 (2012).

80. E. de Goede, P. Mallon, H. Pasch, Fractionation and analysis of an impact poly(propylene) copolymer by TREF and SEC-FTIR, Macromolecular Materials and Engineering, 295, p 366 (2010).
81. E. de Goede, P. Mallon, H. Pasch, Using crystallization fractionation to monitor thermo-oxidative degradation of impact poly(propylene) copolymers, Macromolecular Materials and Engineering, 297, p 26 (2012).
82. I. Saurez, M. J. Callero, B. Coto, A fast and reliable procedure to determine the copolymer composition by GPC-IR: Application to ethylene/propylene copolymers and comparison with ^{13}C NMR, Polymer Engineering and Science, p 317 (2011).
83. Y. Chen, Y. Chen, W. Chen, D. Yang, Multilayered core-shell structure of the dispersed phase in high-impact polypropylene, Journal of Applied Polymer Science, 108, p 2379(2008).
84. N. C Basson, The effect of molecular architecture on the properties of propylene impact copolymers, MSc thesis, University of Stellenbosch, South Africa, 2010.
85. George Hopple, Microstructural Science, Editors M. E Blum, P. M. French, R. M. Middleton, and G. F. Vander Voort, Volume 15, 451-467.
86. N. S. Allen, J. Homer, J. F. McKellar, The use of luminescence spectroscopy in aiding the identification of commercial polymers, Analyst, 101, p 260 (1976).
87. M. Zhang, J. Duhamel, M. van Duin, P. Meessen, Characterization by fluorescence of the distribution of maleic anhydride grafted onto ethylene-propylene copolymers, Macromolecules, 37, p 1877 (2004).
88. J. M. Muretta, A. Kyrychenko, A. S. Ladokhin, D. J. Kast, G. D. Gillispie, D. D. Thomas, High-performance time-resolved fluorescence by direct waveform recording, Review of Scientific Instruments, 81, 103101-1 (2010).
89. V. Tsyalkovsky, V. Klep, K. Ramaratnam, R. Lupitskyy, S. Minko, I. Luzinov, Fluorescent reactive core-shell composite nanoparticles with a high surface concentration of epoxy functionalities, Chemistry of Materials, 20, p 317 (2008).
90. A. N. De Belder, K. Granath, Preparation and properties of fluorescein-labelled dextrans, Carbohydrate Research, 30, p 375 (1973).
91. F. Wilkinson, D. R. Worrall, Photochemistry on surfaces: fluorescence emission of monomers and dimmers and triplet state absorption of acridine orange absorbed on microcrystalline cellulose, SpectrochimicaActa, 48 A (2), p 135 (1992).
92. Q. Yang, X. Pan, A facile approach for fabricating fluorescent cellulose, Journal of Applied Polymer Science, 117, p 3639 (2010).

93. L. J. Nielsen, S. Eyley, W. Thielemans, J. W. Aylott, Dual fluorescent labelling of cellulose nanocrystals for pH sensing, Chemical Communications, 46, p 8929 (2010).

94. U. Zettl, M. Ballauff, L. Harnau, A fluorescence correlation spectroscopy study of macromolecular tracer diffusion in polymer solutions, Journal of Physics: Condensed Matter, 22, 494111 (2010).

95. C. Wu, Y. Zheng, C. Szymanski, J. Mcneill, Energy transfer in a nanoscalemultichromophoric system: Fluorescent dye-doped conjugated polymer nanoparticles, Journal of Physical Chemistry C, 112, p 1772 (2008).

96. M. G. Lagorio, E. San Roman, A. Zeug, J. Zimmermann, B. Roder, Photophysics on surfaces: Absorption and luminescence properties of pheophorbide-a on cellulose, Physical Chemistry Chemical Physics, 3, p 1524 (2001).

97. L. F. Vieira Ferreira, M. Rosario Freixo, A. R. Garcia, F. Wilkinson, Photochemistry on Surfaces: Fluorescence emission quantum yield evaluation of dyes absorbed on microcrystalline cellulose, Journal of the Chemical Society, Faraday Transactions, 88 (1), p 15 (1992).

98. H. B Rodriguez, A. Iriel, E. San Roman, Energy transfer among dyes on particulate solids, Photochemistry and Photobiology, 82, p 200 (2006).

99. T. A. Fayed, S. El-Din H. Etaiw, Fluorescence characteristics and photostability of benzoxazole derived donor-acceptor dyes in constrained media, Spectrochimica Acta Part A, 65, p 366 (2006).

100. F. Bezati, D. Froelich, V. Massardier, E. Maris, Addition of tracers into the polypropylene in view of automatic sorting of plastic wastes using x-ray fluorescence spectrometry, Waste Management, 30, p 591 (2010).

101. G. Binnig, C. F. Quate, Ch. Gerber, Atomic force microscope, Physical Review Letters, 56 (9), p 930 (1986).

102. J. C. Bastidas, R. Venditti, J. Pawlak, R. Gilbert, S. Zauscher, J. F. Kadla, Chemical force microscopy of cellulosic fibers, Carbohydrate Polymers, 62, p 369 (2005).

103. D. V. Vezenov, A. Noy, P. Ashby, Chemical force microscopy: probing chemical origin of interfacial forces and adhesion, Journal of Adhesion Science and Technology, 19 (3-5), p 313 (2005).

104. H. Takano, J. R. Kenseth, S.-S. Wong, J. C. O'Brien, M. D. Porter, Chemical and biochemical analysis using scanning force microscopy, Chemical Revision, 99 (10), p 2845 (1999).

105. G. G. Baralia, A.-S. Duwez, B. Nysten, A. M. Jonas, Kinetics of exchange of alkanethiol monolayers self-assembled on polycrystalline gold, Langmuir, 21, p 6825 (2005).

106. M. Meincken, R. D. Sanderson, Advantages of scanning probe microscopy in polymer science, South African Journal of Science, 100, p 256 (2004).

107. G. S. Oporto, D. J. Gardner, D. J. Neivandt, Adhesion properties of wood-plastic composite surfaces: atomic force microscopy as a complimentary analysis tool, Contact Angle, Wettability and adhesion, 6, p 341 (2009).

108. A. Klash, Localisation and quantification of chemical functional groups on pulp fibers, PhD thesis, University of Stellenbosch, South Africa, 2010.

CHAPTER 3 EXPERIMENTAL

3.1 Materials

3.1.1 Polymers

The impact polypropylene copolymers were supplied by Sasol Polymers (CMR648, ethylene content 12 %, MFI = 8.5 g/ 10 min and CKR 448, ethylene content 9.5 %, MFI = 4.5 g/ 10 min). The CKR 448 polymer was renamed CMR 448 for the purposes of this study. These polymers were used as received.

The polymers used as compatibilizers were polypropylene-graft-maleic anhydride (abbreviated as PPgMA, Sigma-Aldrich, maleic anhydride content 8 -10 wt %, melting temperature (Tm) = 156 °C, Mw = 9600 g/mol, Mn = 3900 g/mol, determined by GPC), and poly(ethylene-co-vinyl alcohol) (abbreviated as EvOH, 44 mole% ethylene, Tm = 191 °C, glass transition temperature (Tg) = 55 °C). The compatibilizers were pre-treated before use, as follows:

Typically, PPgMA (3 g) was dissolved at 135 °C in 75 mL xylene (Kimix Chemicals, mixture of ortho, meta and para isomers), cooled, precipitated with and washed in acetone (KIMIX chemicals). The precipitated polymer was filtered and dried under reduced pressure. This procedure removed any maleic anhydride contaminant and changed the physical form from the original pellets to a finely divided powder, which was more suited for subsequent mixing experiments.

Similarly, EvOH (3 g) was dissolved in 75 mL dimethyl sulfoxide (DMSO)(UNILAB, 99.5 % assay) at 135 °C, cooled and precipitated in distilled, deionized water.

3.1.2 Wood particles (preparation and characterization)

The wood chips (Pinus radiata) used for the composites were obtained from the Department of Forestry and Wood Science at the University of Stellenbosch. The wood chips were milled in a Drotsky hammer mill with a 4 mm screen, and then dried in an oven at 103 °C for 24 hours. Screenings of these particles were done in a Retch shaker (AS 200). Particles retained in the 180 μm sieve were used in the composites. All particles with a size below 180 μm were used to prepare composites for a comparative study. This is described in Chapter 4, Section 4.4.

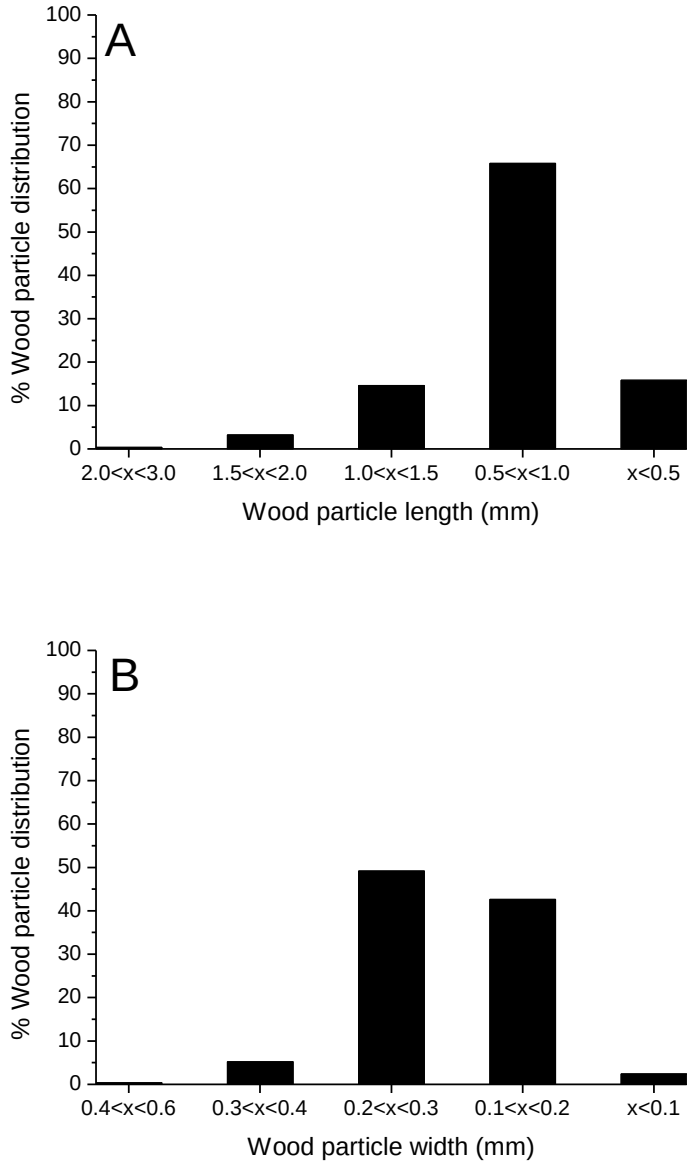

Figure 3.1: Wood particle distribution of the 180 μm sieved particle size; A, particle length and B, particle width.

Length and width measurements of 120 wood particles (as a representative sample) were done using a Leica EZ 4D stereo microscope (10 x magnification). The average length, width and distribution of particles of these dimensions are shown in Figure 3.1 A and B. The average aspect ratio of these particles is 3.76.

3.1.3 Other materials

Organic dyes used in the fluorescence studies were Fluorescein and Rhodamine B (Sigma-Aldrich). The solvent used for the preparative TREF experiments was Xylene (Kimix, mixture of isomers). The xylene was dried by refluxing over sodium metal and then distilling. A mixture of Irgafos 168

and Irganox 1010 (Ciba) was used as stabilizers during the preparation and molding of the composite samples.

3.2 Reactions and composite preparation

3.2.1 Reaction of compatibilizers with dye molecules

The compatibilizers (PPgMA and EvOH) were reacted with the dyes (Rhodamine B and Fluorescein) to prepare materials that could be used in fluorescence studies. The reaction schemes are given below (Schemes 3.1 A (reaction of Rhodamine B with PPgMA and 3.1 B (reaction of Fluorescein with EvOH).

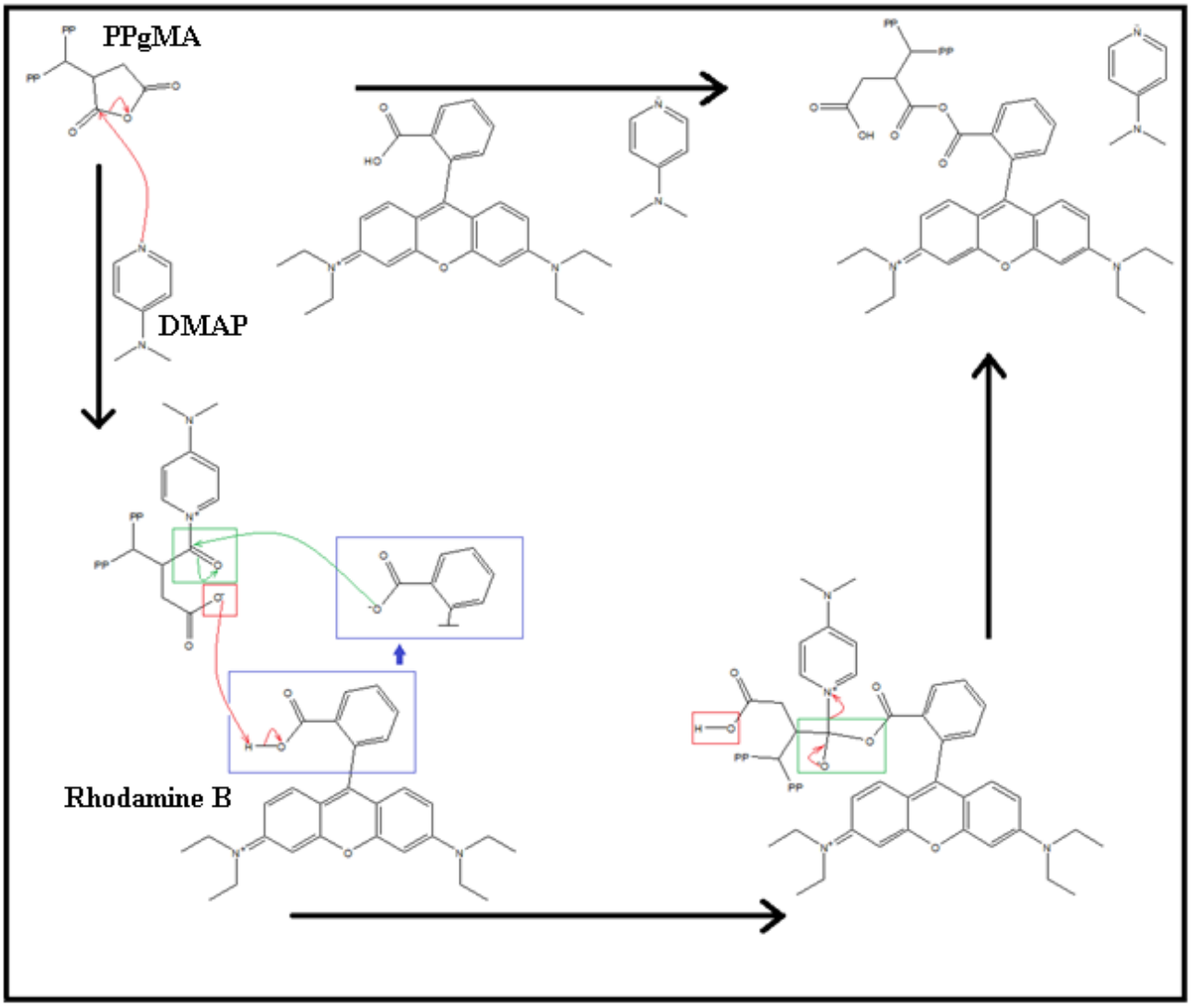

Scheme 3.1 A: Reaction of Rhodamine B with PPgMA.

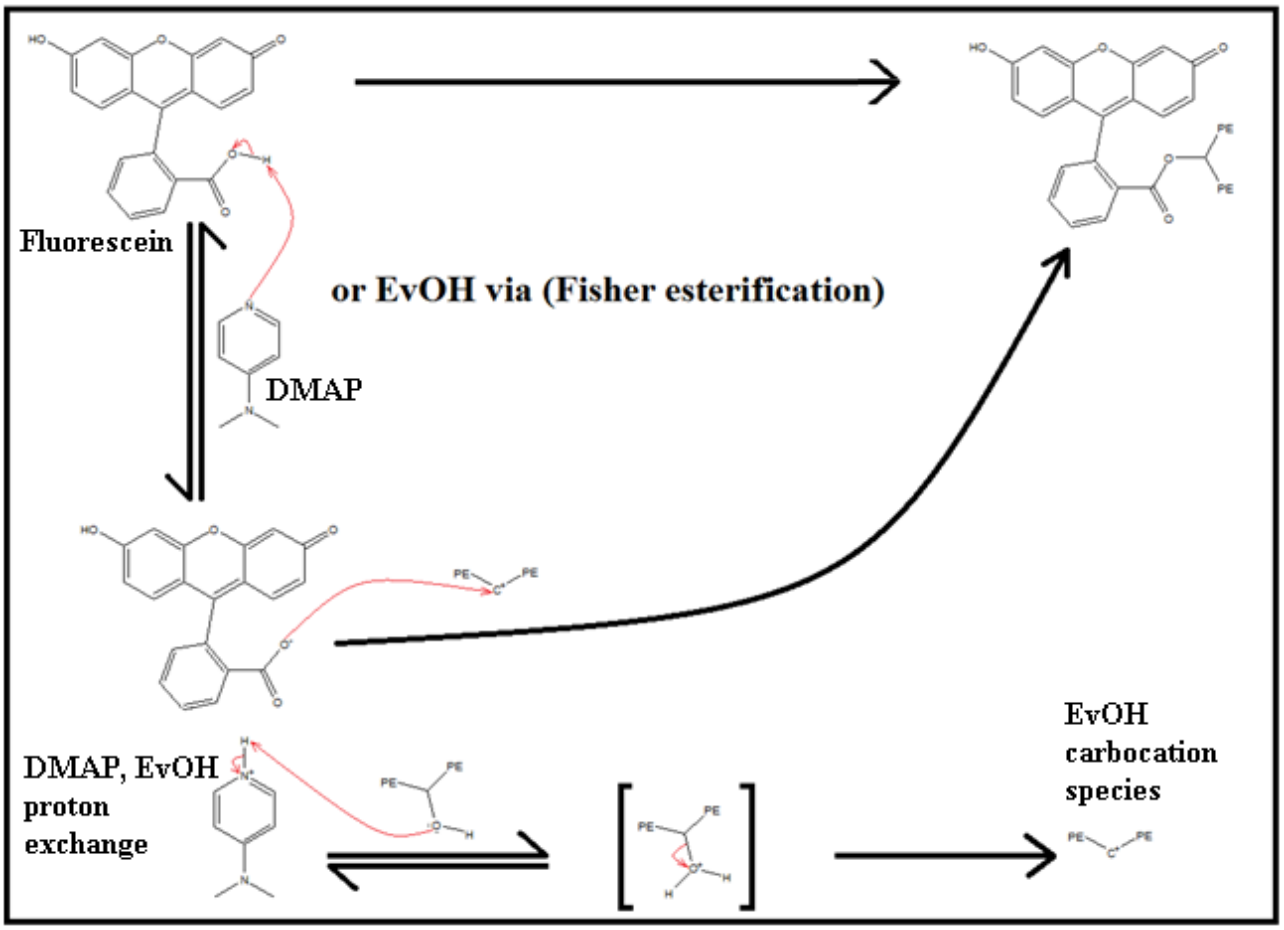

Scheme 3.1 B: Reaction of Fluorescein with EvOH.

PPgMA was reacted with Rhodamine B according to the following example:

The maleic anhydride content of 2 g PPgMA was calculated based on the assumption that the polymer contains a minimum of 8 wt% MAH. It was first assumed that the reaction between the maleic anhydride moiety and Rhodamine B would take place in a 1:1 ratio, but it soon became apparent that this was not the case. In addition it was also seen that a very small amount of dye is necessary to attain a large enough fluorescence signal. Using a calculated 10% (based on MAH content) of the dye was enough, and also reduced the amount of unreacted dye that had to be removed during the washing process.

Typically, therefore, PPgMA and Rhodamine B were reacted in 50 mL xylene. The dye was first dissolved in a very small amount of acetone, which was required to ensure that the dye remained in solution during the reaction. The reaction was done at 135 °C. DMAP (0.5 mol%[1] relative to MAH content) was used as catalyst. The reaction was allowed to continue for two hours.

The product was precipitated, filtered and washed with acetone until the filtrate had showed no traces of dye. The product was redissolved in xylene at 135 °C, and the precipitation, filtration and wash procedure repeated to make sure all unreacted dye was removed. The product was dried under vacuum for 24 hours before use.

EvOH was reacted with Fluorescein according to the following example:

EvOH with 44 mole % ethylene content were used, thus we assumed that 56 mole % is vinyl alcohol content. The molecular weight for the vinyl alcohol repeat unit of EvOH was calculated at 72.1062 g/mol. It is thus possible to calculate a relative amount of moles of alcohol content in a certain mass of EvOH. The amount of DMAP catalyst used was 0.5 mol % based in the hydroxyl content of the EvOH used. The amount of Fluorescein dye used was calculated in the same $1/10^{th}$ ratio as described above for Rhodamine B.

3.2.2 The preparation of joint compatibilizers

As it was found that using compatibilizers (PPgMA and EvOH) by themselves resulted in wood-polymer composites with inferior properties compared to those composites where a combination of the compatibilizers were used, it was decided to pre-react the compatibilizers in varying ratios before use. This was done pre-empt possible reaction of the functional groups of the compatibilizers (maleic anhydride and hydroxyl groups) during the preparation and molding of composite samples. Three different approaches were tried.

Method1

Composite samples of 3 g were prepared with joint compatibilizers, containing PPgMA and EvOH in different ratios. The copolymer was dissolved at 135 °C in 75 mL xylene and the compatibilizers were dissolved separately at 135 °C in 5mL xylene and 5 mL dimethyl sulfoxide (DMSO), respectively. Then they were added to the copolymer while stirring, together with the wood particles at 135 °C for 2 minutes.

The blend was cooled to room temperature, precipitated in acetone, filtered and dried.

Method2

The compatibilizers were first reacted in solution, using just heat to effect the esterification reaction. The EvOH and PPgMA were dissolved in 5 mL DMSO. DMSO was used, because PPgMA can partially melt and dissolve in this solvent and specifically since EvOH dissolves easily in this solvent. Other solvents proved ineffective.

The copolymer was dissolved as described previously and the compatibilizers were allowed to react for 15-20 minutes at 135 °C before they were added to the polymer solution, and the addition of wood particles followed as described in method 1.

Method 3

Composite samples were prepared in the same manner as described above, but with 5 mole % DMAP catalyst added to the mixture of the two compatibilizers. No other esterification methods were used,[2-4] as we were concerned that increasing esterification could lead to unwanted cross linking, that could take place. In a similar reaction, a joint compatibilizer of PPgMA and EvOH was prepared, using compatibilizers that had first been reacted with the respective dyes (see Section 3.2.1); this product was used during the fluorescence study (see Section 5.3.2, Chapter 5).

3.2.3 Composite preparation

3.2.3.1 Polymer-wood composites without compatibilizer

Composites (total mass 3 g each) were prepared in replicates of four. The wood content was 10, 20 or 30 wt %. This was done in order to determine the optimum wood loading. 2 wt % stabilizers (a mixture of Irganox 1010 and Irgafos 168, donated by Sasol Polymers) were added to prevent degradation.

Typically, the composite samples were prepared by dissolving the impact copolymer in 75 mL xylene at 135 °C and then adding the wood into the solution. Stirring and cooling to room temperature was followed by precipitation in acetone. The samples were then filtered (Whatman, 24 cm) and allowed to dry in a constant air flow at room temperature for two days. This solution mixing method considered was the best option, as no melt mixing instrumentation was available. For example, 2.7 g polymer would be used with 0.3 g wood, or 2.1 g polymer and 0.9 g wood. In each case 2 wt % stabilizer would be added, calculated on the amount of polymer present.

Eventually a wood content of 10 wt % was selected as standard for all samples, as it was found that this allowed for easy sample preparation for physical testing (injection molding) and resulted in good properties of the composites (see Chapter 4). It was, for example, very difficult to injection mold samples with 30 wt % wood.

3.2.3.2 Polymer-wood composites with compatibilizer

Composites (total mass of 3 g) were prepared in replicates of four with a wood content of 10 wt %, but in this case with compatibilizer added. Compatibilizer content varied from 2 to 10 wt %. The amount of compatibilizer was calculated on the total polymer content.

The best mechanical properties (see Chapter 4) were achieved at 6 % compatibilizer content, which was therefore used as a standard for all samples. To prepare the composites, the impact copolymer was dissolved in 75 mL xylene at 135 °C and the compatibilizer was added to the dissolved polymer solution while stirring. The wood particles were then added as described in Section 3.2.3.1.

3.2.3.3 Polymer-wood composites with joint compatibilizer

Refer to Section 3.2.2 for the details on the preparation of the composites. In this case, the amount of individual compatibilizers making up the "joint" compatibilizer was varied, but the overall compatibilizer content was kept at 6 wt %.

3.3 Preparation of test specimens

3.3.1 Film pressing

A Graseby Specac mini bench top film press was used to mold films of fractionated polymer matrix (see Section 3.3.5) with compatibilizer, dye-reacted compatibilizer, or joint compatibilizer. A total of 12 wt % compatibilizer was added to each polymer fraction. The films were prepared at 180 °C with the following procedure:

1. The sample (polymer and compatibilizer) was placed between two Mylar ® films in the mold.
2. Temperature was maintained at 180 °C for 2 minutes 30 seconds, no applied pressure.
3. 5 t pressure was applied at 180 °C for 1 minute.
4. 5 t pressure was re-applied at 180 °C for 1 minute.
5. The sample was removed and cooled to room temperature inside a sample container, cooled with water cooling.

3.3.2 Bench top injection molding

Composite samples were molded into tensile bars with a HAAKE Mini Jet II from Thermo Scientific (type 557-2290). Four samples were prepared of each composite for impact testing and tensile testing. In order to obtain accurate and reproducible results during physical tests all samples were injection molded prior to testing.[5-8] The following settings were used:

1. Cylinder temperature: 250 °C.
2. Mold temperature: 60 °C.
3. Injection pressure: 250 bar.
4. Post (hold) pressure: 250 bar.
5. Removal of sample.

The sample dimensions were: gauge length 37.58 mm, width 4.98 mm, thickness 1.45 mm.

3.3.3 Microtome

Sections between 20 and 40 μm thick were cut from the injection molded, tensile fractured samples with a Leica RM 2245 Rotary Microtome with 16 cm steel blades.

3.3.4 Atomic force microscope tip modifications

Suitable AFM tips were gold coated (50 nm layer), under vacuum with Argon/ nitrogen gas deposition support, then reacted with a thiol[9-10] and functionalized with either PPgMA or EvOH.

The tip modification involved the following steps:

1. Preparation of a 1 mM solution of 11-mercapto-1-undecanol, 1-octadecanethiol and11-mercapto undecanoic acid (all from Sigma Aldrich, used as received) in ethanol (KIMIX).
2. Gold tips were submerged in this thiol solution and allowed to react for 2 hours at room temperature under Argon gas.
3. Tips were then repeatedly washed with ethanol and n-heptane (KIMIX) and dried under Argon gas.
4. A 2 mM PPgMA solution was prepared in xylene at elevated temperature, and then allowed to cool.
5. A 2 mM EvOH) solution was prepared with a ratio of 70: 30 isopropanol (KIMIX) and distilled deionized water.
6. The thiol coated tips were allowed to react with the PPgMA and EvOH solutions individually to prepare functionalized tips with PPgMA and EvOH, respectively. The conditions and experimental procedure remained the same as described during the thiol preparation steps, and a temperature of 40 °C, were used to improve the reaction rate.

Films of PPgMA, EvOH, Lignin (Sigma Aldrich) and α-Cellulose (Sigma Aldrich), as well as polymeric materials obtained from the TREF fractionation of the impact copolymers were prepared. The TREF fractions were melted on freshly cleaved mica between two glass slides. This was done in order to obtain a flat surface suitable for AFM analysis. EvOH and PPgMA were melted and films prepared in the same manner. The lignin was precipitated with reaction grade acetone (99.9 % pure, KIMIX) and dried to evaporate all the acetone. α-Cellulose fibers were compressed between two glass slides and melted.

Confirmation of thiol tip modification was determined from differences in adhesive force distance curves, between analyses of different chemically modified tips on the same test sample. SEM was

used to confirm reaction and successful preparation of PPgMA and EvOH tips, as shown in Figure 3.2 A and B.

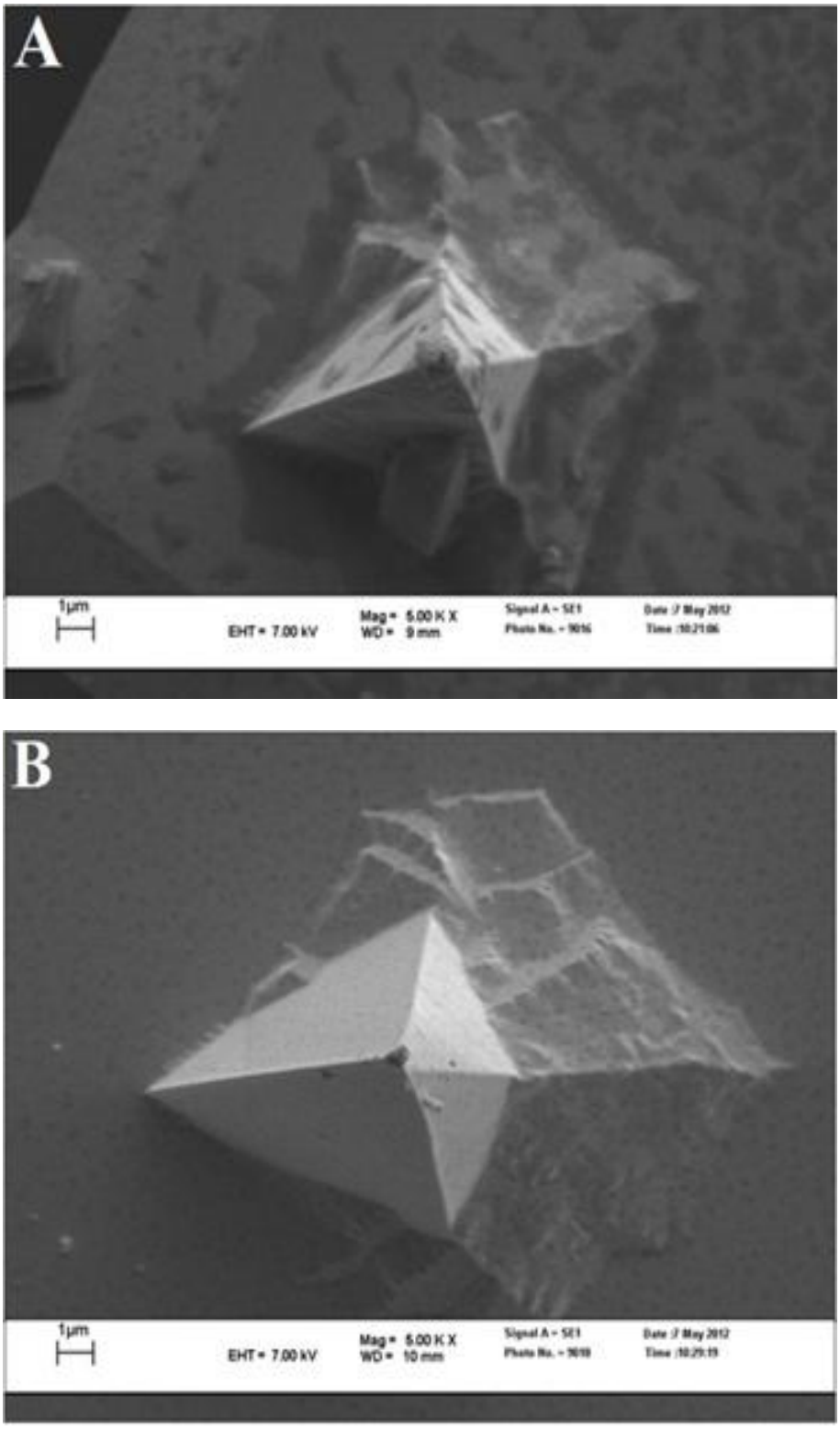

Figure 3.2: A; PPgMA modified AFM tip and B; EvOH modified AFM tip.

3.3.5 Temperature rising elution fractionation (TREF)

A preparative TREF instrument built in-house was used for this part of the study [11, 12]. Typically 3 g of a sample) was dissolved in 300 mL of xylene (stabilised with a mixture of Irganox 1010 and Irganox 168) at a temperature of 135 °C in a glass reactor. Pre-heated sea sand (Sigma Aldrich) was added to this hot solution, ensuring that the sand covered the solution completely. The sand/ polymer solution mixture was then cooled in a controlled fashion at 1 °C/ hour to a room temperature of 20 °C. When the mixture reached room temperature, the sand support and residual solvent was transferred to an elution column, and placed in a modified oven. Elution with xylene (stabilized with beta-hydroxytoluene, Ciba Switzerland) at set temperature intervals (25 °C, 40 °C, 60 °C, 80 °C, 90 °C, 100 °C, 110 °C, 120 °C, 140 °C) and subsequent evaporation of the xylene and precipitation with acetone lead to fractions of the polymer being isolated. These fractions were dried under vacuum to constant weight. Samples were analyzed in combination with SEC-FTIR as described below in Section 3.4.1.

Each temperature fraction consisted of segments of polymer material, separated during elution as explained below:

25 °C Fraction: All polymer material eluting up to 25 °C.

40 °C Fraction: All material between 26 °C and 40 °C.

60 °C Fraction: All material between 41 °C and 60 °C.

80 °C Fraction: All material between 61 °C and 80 °C.

90 °C Fraction: All material between 81 °C and 90 °C.

100 °C Fraction: All material between 91 °C and 100 °C.

110 °C Fraction: All material between 101 °C and 110 °C.

120 °C Fraction: All material between 111 °C and 120 °C.

140 °C Fraction: All material between 121 °C and 140 °C.

3.4 Characterization

3.4.1 Size exclusion chromatography coupled with Fourier transform infrared spectroscopy (SEC-FTIR)

SEC was conducted using a PL220 Chromatograph (Polymer Laboratories, Varian Inc., Church Stretton, Shropshire, England). Analysis was done at 150 °C using three 300 mm x 7.5 mm PLgel Olexis columns, a PLgel Olexis Guard and a refractive index detector. Samples were prepared by

dissolution in trichlorobenzene (TCB, Sigma-Aldrich South Africa, refluxed over sodium and freshly distilled and filtered) at 160 °C. Sample concentration was 2 $mg.ml^{-1}$ for the SEC-FTIR experiments and 0.5 mg/mL for the SEC analyses. An automated sample injection system was used with TCB as the mobile phase. The mobile phase flow rate was 1.0 $mL.min^{-1}$. Sample injection volume was always 200 µl. For SEC experiments, calibration was done by using polystyrene standards (PSS GmbH, Mainz, Germany).

For the SEC-FTIR experiments, the column outlet was connected to a LC Transform (solvent evaporation FTIR interface, Series 300, Lab Connections, Carrboro, USA). The deposition stage was at 165 °C and the spray nozzle at 150 °C. The line connecting the nebulization compartment and the high temperature chromatograph was kept at 150 °C. Overheating of the nozzle was prevented by a constant flow of compressed air. Deposition of the solutes onto a heated germanium disk was followed by FTIR analysis (Nicolet iS10 Spectrometer, (Thermo Electron, Waltham, USA). Data analysis was done with the Omnic software package (Thermo Electron). FTIR was done in ATR mode (64 scans, 4 cm^{-1} resolution).[14, 15]

3.4.2 Fluorescence microscopy and spectroscopy

Samples prepared as described above (Section 3.3) were analyzed with fluorescence microscopy. The Mylar ® film was removed and four surface images of each sample were taken in order to calculate an average grey value for each sample, as well as four fluorescence images taken per sample. The instrumentation setup is described below.

The samples were analyzed on an Olympus Cell'R, attached to an IX-81 inverted fluorescence microscope and equipped with an F-view-II cooled CCD camera (Soft imaging Systems).

A Xenon-Arc burner (Olympus Biosystems GMBH) was used as light source. Images were acquired with a 492 nm and 572 nm excitation filter. Emission collected with a UBG triple band pass emission filter cube. Image acquisition and analysis was done with a 10 x magnification objective (Olympus Plan Apo N) and the Cell'R imaging software.[16]Images were divided into four representative regions of interest and an average grey value was determined for each region.

3.4.3 Scanning electron microscopy

Scanning electron microscopy (SEM) was performed with a Leo® 1430VP scanning electron microscope. Each sample was placed on a SEM stage with double-sided carbon tape and coated with a thin gold layer, before imaging. The analysis was done at high vacuum (6 – 10 Pa) and the energy of the electron beam set to between 4 and 7 keV. Images were acquired at 50 x, 250 x and 500 x magnification.

3.4.4 Field emission scanning electron microscopy

Field emission scanning electron microscopy (FE SEM) was performed on 20-40 µm thick slices cut with a microtome. The FE SEM unit used is a FEI Nova nano FEG SEM 230. The samples were mounted on aluminum stubs, carbon coated and images were acquired with a vCD detector while the microscope was operated in beam deceleration mode with an energy of 2 KeV, a spot size of 2.5 and magnifications at 1000 x, 5000 x and 10 000 x.

3.4.5 Hardness testing

An UHL VMHT micro hardness tester was used to analyze the hardness of the samples at 50 gram force (0.5 N), a dwell time of 15 seconds and indentation speed of 25 µm/second and 15 measurements per sample, to obtain an average hardness value and standard deviation value.[17-23]

3.4.6 Tensile testing

A LRX (LLOYD instruments) tensile tester was used for tensile tests of the composite samples. A preload of 30 N was applied and a standard test speed of 50.0 mm/min was used. Four samples were analyzed for each composite to obtain average values. The sample dimensions were: gauge length 37.58 mm, width 4.98 mm, thickness 1.45 mm.

3.4.7 High speed tensile impact testing

A CEAST Torino high speed tensile impact tester was used to study the impact strength of the composite samples. Tensile molded composite samples were subjected to a 15 Joule hammer weight and (type 0.96) front weight at a 90° angle.

3.4.8 Differential scanning calorimetry

Differential scanning calorimetry (DSC) was performed on a DSC Q100 (TA instruments) with standard aluminum pans, under a nitrogen atmosphere (purge gas flow of 2ml/ min, analysis gas flow of 50 ml/ min) at an equilibrating temperature of 25 °C. Samples were heated at 10°C/ min to 220 °C, held isothermally for 10 minutes, cooled to -40 °C at the same rate, left to equilibrate at -40 °C and then heated to 200 °C at 10 °C/min, to record the crystallization and melting behavior.

In order to monitor isothermal crystallization, the following method was used: samples were first equilibrated at -40 °C and then heated to a rate of 10 °C/ min to 200 °C, after which they were cooled down to 110 °C at a rate of -20 °C/ min and kept isothermal for 20 min. From there they were further cooled down to -40 °C at a rate of 10 °C/min and equilibrated at -40 °C.[24-26]

3.4.9 Atomic force microscopy (AFM)

An Easy Scan 2 AFM from Nanosurf (Switzerland) was used for AFM analysis in the spectroscopy mode. A contact cantilever from Nanosensors, with a spring constant of 0.2 N/ m was used and the tips were chemically modified. Adhesive force-distance curves were obtained, and were used to determine adhesive forces between chemically modified tips (thiol and compatibilizer functionalities) and polymer, lignin and α-cellulose surfaces.[27]

3.4.10 Thermogravimetric analysis (TGA)

Samples were heated at a temperature ramp of 20 °C/ min, from 27 °C up to 840 °C, on a Perkin Elmer thermogravimetric analyzer (TGA 7).

3.4.11 ^{13}C Nuclear magnetic resonance spectroscopy (NMR)

Carbon -13 NMR spectra were recorded with a Varian Inova spectrometer, 600 MHz, at 126.5 °C. Solutions of PPgMA-EvOH joint compatibilizer sample were prepared by dissolving 50 mg of sample in dimethyl sulfoxide-d_6. The spectral width was 41500, the number of scans 5312 and a relaxation delay time of 15 seconds between pulses was used. This should lead to quantitative spectra, provided analyses of only those carbons with relaxation delays of less than 3 seconds are used.

3.5 References

1. A. Sakakura, K. Kawajiri, T. Ohkubo, Y. Kosugi, K. Ishihara, Widely useful dmap – catalyzed esterification under auxiliary base- and solvent-free conditions, Journal of American Chemical Society, 129, p 14775 (2007).
2. G. D. Yadav, M. B. Thathagar, Esterification of maleic acid with ethanol over cation-exhange resin catalysts, Reactive and Functional Polymers, 52, p 99 (2002).
3. B. Neises, W. Steglich, Simple method for the Esterification of Carboxylic Acids, AngewandteChemie International Edition English, 17, p 522 (1978).
4. Y. Zhang, Y. Xue, H. Toghiani, J. Zhang, C. U. Pittman Jr., Modification of wood flour surfaces by esterification with acid chlorides: use in HDPE/ wood flour composites, Composite Interfaces, 16, 671 (2009).
5. F. M. B. Coutinho, T. H. S. Costa, Performance of propylene-wood fiber composites, Polymer testing, 18, p 581 (1999).
6. V. Hristov, Melt flow instabilities of wood polymer composites, Composite Interfaces, 16, p 731 (2009).
7. A. K. Bledzki, O.Faruk, Injection moulded microcellular wood fiber-polypropylene composites, Composites: Part A, 37, p 1358 (2006).
8. A. K. Bledzki, O. Faruk, Wood fiber reinforced polypropylene composites: Compression and injection molding process, Polymer Plastics Technology and Engineering, 43 (3), p 871 (2004).
9. G. G. Baralia, A.-S. Duwez, B. Nysten, A. M. Jonas, Kinetics of exchange of alkanethiol monolayers self-assembled on polycrystalline gold, Langmuir, 21, p 6825 (2005).
10. A. Klash, Localisation and quantification of chemical functional groups on pulp fibers, PhD thesis, University of Stellenbosch, South Africa, 2010.
11. A. J. Rabie, Blends with low density polyethylene (LDPE) and plastomers, MSc thesis, University of Stellenbosch, South Africa, 2004.
12. G. W. Harding, A. J. van Reenen, Fractionation and Characterisation of Propylene-Ethylene Copolymers: Effect of the Comonomer on Crystallization of Poly(propylene) in the γ-phase, Macromolecular Chemistry and Physics, 207, p 1680 (2006).

13. P. J. Deslauriers, D. C. Rohlfing, E. T. Hsieh, Quantifying short chain branching microstructures in ethylene 1-olefin copolymers using size exclusion chromatography and fourier transform infra red spectroscopy (SEC-FTIR), Polymer, 43, p 159 (2002).

14. S. de Goede, R. Brull, H. Pasch, N. Marshall, Monitoring thermo-oxidative degradation by CRYSTAF and SEC-FTIR, Macromolecular Symposia, 193, p 35 (2003).

15. Fractionation and analysis of an impact poly(propylene) copolymer by TREF and SEC-FTIR, Macromolecular Materials and Engineering, 295, p 366 (2010).

16. B. Loos, S. Genade, B. Ellis, A. Lochner, A. M. Engelbrecht, At the core of survival: Autophagy delays the onset of both apoptotic and necrotic cell death in a model of ischemic cell injury, Experimental Cell Research,317 (10), p 1437 (2011).

17. G. H. Michler, F. J. Balta-Calleja, I. Puente, M. E. Cagiao, K. Knoll, S. Henning, R. Adhikari, Microhardness of styrene/ butadiene block copolymer systems: Influence of molecular architecture, Journal of Applied Polymer Science, 90, p 1670 (2003).

18. F. J. Balta-Calleja, Dependence of micro-indentation hardness on the superstructure of polyethylene, Colloid & Polymer Science, 254, p 258 (1976).

19. G. H. Michler, F. J. Balta-Calleja, R. Adhikari, K. Knoll, Microindentation hardness of SB-block copolymers relating to nano mechanical mechanisms, Journal of Materials Science, 38, p 4713 (2003).

20. F. J. Balta-Calleja, M. E. Cagiao, R. Adhikari, G. H. Michler, Relating microhardness to morphology in styrene/ butadiene block copolymer/ polystyrene blends, Polymer, 45, p 247 (2004).

21. M. Krumova, J. Karger-Kocsis, J. Balta-Calleja, S. Fakirov, Strain-induced β-α polymorphic transition in iPP as revealed by microhardness, Journal of Materials Science, 34, p 2375 (1999).

22. S. Osawa, R. S. Porter, Anistropy in mechanical properties of forged isotactic polypropylene, Polymer, 37 (11), p 2095 (1996).

23. F. J. BaltaCalleja, L. Giri, G. H. Michler, I. Naumann, Kinetics of chlorosulfonating and OsO_4 attack in the interlamaller regions of low and high density polyethylene studied by microhardness, Polymer, 38 (23), p 5769 (1997).

24. J. Li, C. Zhou, G. Wang, Y. Tao, Q. Liu, Y. Li, Isothermal and nonisothermal crystallization kinetics of elastomeric polypropylene, Polymer Testing, 21, p 583 (2002).

25. A. Gradys, P. Sajkiewicz, A. A. Minakov, S. Adamovsky, C. Schick, T. Hashimoto, K. Saijo, Crystallization of polypropylene at various cooling rates, Materials Science and Engineering, A 413-414, p 442 (2005).

26. B. Wielage, T. Lampke, G. Marx, K. Nestler, D. Starke, Thermogravimetric and differential scanning calorimetric analysis of natural fibers and polypropylene, ThermochimicaActa, 337, p 169 (1999).

27. G. S. Oporto, D. J. Gardner, D. J. Neivandt, Adhesion properties of wood-plastic composite surfaces: Atomic force microscopy as a complimentary analysis tool, Contact Angle, Wettability and Adhesion, 6, p 341 (2009).

CHAPTER 4 DETERMINATION OF PHYSICAL PROPERTIES

In the initial phase of the work, a baseline was established in terms of preparation and evaluation of the physical properties of composites prepared with and without added compatibilizers. The effect of combining compatibilizers was also evaluated in an initial study. This chapter is organized in the evaluation of the types of composite prepared, and the evaluation of hardness, tensile impact properties and tensile properties of each of the types of composite. Where applicable, comparisons were made, and some initial conclusions drawn.

4.1 Wood-polymer composites with no compatibilizer

4.1.1 Hardness testing

The hardness to impact balance of a polymer material is an important factor to consider in physical property determinations. The complex morphology of impact polypropylene, specifically with regards to rubber content and distribution in the isotactic polypropylene matrix of this polymer, is important. Since the hardness of the polymer can be greatly influenced by the rubber content of the material, the interactions of the rubber material and the isotactic polypropylene fractions with the wood particles in wood polymer composites needs to be studied. The changes in the hardness to impact balance, with regards to interaction of this specific polymer with the wood particles, upon compatibilization, must be considered. While it is true that the hardness of a wood-polymer composite is largely due to the hardness of the wood species, it is also true that improper distribution of the wood particles could lead to aggregation and areas of the surface of the composite that is devoid of wood; thus leading to an apparently much softer material. Thus the average deviation in the hardness values of the wood-polymer composite could be indicative of the effective distribution of the wood particles within the composite.

In Figure 4.1, the hardness values for the composites made with CMR 648 and CMR 448 are shown.

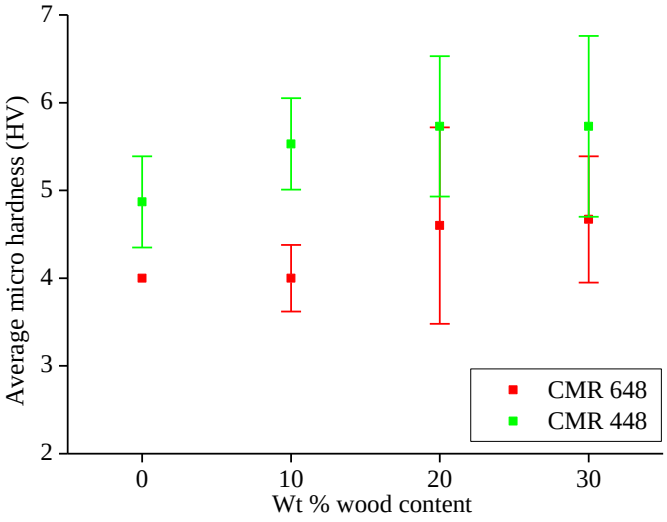

Figure 4.1: Hardness of the composites of CMR 448 and CMR 648 without compatibilizer.

From Figure 4.1 it is evident that the hardness for both impact copolymers increases when wood is present, as could be expected. What is also clear is that the standard deviation for the hardness values increases quite significantly as the wood content is increased. This is in conjunction with a general increase in the average hardness value as the wood content increases, at least up to a wood loading of 20 wt %. The large standard deviation in the average hardness values indicates that there is generally poor distribution of the wood particles in these composites, possibly due to the absence of compatibilizer.

The hardness values should be evaluated with the impact resistance values for the same composites.

4.1.2 High speed tensile impact testing

The high speed tensile impact results for the non-compatibilized composites are shown in Figure 4.2.

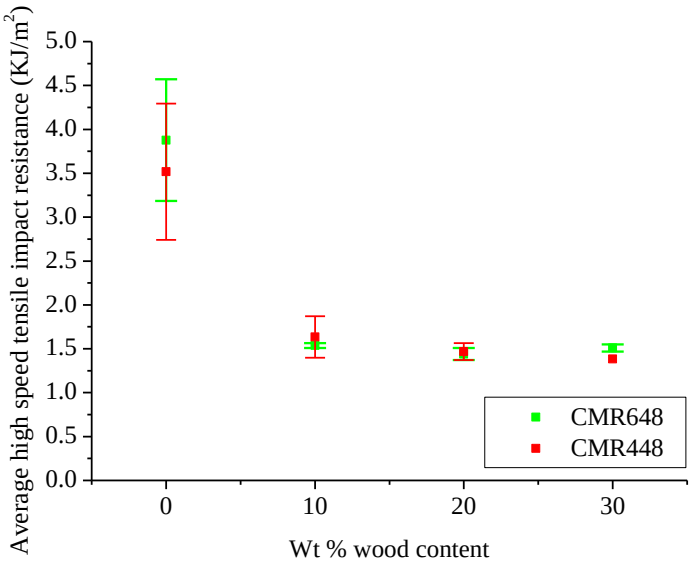

Figure 4.2: High speed tensile impact resistance of the composites of CMR 448 and CMR 648 without compatibilizer.

Figure 4.2 shows that the impact resistance is significantly reduced when wood is added to the virgin polymer. This was to be expected, as the presence of the wood particles could disrupt the distribution of rubber domains in the polymer matrix. This disruption will be more severe in the case where little or no interaction between the polymer and the wood particles is present. This will cause poor distribution of the wood particles, and the resultant large decrease in impact resistance. In fact, SEM micrographs show clear separation between the wood particles and the polymer. This will be discussed at a later stage (see Section 5.1.1 Chapter 5). The impact resistance remained constant after 10 wt % wood content.

It is interesting to note though, that the standard deviation is large for the virgin polymer. Here the effect of the complex nature of the virgin polymer plays a significant role in the impact properties,[1] the effect disappears when the polymer is mechanically mixed with wood. The small standard deviation after the addition of wood suggests that the fracture of these composites, specifically at the wood polymer interface is immediate and little interaction is present. This is thought to be the primary reason for the poor impact resistance of the composites.

If we now take the results shown in Figures 4.1 and 4.2 together, we get an indication of the hardness/ impact balance of the composites with no compatibilizer. A relatively small increase in hardness (about 10 – 15 %, albeit with a large standard deviation) is offset by a sharp decrease in the impact resistance. The differences in hardness for the two types of composites is related to the difference in

chemical composition (ethylene content), yet the impact resistance of the two polymers (under these test conditions) are essentially similar, without and with added wood.

4.1.3 Tensile testing

The strength of materials is an important factor to consider in any discussion, and in this section the focus will be on the tensile properties of the polymer composites. Figure 4.3 gives the average maximum stress and Figure 4.4 the average maximum strain attained by the CMR 648 and CMR 448 composites under tensile test conditions.

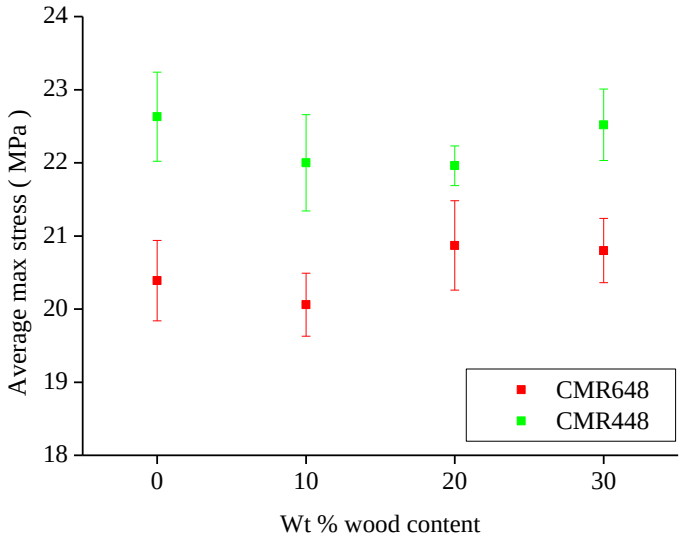

Figure 4.3: Average maximum stress of the composites of CMR 448 and CMR 648 without compatibilizer.

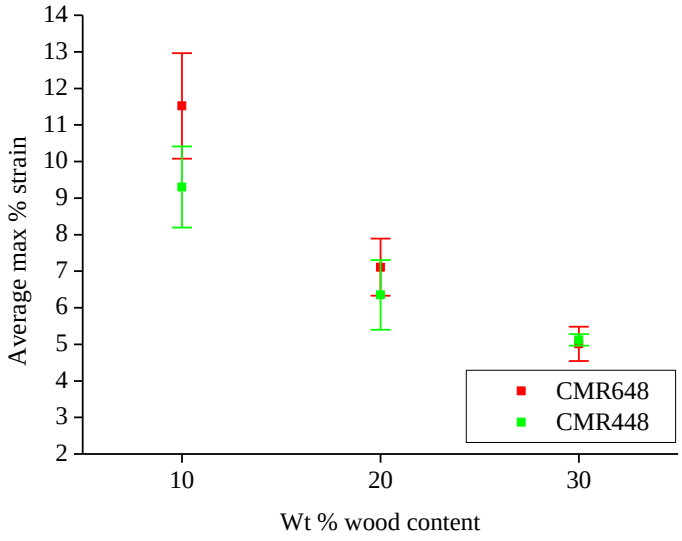

Figure 4.4: Average maximum strain of the composites of CMR 448 and CMR 648 without compatibilizer.

From the results presented in Figures 4.3 and 4.4 it is clear that the average tensile stress of the composites is largely unchanged for the wood-polymer composites (compared to the virgin polymer). The CMR 448 samples vary between 22 and 23 MPa, with the CMR 648 slightly weaker at 20 – 21 MPa. The wood therefore seems to have no effect. The tensile strength of the polymer would result from the isotactic polypropylene matrix, and thus the results indicate that there is little or no interaction between the wood particles and the crystalline portions of the polymer.

The maximum attainable strain, however, decreases considerably as the wood content is increased. The virgin polymer has a maximum strain of over 100 % (not shown here). At a wood content of just 10 wt %, a decrease around 80-90 % in the maximum attainable strain is observed. This indicates that, whilst the interaction of the wood particles with the polymer is not sufficient to increase or affect the tensile strength, they do interfere with the deformation of the polymers under stress. The wood particles are rigid and unable to deform, so some form of interaction with parts of the polymer matrix must be present. The question would be if the wood does interact with the rubbery domains, and if so, will this affect the strain behaviour? Or is it merely a case of yield and flow of the crystalline domains being hampered by the presence of the wood particles?

Good compatibility between polymer and wood is expected to be necessary to improve the tensile strength, which means a suitable compatibilizer to bridge the interface between polymer and wood. Evidence of a good interaction between polymer and wood would be the transfer of strength from the wood particles to the polymer matrix to prevent fibre pull out and rather promoting fibre fracture. Some of these results will be discussed later (see Section 5.1 Chapter 5).

4. 2 Wood-polymer composites with compatibilizer

In order to evaluate the effect of the compatibilizers, we initially prepared composites with (a) PPgMA as compatibilizer and (b) EvOH as compatibilizer. Results are given below, and are discussed as in Section 4.1, under the headings of methods of physical testing.

4.2.1 Hardness testing

The results of the evaluation of hardness for the composites containing PPgMA as compatibilizer are shown in Figure 4.5, while the results for the composites with EvOH as compatibilizer are shown in Figure 4.6. Based on the results we obtained (Section 4.1) we decided to standardize the wood loading at 10 wt % for comparative purposes.

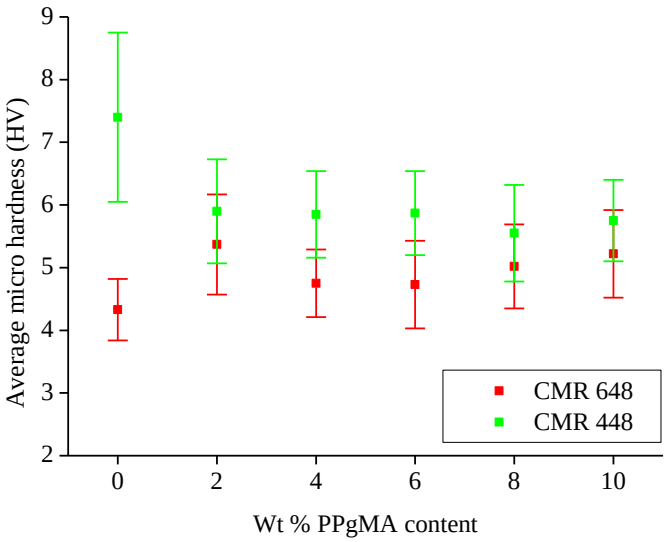

Figure 4.5: Hardness of the composites of CMR 448 and 648 with PPgMA as compatibilizer, (10 wt % wood).

From Figure 4.5 we see that, for the composites with no compatibilizer (10 wt % wood) there appears to be a large standard deviation (particularly for the CMR 448 composites) in the hardness values. With the addition of the compatibilizer, the hardness values are much more constant, and the standard deviation decreases significantly. Of interest here is also the fact that the average hardness values for the CMR 648 composites are higher (at 10 wt % wood) than for the non-compatibilized composites (Figure 4.1). As the amount of PPgMA in the composite is increased, very little change in the average hardness was observed. Once again, when we view these results in conjunction with the tensile impact results, we could make a selection as to the optimum amount of compatibilizer that we would use (about 6 wt %, see Section 4.2.2).

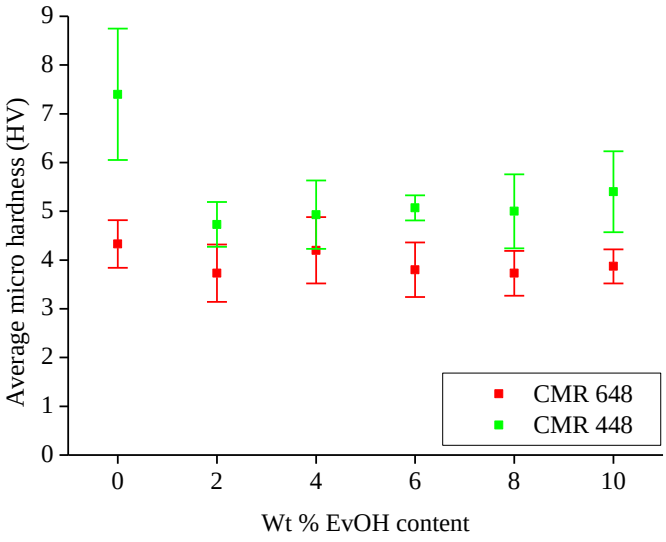

Figure 4.6: Hardness of the composites of CMR 448 and CMR 648, with EvOH as compatibilizer, (10 wt % wood).

Once again we see more reproducible hardness results when the compatibilizer has been added. In this case, the addition of the EvOH appears to have less of an effect on the hardness of the CMR 648 composites than the addition of PPgMA, but the decrease in hardness of the CMR 448 composites was more pronounced by the addition of EvOH than in the case of the PPgMA.

The results obtained with the addition of the two compatibilizers to the composites prepared with 10 wt % wood and either CMR 648 or CMR 448 as polymer indicates several important aspects. In the first place, the addition of compatibilizer assists in the more even distribution of wood particles, as is evidenced in the reproducibility of the hardness results. Second, the effect of the two compatibilizers is different, both when comparing polymeric matrices (for example EvOH in CMR 648 vs. CMR 448), or when comparing compatibilizers within a specific matrix (for example PPgMA and EvOH in CMR 648). The latter clearly indicates that the interaction of the compatibilizer with the impact copolymer is dependent on the chemical composition distribution of the impact copolymer and the chemical composition of the compatibilizer. In addition to that, the interaction between the compatibilizer and the wood will differ depending on the type of compatibilizer, and presumable, this will lead to different levels of interaction with the wood particles and the various components of the impact copolymers.

4.2.2 High speed tensile impact testing

Figures 4.7 and 4.8 show the tensile impact results for composites of CMR 648 and CMR 448 (10 wt % wood) prepared with PPgMA and EvOH as compatibilizer.

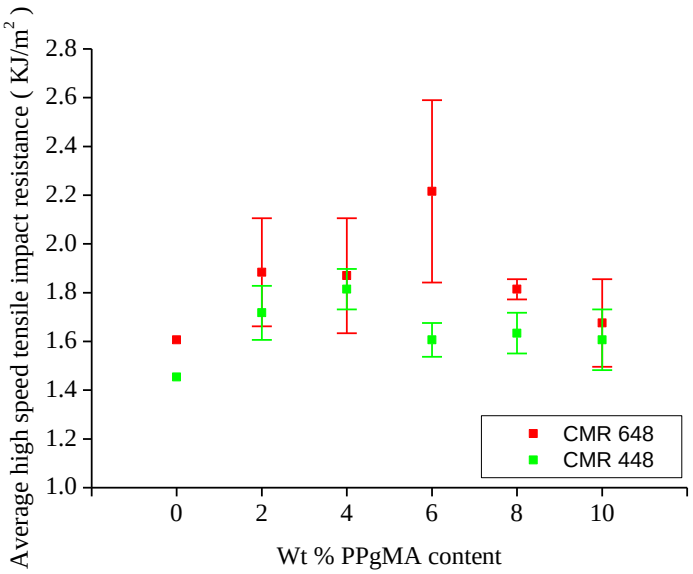

Figure 4.7: High speed tensile impact resistance of the composites of CMR 448 and CMR 648, with PPgMA as compatibilizer, (10 wt % wood).

It is clear that the impact resistance for the composites containing PPgMA (Figure 4.7) increase compared to WPCs with no compatibilizer (see Figure 4.3). The maximum impact resistance is obtained around 6 wt % compatibilizer for the CMR 648 composites, and at around 4 wt % for the CMR 448 composites. The CMR 648 polymer composite shows a large standard deviation for the 6 wt % compatibilizer, although the average values are not statistically significantly different. The CMR 448 polymer composite shows lower standard deviations, which could be due to the differences in the molecular structure of the polymer matrix (compared to CMR 648) and the effect this has on the impact resistance of the composite. What is of importance here is that the impact resistance increases, which is a clear indication of better distribution of the wood particles as well as good interaction between the particles and the polymer matrix. Thus the hardness-impact balance is better than for the non-compatibilized composites; not only is the hardness of the CMR 648 composites increased, but the impact resistance decrease upon the addition of wood is not as pronounced as in the case of the non-compatibilized composites. In the case of the CMR 448 composites the same applies with respect to the impact resistance, although the hardness values decreased slightly upon addition of the PPgMA.

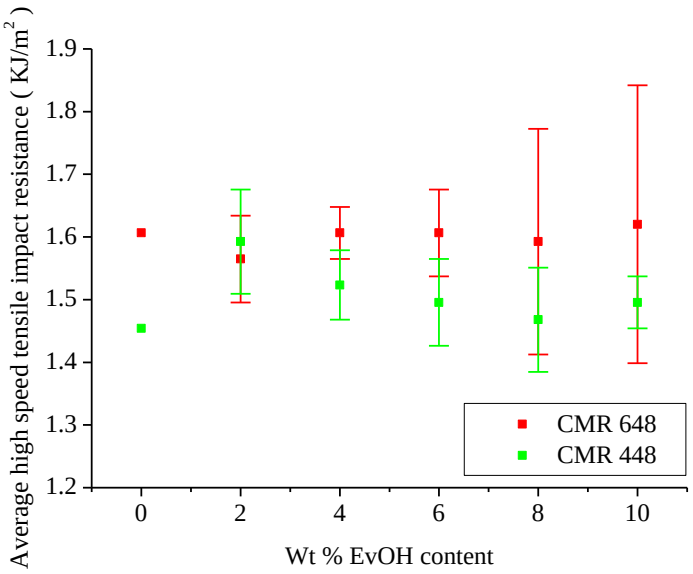

Figure 4.8: High speed tensile impact resistance of the composites of CMR 448 and CMR 648, with EvOH as compatibilizer, (10 wt % wood).

The results presented in Figure 4.8 indicates that EvOH has no effect on the impact resistance of the WPCs in the case of the CMR 648 copolymer, and decreases it for the CMR 448 composite although the impact resistance is slightly better for the composite containing 2 wt % EvOH compared to the composite with no EvOH. Generally the impact resistance of CMR 448 composites are lower than that of CMR 648, which is to be expected, as the latter copolymer has a higher rubbery content.[1] At increasing EvOH contents, specifically at 8 and 10 wt %, the standard deviation for the CMR 648 polymer composite becomes extremely high compared to the CMR 448 polymer composite, suggesting that the differences in the polymer matrices effects the standard deviation to a significant degree when using EvOH as compatibilizer. At large EvOH contents, a good dispersion of the compatibilizer in the polymer matrix might no longer be possible, which could lead to phase segregation, or the EvOH might be interfering with the rubber/ copolymer interface.

4.2.3 Tensile testing

The maximum stress and strain values for CMR 648 and CMR 448 composites with PPgMA and EvOH as compatibilizer are represented in Figures 4.9 and 4.10, while the Young's modulus values are given in Figure 4.11.

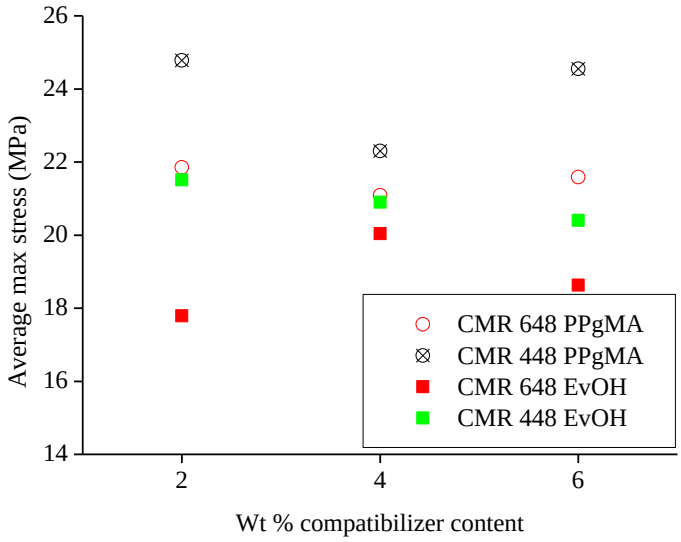

Figure 4.9: Average maximum stress of the composites of CMR 448 and CMR 648, with compatibilizer, (10 wt % wood).

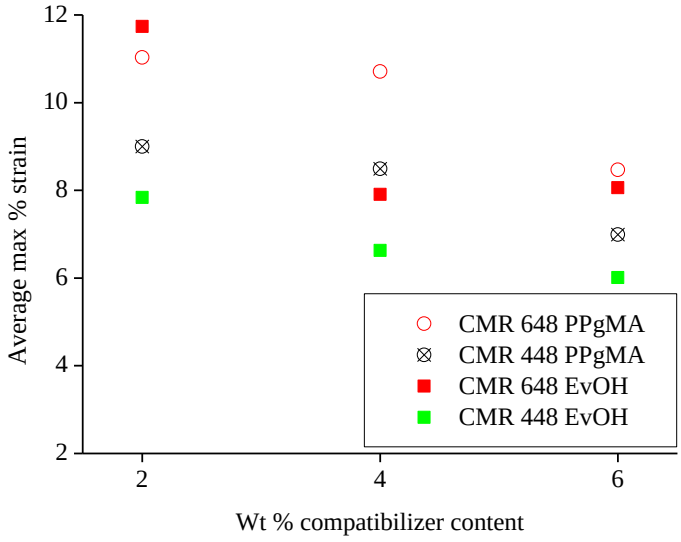

Figure 4.10: Average maximum % strain of the composites of CMR 448 and CMR 648, with compatibilizer (10 wt % wood).

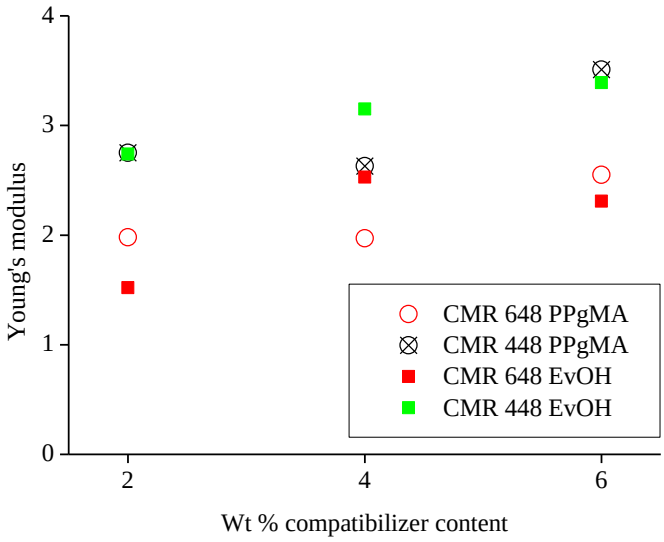

Figure 4.11: Young's modulus of the composites of CMR 448 and CMR 648, with compatibilizer (10 wt % wood).

The results presented in Figure 4.9 shows that (a) the average tensile stress for the composites containing PPgMA is higher than for the composites containing EvOH, when comparing the same polymer matrix, and (b) that the presence of EvOH as compatibilizer results in maximum attainable stresses lower than in the case of the non-compatibilized composites (Figure 4.4). This is in contrast to the PPgMA compatibilized composites which result in increased maximum stress values. As the maximum stress values should be due to the deformation of the more crystalline (iPP) part of the copolymer, the results seem to indicate that the PPgMA affords interaction between the wood particles and the crystalline PP matrix, resulting is a stronger material.

The EvOH compatibilizers lower the stress attainable, indicating that whilst the EvOH interacts with the wood particles, allowing for a more even dispersion of the filler, the interaction of the EvOH with the impact copolymer matrix results in a decreased ability to resist deformation. This probably indicates that the EvOH facilitates interaction between the wood and the ethylene-rich areas of the copolymer (rubbery EPR and ethylene-rich copolymers) and does little to facilitate stress transfer to the more crystalline areas of the copolymers.

The maximum % strain (Figure 4.10) decreases in all cases as the compatibilizer content increases, suggesting that an increase in compatibilizer, whether PPgMA or EvOH, resists deformation in the composite. This indicates a better interaction between the wood fibre and the matrix compared to the wood-polymer composites in the absence of compatibilizer. What is interesting here is that the addition of a small amount (2 wt %) of compatibilizer does little to affect the strain values (see also Figure 4.4), but that increasing the amount does affect the strain behaviour. The fact that the effect of EvOH on the strain decrease is not as marked (in comparison to PPgMA), as in the case of the

maximum stress values, does indicate that the EvOH interacts with a different part of the polymer than the PPgMA.

The Young's modulus (Figure 4.11) confirms that the stiffness of the material increases with increasing compatibilizer content.

The difference in Young's modulus between the composites indicates that EvOH plays a stronger role in the CMR 648 polymer composite than in the case of the CMR 448 composites. This must be related to the difference in interaction of EvOH with the different polymer matrices (see Section 5.3, Chapter 5). The Young's modulus also remains relatively unchanged between a PPgMA content of 2 - 4 wt %, which indicates that an increase in PPgMA does not have such an adverse effect on the polymer matrix as EvOH, and suggests that the different polymer matrices do not play such a large role when PPgMA is used. This further indicates that the interaction of the PPgMA is primarily with the isotactic PP fraction of the copolymer, while the EvOH interacts more with the rubbery and copolymer fractions of the copolymers.

The morphology, specifically the dispersion of the compatibilizer in the matrix is discussed in Section 5.2 (Chapter 5) for the CMR 648 polymer matrix only.

4.3 Combining compatibilizers

The initial results (Sections 4.1 and 4.2) clearly show that the use of compatibilizers improve the dispersion of the wood particles and the interaction of the wood particles with the polymer matrix. The initial results also show that the two compatibilizers (PPgMA and EvOH) interact with different parts of the polymeric matrix. It was therefore decided to use the compatibilizers jointly, and to evaluate the results that were obtained.

In the first series of experiments, we tried combinations of the two compatibilizers, simply mixing the two compatibilizers and then preparing the composites as described in Chapter 3. The total compatibilizer concentration was set at 10 wt % for the initial experiments. This was higher than the so called "optimum" value of 6 wt % that was used for comparative studies that were described in the first part of this chapter.

4.3.1 Hardness testing

Figure 4.12 shows the results of the hardness tests for the composites of CMR 648 and CMR 448 prepared with a mixture of two compatibilizers. The ratios are expressed as the proportions used to make up 10 wt % total compatibilizer content. Therefore, for example, 5/5 represents 5 wt % EvOH and 5 wt % PPgMA, whilst 8/2 represents 8 wt % PPgMA and 2 wt % EvOH. Note that the ratios 4/6, 3/7 and 2/8 were not evaluated.

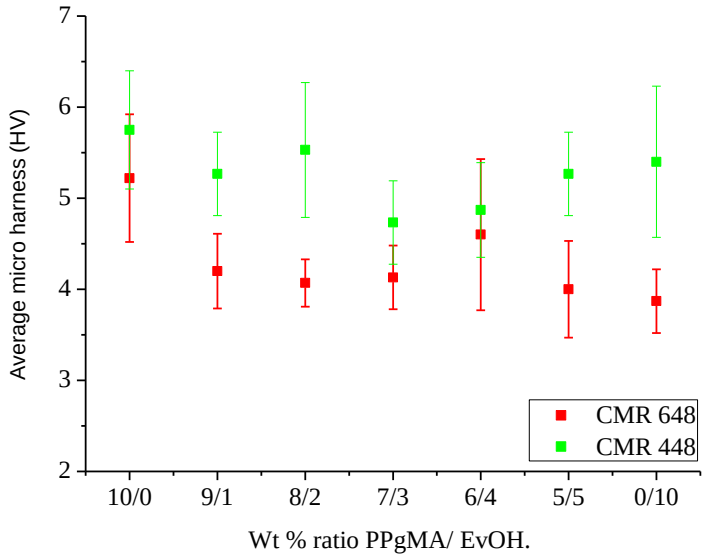

Figure 4.12: Hardness of the composites of CMR 448 and CMR 648, using a combination of PPgMA and EvOH as compatibilizer, (10 wt % wood).

The first stage of the "joint compatibilizer" system involved combining different amounts of PPgMA and EvOH, to the wood-polymer composites. In this case there was no attempt to pre-react these compatibilizers. The hardness values show large standard deviations and no consistent trend or order for either of the polymer composites, regardless of the compatibilizer ratios. We concluded that some partially uncontrolled reactions between the functional groups present in the two compatibilizers could have occurred to cause this result, and we were forced to reassess our strategy for using the compatibilizers in a combination system.

As a first attempt we simply pre-treated the 2 compatibilizers by heating them together (see Chapter 3) before adding them to the wood-polymer composite. In the second approach, we used DMAP as catalyst during the pre-reaction process. This reaction product we named a joint compatibilizer. We expected the second approach (DMAP catalysed reaction) to result in a more controlled reaction between PPgMA and EvOH. DMAP as catalyst was preferred, as acid catalysts could not be used, as these resulted in dehydration of the EvOH.

All the composites prepared with the "joint compatibilizers" contained a total compatibilizer content of 6 wt %. Thus a PPgMA/ EvOH ration of 3/3 denotes a joint compatibilizer constructed by pre-reacting 3 wt % (based on total polymer mass) of PPgMA and 3 wt % EvOH. Figure 4.13 show the hardness values obtained with CMR 648 and CMR 448 composites (10 wt % wood) with PPgMA pre-reacted by just heating. This method of pre-treatment is denoted by the letter H in the legend of the figures. Figure 4.14 compares the hardness values for the CMR 648 composites prepared with a joint

compatibilizer either just pre-reacted by heat (H) or by heating in the presence of DMAP. This method of pre-treatment is denoted with the letter D.

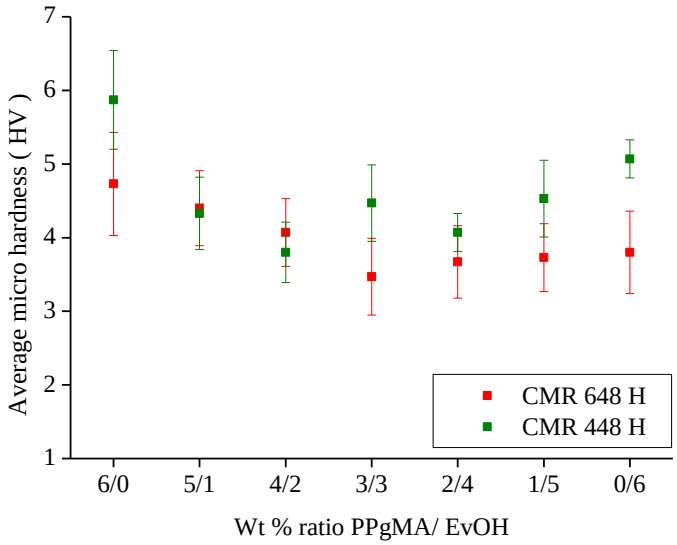

Figure 4.13: Hardness of the composites of CMR 448 and CMR 648, prepared with joint compatibilizers (pre-reacted by heating (H)), (10 wt % wood).

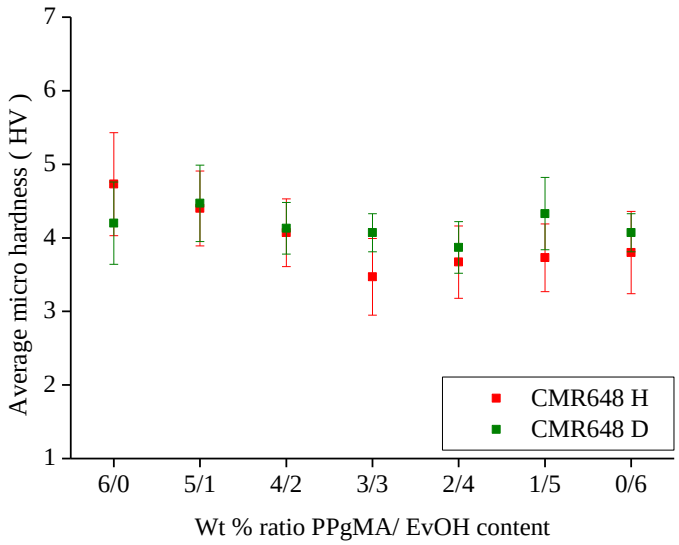

Figure 4.14: Hardness of the composites of CMR 648, prepared with joint compatibilizers either pre-reacted by heating (H) or by heating in presence of a catalyst (D), (10 wt % wood).

The results presented in Figure 4.13 shows, for the CMR 648 composite, a decrease in the hardness values as the EvOH content increase, followed by a levelling off of the hardness. For the CMR 448 composite, we see roughly the same trend, and with higher EvOH content (1/5 and 0/6) we observe an increase in hardness. This is roughly what we observed with the unreacted compatibilizers as well

(Figure 4.12), but the standard deviation is much smaller than in the case of the heat-treated (pre-reacted) joint compatibilizers.

If we monitor the effect of DMAP catalysis on the esterification process, (only studied for the CMR 648 composite), we can see that the initial decrease in hardness in the absence of the DMAP disappears. In fact, the hardness values remain fairly constant across the whole range of joint compatibilizers evaluated. This is a clear indication that a uniform dispersion of the wood particles is achieved. On the face of this evidence, then, it appears that pre-reacting the compatibilizers by heating in the presence of a suitable catalyst leads to a product that can be used to study the effect of compatibilization by different chemical moieties in a complex matrix.

4.3.2 Strain hardening effects

As we subjected the composites prepared with the joint compatibilizers to tensile test measurements, we decided to see the effect of strain hardening on the composites (after breakage).

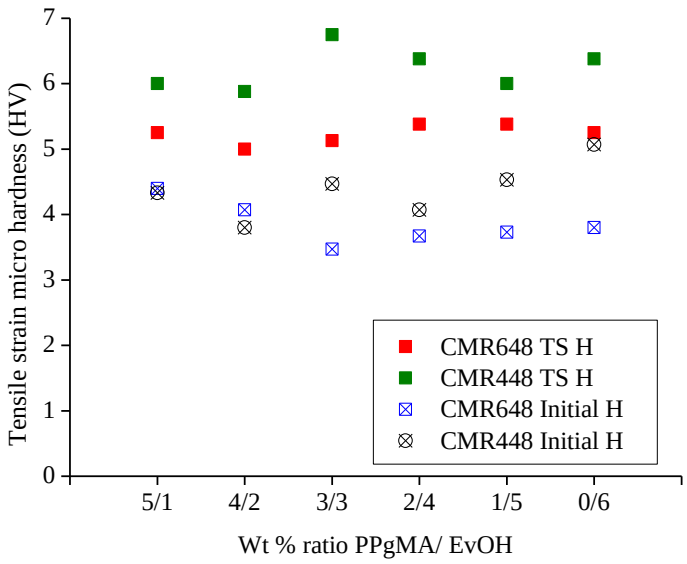

Figure 4.15: Hardness (H) measured after tensile strain (TS) for the CMR 648 and CMR 448 composites, DMAP treated, (10 wt % wood).

In Figure 4.15, the hardness values for WPC samples subjected to tensile testing (a severely destructive technique) are presented. It is clearly visible in all cases that strain hardening occurs. This indicates that drawing and recrystallization occurs, as well as the alignment of the wood particles. Not that error bars are not included, as this affects the clarity of the data in the figure. All of the relevant data can be found in the Appendix. The greatest increase in hardness after tensile strain appears for a 3/3 wt % ratio of PPgMA and EvOH, particularly for the CMR 448 composite. On the other hand, the range of strain hardening remains relatively constant for the CMR 648 composite when the EvOH

content increases (3/3, 4/2, 1/5 and 0/6). These hardness measurements serve to show that the interaction between the wood and polymer is uniform, and that the hardness values are only dependent on the dominant species on the surface of the samples, be it polymer or wood particles. The joint compatibilizer, created by DMAP catalysed esterification reactions, function well and creates a composite where there appears to be good interaction between the polymer and wood. Even under stress, the distribution of the wood in the polymer matrix appears to be consistent.

4.3.3 High speed tensile impact testing

In Figure 4.16, the results of the high speed tensile impact resistance tests for the CMR 648 and CMR 448 composites with joint compatibilizer (6 wt %, heat-treated (H)) are presented, while the CMR 648 composites are compared with those treated with DMAP catalysed joint compatibilizer (D) in Figure 4.17.

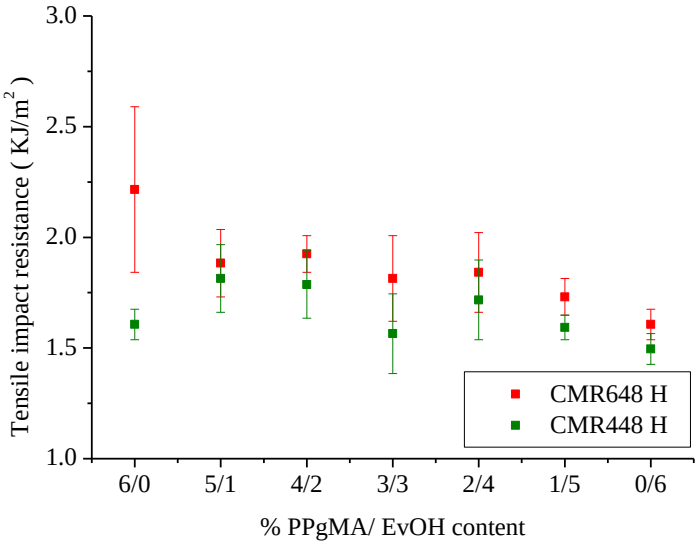

Figure 4.16: High speed tensile impact resistance of the composites of CMR 448 and CMR 648. The compatibilizer content was kept at 6 wt %, the wood content at 10 wt %. The pre-reaction between the compatibilizers were heat (H) assisted.

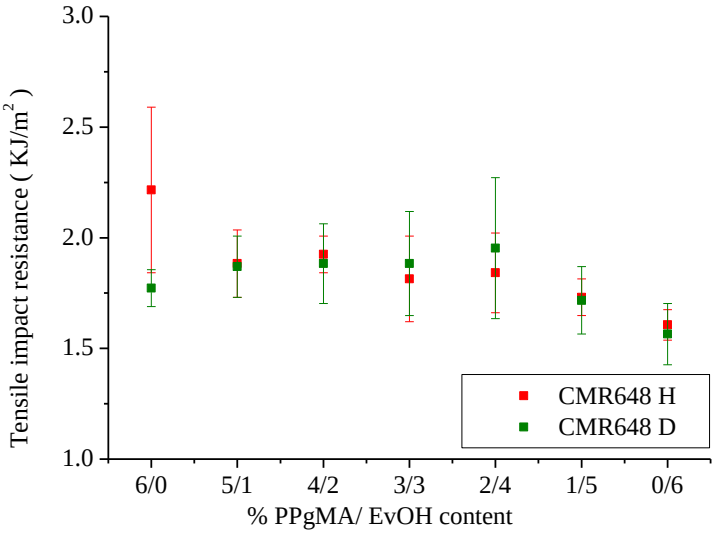

Figure 4.17: High speed tensile impact resistance of the composites CMR 648. The compatibilizer content was kept at 6 wt %, the wood content at 10 wt %. The pre-reaction between the compatibilizers were heat (H) and DMAP (D) assisted.

The results shown in Figures 4.16 indicate that the effect of EvOH addition results in a decrease in the impact resistance of the CMR 648 composite, and has little effect on the CMR 448 composites. Figure 4.17 shows that the use of EvOH in the joint compatibilizer pre-treated by heating in the presence of DMAP initially has little effect on the impact properties, but at high EvOH content (1/5 and 0/6) the impact resistance decreases. The standard deviation of the DMAP treated joint compatibilizer-treated CMR 648 composites is about 20 – 30 % lower than for the heat-treated system. This is significant, as it allows for better control over the composite properties.[2] What is also really interesting is that the impact resistance values of the CMR 648 (D) series of composites are about the same as the values for the PPgMA-compatibilized CMR 648 composites (Figure 4.7, 1.6 – 1.8 kJ/ m^2), except for the high EvOH content (1/5 and 0/6) which are, unsurprisingly, the same as for the EvOH compatibilized CMR 648 composites (Figure 4.8).

4.3.4 Tensile testing

The tensile test results for the (H) series of composites, CMR 648 and CMR 448, prepared by the joint compatibilizers are shown in Figure 4.18 (maximum stress (H)), Figure 4.19 (maximum strain, (H)) and Figure 4.20 (Young's modulus (H)). Similarly Figures 4.21 – 4.23 represent a comparison of the (H) and (D) series of CMR 648 composites.

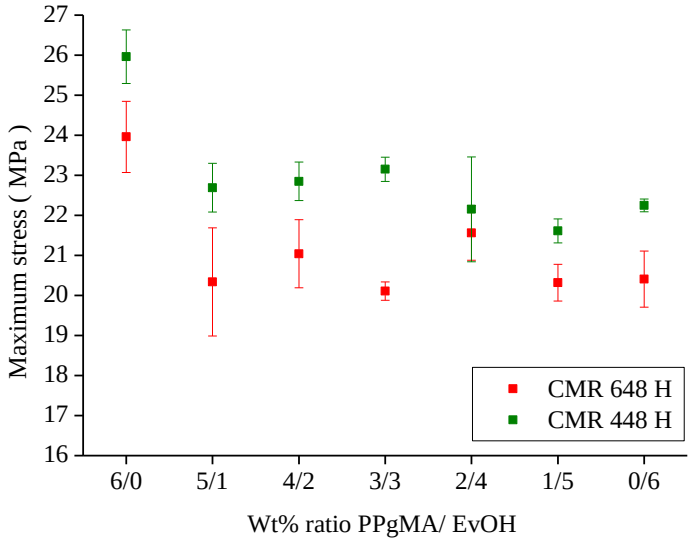

Figure 4.18: Average maximum stress of the CMR 648 and CMR 448 composites with 10 wt % wood and 6 wt % compatibilizer. The pre-reaction between the compatibilizers were (H) heat-assisted.

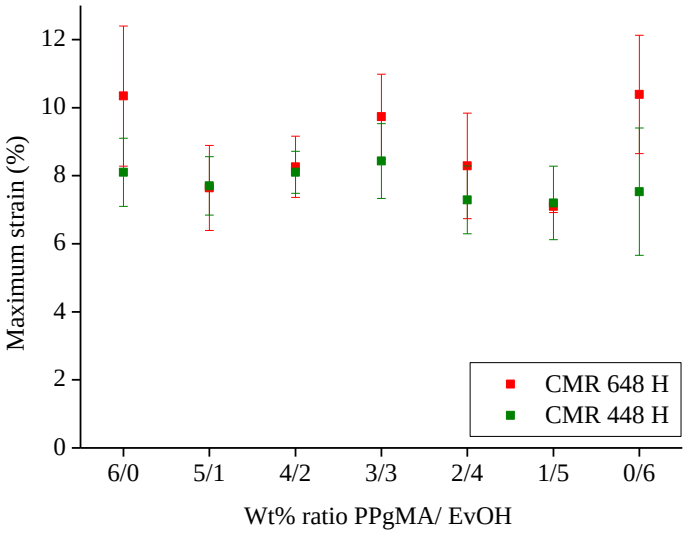

Figure 4.19: Average maximum % strain of the CMR 648 and CMR 448 composites with 10 wt % wood and 6 wt % compatibilizer. The pre-reaction between the compatibilizers were (H) heat-assisted.

Figure 4.18 shows that the CMR 448 polymer composite is able to withstand a higher maximum stress than the CMR 648 polymer composite, which can mostly be attributed to the higher rubber content in the CMR 648 polymer.

A large drop in the average maximum stress of 10 to 18 % can be observed from pure PPgMA (6/0) to a 5/1 PPgMA/ EvOH ratio for both composite systems. Thereafter the maximum attainable stress is roughly constant for the whole range of joint compatibilizers. Interestingly the composites with the joint compatibilizer, containing EvOH, exhibit maximum stress values very similar to that of the composites with just 6 wt % EvOH as compatibilizer. If we follow the argument put forward in

Section 4.2, then the PPgMA interacts between the iPP and the wood, creating a material that is stronger than the non-compatibilized composites. It appears that the presence of even a small amount of EvOH interferes with this interaction to a certain extent. The strain values presented in Figure 4.19 indicate little change as the EvOH content is increased. If this is taken together with the results of Figure 4.18, we see, while the presence of EvOH decreases the maximum stress the material can take; it has little or no effect on the deformability as measured by the maximum strain. Once again this indicates that the two components of the joint compatibilizer interact with different parts of the polymer. The standard deviation in the results obtained for the heat-reacted compatibilizer indicates that this method is possibly not that successful in combining the PPgMA and the EvOH.

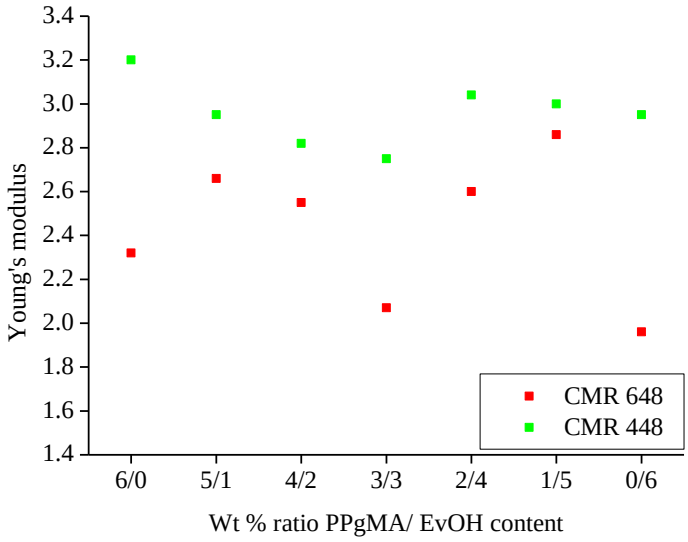

Figure 4.20: Change in Young's modulus of the CMR 648 and CMR 448 composites with 10 wt % wood and 6 wt % compatibilizer. The pre-reaction between the compatibilizers were (H) heat-assisted.

Figure 4.20 shows the change in Young's modulus with changing compatibilizer ratio. A clear difference due to the polymer matrices can be observed: For the CMR 448 polymer the Young's modulus is generally higher than for the CMR 648 polymer.

In the CMR 648 polymer matrix, the Young's modulus shows sudden changes, it first increases and then decreases and then increases again, with a minimum at a 3/3 wt % ratio. These results show clearly that the stiffness changes of the composites are much larger for the CMR 648 polymer matrix, which is more affected by the change in the compatibilizer content, specifically the EvOH content. Comparing the stiffness for pure PPgMA, 6/0 wt % ratio, and pure EvOH, 0/ 6 wt % ratio, it is obvious that PPgMA leads to higher stiffness in the CMR 648 matrix, with even increased stiffness for joint wt % ratios of PPgMA and EvOH.

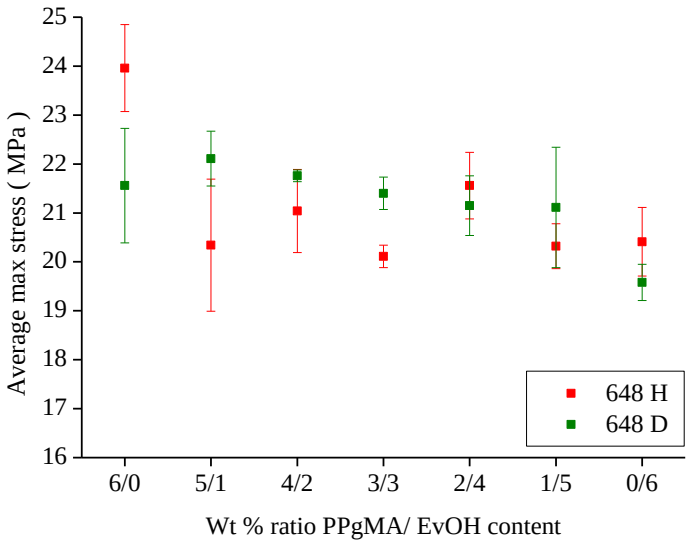

Figure 4.21: Average maximum stress of the CMR 648 composite, with 10 wt % wood content; wt % ratio PPgMA/ EvOH content jointly 6 %, heat (H) and DMAP (D) assisted.

Once again, the DMAP-assisted esterification reaction is evaluated by comparing the CMR 648 composites of the (D) series with the (H) series of compatibilizers. Overall, we see lower standard deviations, indicating a more uniform product with respect to the compatibilizer (D) series. This is particularly noticeable with the 3/3 ratio. In general the same trends are observed for the maximum stress, in that it remains essentially constant until high EvOH content is reached.

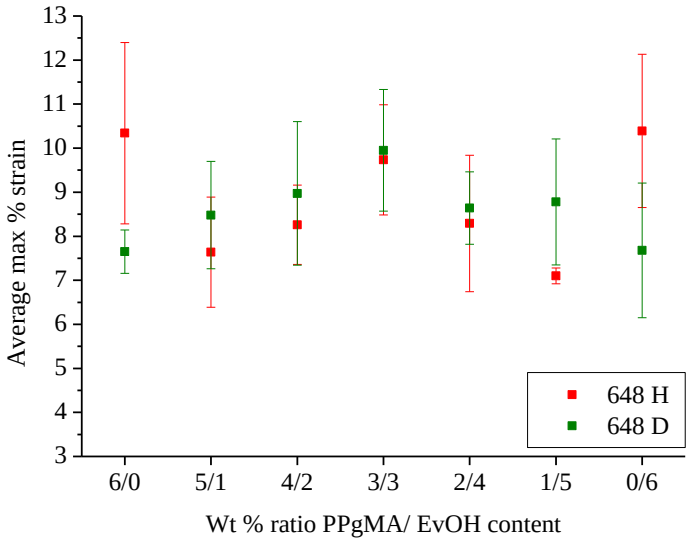

Figure 4.22: Average maximum % strain of the CMR 648 composite, with 10 wt % wood content; wt % ratio PPgMA/ EvOH content jointly 6 %, heat (H) and DMAP (D) assisted.

The results in Figure 4.22 are quite interesting from a standard deviation perspective. With the exception of the pure PPgMA, the standard deviation is large for all of the samples. The question now arises, why would the (H) and (D) results for pure PPgMA vary? As DMAP was added to all the samples prepared in the (D) series, one has to assume that the catalyst was instrumental in increasing permanent esterification between the PPgMA and EvOH and the hydroxyl groups on the cellulose of the wood. This of course means that the addition of DMAP introduces a further, non-quantifiable interaction parameter to the wood-compatibilizer interaction. This needs to be kept in mind while evaluating results of the physical tests. Overall though, it seems as if using PPgMA and EvOH jointly results in better control of the physical properties, indicated by the generally smaller standard deviations.

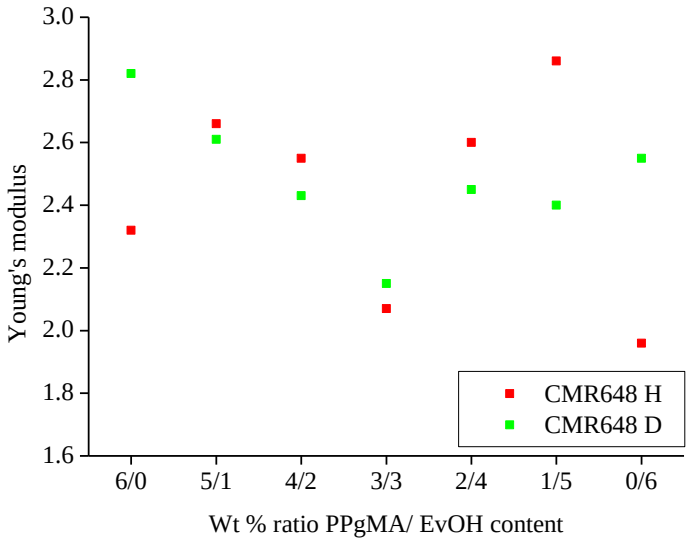

Figure 4.23: Change in Young's modulus of the CMR 648 composites, with 10 wt % wood content. The compatibilizers were pre-reacted with heat (H) or DMAP (D).

Figure 4.23 shows the same trend for the Young's modulus of the heat and catalyst reacted composites, a decreasing trend to a 3/3 wt % ratio PPgMA/ EvOH content, which increases again for higher EvOH wt % ratios.

The results show that the composite with a joint compatibilizer, wt % ratio of 3/3 PPgMA/ EvOH, can on average withstand a stress of relatively the same force as the other composites, but its stiffness is lower and it is able to undergo more deformation per unit of stress than the other composites, before failing.

4.4 Effect of wood loading and particle size

This section deals with a separate set of data produced during the assessment of the effect of wood loading and wood particle size. Whilst we set the parameters regarding the wood type (Pinus radiata) and particle size (180 um), and the wood content (10 wt %), we did investigate the effect of wood loading and particle size on compatibilized composites. The same sets of physical tests were conducted on the composites produced as were done on all the other composites (Sections 4.1 – 4.3).

4.4.1 Hardness testing

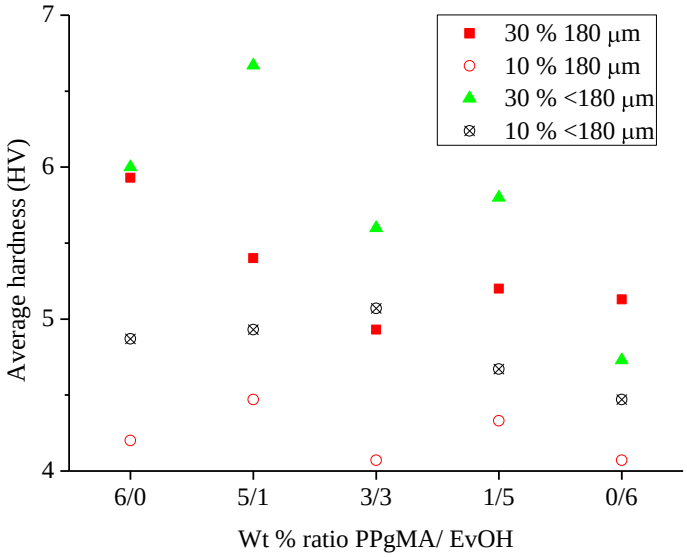

Figure 4.24: Average hardness of the CMR 648 composites with 10 and 30 wt % wood content (particle sizes of 180 µm and smaller than 180 µm) and 6 wt %, compatibilizer (D).

The results presented in Figure 4.24 clearly indicate that (a) the composites with 30 wt % wood are harder than the those containing 10 wt % wood, and (b) in general the composites made with the smaller wood particles are harder than the ones made with the 180 µm wood particles. The latter is more noticeable in the case of the lower wood content. Interestingly, the composition of the joint compatibilizer has a larger effect with the 30 wt % wood composites than in the case of the 10 wt % wood composites.

The hardness shows an overall decrease as the wt % EvOH content in the compatibilizer increases. This more pronounced for the 30 wt % wood composites (with the exception of the one composite with a 5/1 ratio and small wood particles

The decrease in wood particle size from 180 µm to a particle size less than 180 µm do point out that the hardness properties become more stable and smaller increases or decreases in hardness values compared to the larger wood particle size of 180 µm. This is to be expected, since the hardness

properties can vary significantly when the wood particle size increases. Improved interaction between polymer matrix and wood particle exist as the particle size is reduced, and hardness properties should remain more consistent, with smaller differences as the compatibilizer content changes, as the results indicate.

4.4.2 High speed tensile impact testing

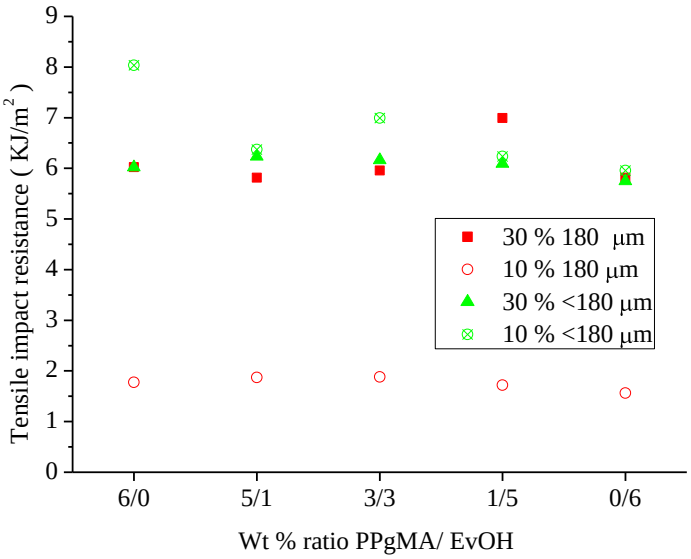

Figure 4.25: Average high speed tensile impact resistance of the CMR 648 composites with either 10 or 30 wt % wood content (particle sizes of 180 μm and smaller than 180 μm). The pre-reaction of the compatibilizers were heat and DMAP assisted.

Figure 4.25 shows the high speed tensile impact resistance results for the joint compatibilizer system used. The standout results here are the impact resistance values of the 10 wt % wood composites when the smaller wood particles are used. These are in the same range as the 30 wt % wood composites. Overall the impact resistance is unchanged with a change in compatibilizer composition.

4.4.3 Tensile testing

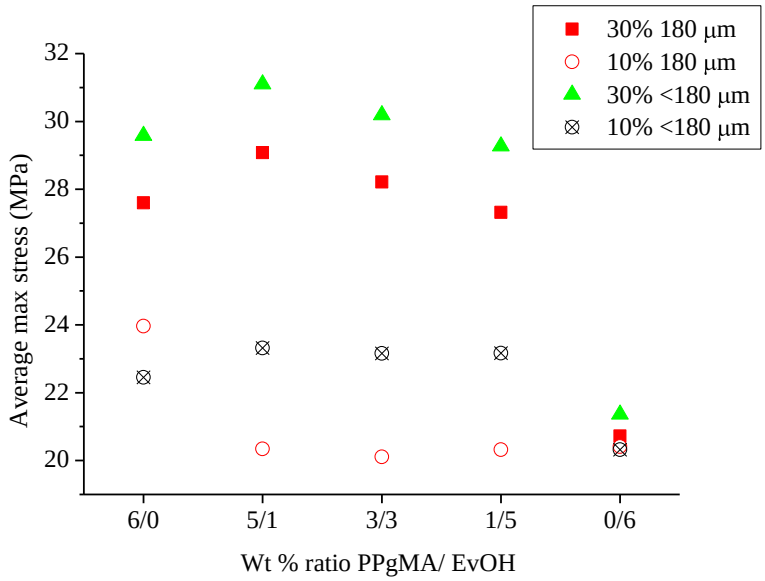

Figure 4.26: The average maximum stress of the CMR 648 composites with either 10 or 30 wt % wood content (particle sizes of 180 µm and smaller than 180 µm). The pre-reaction of the compatibilizers were heat and DMAP assisted.

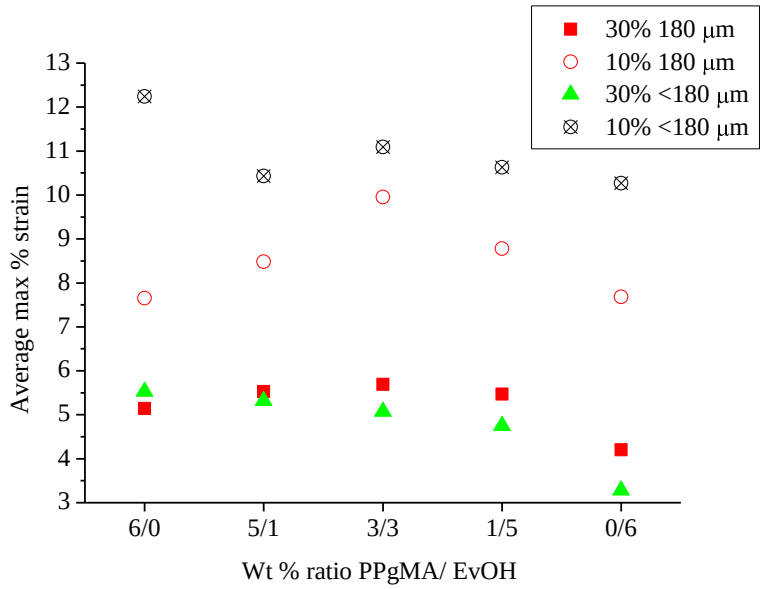

Figure 4.27: The average maximum strain for CMR 648 composites with either 10 or 30 wt % wood content (particle sizes of 180 µm and smaller than 180 µm). The pre-reaction of the compatibilizers were heat and DMAP assisted.

From the results shown in Figure 4.26, for 10 wt % wood, and with a particle size of 180 µm, we see, as before, a general decrease in the maximum stress as the amount of EvOH in the compatibilizer increases. When the same composite is made, but with a smaller wood particle, we do not see this

trend, until we reach the point where pure EvOH is used. For the higher wood content (30 wt %) composites we observe an apparent maximum at a compatibilizer composition of 5/1, where after a steady decrease is observed, until we reach the composite where pure EvOH is used as compatibilizer. In fact, the maximum tensile stress for all the composites with EvOH as compatibilizer is the same, irrespective of wood loading or wood particle size. The strain results (Figure 4.27) also indicate that, for the higher wood content composites of CMR 648 we see essentially no change except for the pure EvOH compatibilizer. For the 10 wt % wood content CMR 648 composites there appears to be a relationship with the compatibilizer composition, with a "peak" at around 3/3.

4.5 Reaction between the compatibilizers

The one obvious question that arose during this research was to which extent the pre-reaction between the compatibilizers occurred. In other words, did any esterification occur during the pre-reaction? In order to investigate this aspect, we focussed on the DMAP-assisted reaction and attempted to see if we could see any indication of the reaction by ^{13}C NMR. It was assumed that we would be able to use the shift or disappearance of the carbonyl peak to show this reaction. However, the first analyses were without success, as no indication of the carbonyl peak associated with the PPgMA could be found either for the 3/3, 5/1 or 1/5 ratios of PPgMA/ EvOH (pre-reacted) compounds. The 3/3 reaction product is shown in Figure 4.28.

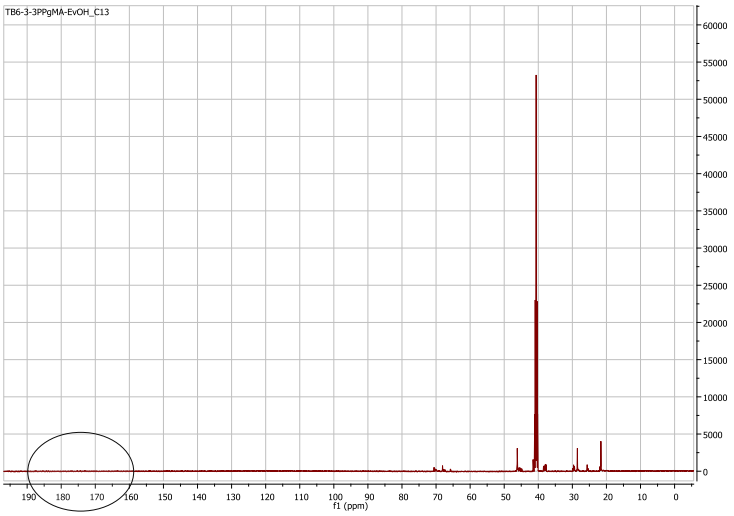

Figure 4.28: ^{13}C NMR spectrum of a pre-reacted 3/3 ration of PPgMA and EvOH

We then found, however, that for even the pure PPgMA we could not detect the carbonyl peak, so we decided to use FTIR to probe the reaction. Results are shown in Figure 4.29.

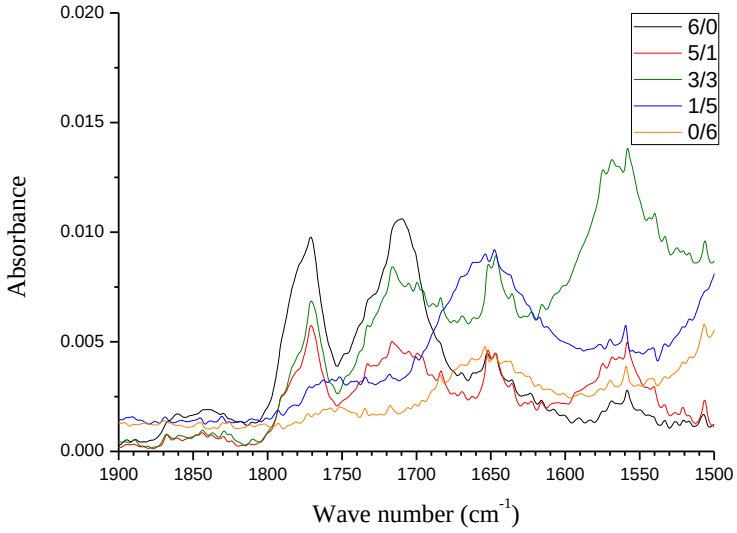

Figure 4.29: FTIR results of the PPgMA-EvOH pre-reacted compatibilizers.

The presence of a carbonyl group in different chemical environments is normally evidenced in the wave number range between 1800 cm^{-1} and 1500 cm^{-1}. Thus we should be able to see shifts due to the anhydride on the PPgMA, the ring-opened anhydride, and the new ester group after reaction with the hydroxyl of the EvOH. The two peaks between 1800 cm^{-1} and 1700 cm^{-1} are due to the two ester carbonyl groups in the closed MAH ring structure of PPgMA (one closer and one further removed from the polymer backbone).

Upon reaction with EvOH, the MAH ring opens up, with the formation of a carboxylic acid and an ester group. These are the peaks at about 1560 cm^{-1} and at 1650 cm^{-1}. It is therefore clear that the reaction does take place.

An attempt was made to qualitatively see differences in these peaks upon esterification, to determine the difference in amount of esterification between the PPgMA. To this end we compared the ratio of the peaks at 1710 cm^{-1} and 1560 cm^{-1}. Results are presented in Table 5.1.

Table 4.1: Peak area ratios of the carbonyl peaks at 1560 and 1710 cm^{-1}.

Sample ID	Peak area ratio $1560cm^{-1}/1710cm^{-1}$
6/0	0.15
5/1	1.44
3/3	4.73
1/5	3.91
0/6	0.09

From Table 5.1 it seems that the largest extent of esterification (little as it may be) occurs when there is an equivalent amount of PPgMA and EvOH used (3/3 wt %). The esterification seen when no EvOH or no PPgMA is present is due to the reaction with DMAP.

4.6 Conclusions

From the results presented in this chapter, we can draw some preliminary conclusions. In the first place, it is quite clear that the use of compatibilizers (in this case PPgMA or EvOH) influences the properties of the impact propylene copolymer-wood composites. It is also clear that the chemical composition distribution of the CMR type copolymers play a role in the properties of the final composites, under the conditions and parameters employed for the comparative studies. By the same token, the interaction of the two different compatibilizers appears to be different with the different polymer matrices. It also seems clear that the interaction of these chemically different compatibilizers is different within the variety of molecularly distinct fractions present in the copolymer matrix.

Simple admixtures of the two compatibilizers and use of these in wood-polymer composites lead to very few discernible trends and large standard deviations in the results of physical testing. Pre-reaction of the two compatibilizers by heating in the presence of a suitable catalyst yield products that, when used in the preparation of impact copolymer-wood composites, give more reproducible results when subjected to physical testing.

The use of these joint compatibilizers indicates that there are definite trends that can be observed when the composition of the compatibilizer is changed. By the same token it was also demonstrated that these trends only hold for the specific parameters that were set in the manufacture of the composites. Changing, for example, the wood loading and the wood particle size resulted in different responses than were originally recorded.

In this light we decided to first investigate the interaction of the compatibilizers with the polymer matrices in question, and then to focus on the fundamental understanding of the interaction of the wood components with the polymer and the compatibilizers, both singly and as a joint product.

4.7 References

1. N. C. Basson, The effect of molecular architecture on the properties of propylene impact copolymers, MSc thesis, University of Stellenbosch, South Africa, 2010.
2. N. C. Basson, A. van Reenen, The effect of compatibilizer on the properties of impact poly(propylene)-wood polymer composites, Macromolecular Symposia, 315, p 30 (2012).

CHAPTER 5 INTERACTION OF THE COMPATIBILIZERS WITH THE POLYMERIC MATRIX

In order to investigate the interaction with the individual fractions present in the copolymer (CMR 648 and CMR 448) that were used to prepare composites, we first needed to fractionate the respective copolymers and to characterize the fractions of these polymers. The results of the preparative temperature rising elution fractionation experiments are given in Section 5.1.

5.1 Preparative temperature rising elution fractionation (pTREF)

The pTREF elution distribution plots for CMR 648 and CMR 448 are shown in Figures 5.1 and 5.2.

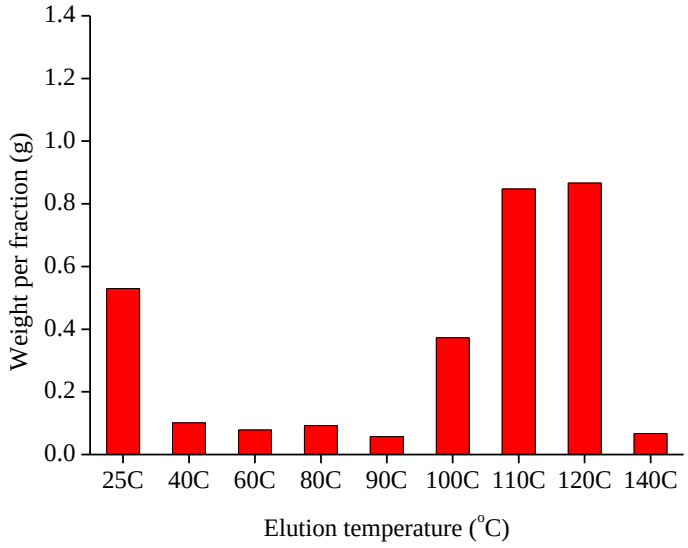

Figure 5.1: TREF elution distribution plot for impact polypropylene CMR 648.

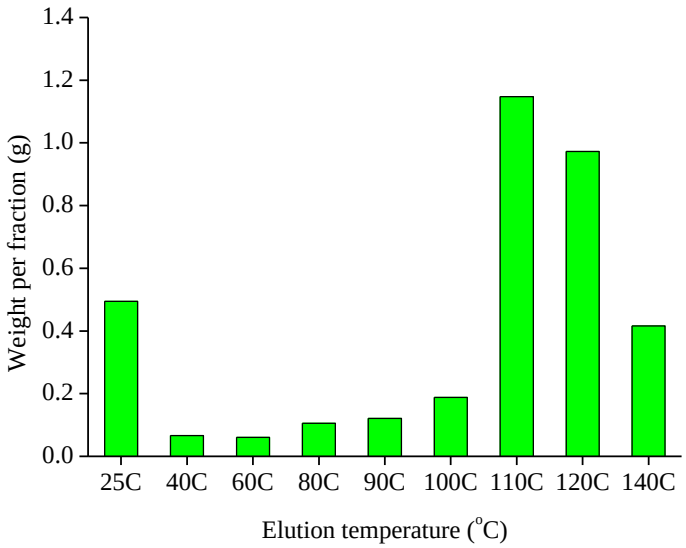

Figure 5.2: TREF elution distribution plot for impact polypropylene CMR 448.

The two impact copolymers were both fractionated according to crystallizability using p-TREF in order to distinguish between the fractions of interest (rubber, co-polymer, crystalline phase). SEC-FTIR measurements were also conducted on the individual fractions of the CMR 648 polymer (see Section 5.2.2). The weight fraction of the 25 °C (rubbery) fraction for both polymers is comparable, as seen in Figures 5.1 and 5.2. The copolymer fractions between these two polymers differ slightly with the largest difference seen in the region of the 90 °C and 100°C fraction, where the CMR 648 copolymer has a larger amount of material present. These fractions typically represent the ethylene rich crystalline copolymers.[1] The higher temperature fractions indicate that the CMR 448 copolymer has a larger percentage of the total material between fractions 110 °C and 140 °C (PP rich crystalline fractions), compared to the CMR 648 copolymer.

Since the most crystalline fractions elute from 110°C onwards, and are mostly PP rich, it appears that the CMR 448 copolymer is more crystalline than CMR 648 and the hardness of CMR 448 should be higher since a larger amount of the bulk of the fractionated material elutes in the crystalline region, as seen in Figure 5.2. This is confirmed by the hardness results described in Chapter 4. Overall it is clear that these two polymers are different with respect to the chemical composition distribution. In particular, a larger semi-crystalline copolymer fraction (possibly ethylene-rich) is present in the polymer with the higher ethylene content (CMR 648). The SEC results for CMR 648 fractions are shown in Section 5.2.1

5.2. Characterization of selected TREF fractions

5.2.1 Size exclusion chromatography

In order to illustrate the molecular weight distribution and the chemical composition distribution of the impact copolymers, we focussed the analysis efforts regarding SEC and SEC-FTIR (Section 5.2.2) on the CMR 648 copolymer. The results of the SEC analysis on the TREF fractions of CMR 648 are shown in Table 5.1.

Table 5.1: Molecular weight (M_w, M_n) and polydispersity (PD) values of the TREF fractions of polymer CMR 648.

Sample ID	M_w (g/ mol)	M_n (g/ mol)	PD
25 °C	336411	106786	3.15
40 °C	206927	77420	2.67
60 °C[1]	248340	80748	3.08
	2569	1693	1.51
80 °C[1]	325629	100884	3.23
	5266	2794	1.88
90 °C[1]	382378	135032	2.83
	9665	3651	2.65
100 °C	82767	28386	2.92
110 °C	172909	70436	2.45
120 °C	216829	81454	2.66
140 °C	213106	81091	2.63

1: Bimodal SEC curves were observed in these cases

The molecular weight shown in Table 5.1, gives a clear indication of the differences in molecular weight distribution between the different TREF fractions from 25 °C to 140 °C. As expected the rubbery fraction has a higher molecular weight than the predominantly crystalline (iPP) fractions (110 – 140 °C fractions). This is typical for these copolymers, as the average MFI of the iPP prepared in the first reactor reads to about 50 – 100% more than that of the final product. What is interesting is the apparent "double" peaks present in the 60 – 90 °C fractions. The molecular weight of the 80 °C and 90 °C fractions is also quite high. The polydispersity is generally between 2 and 3.

The "bimodal" distribution of the copolymer fractions 60 °C, 80 °C and 90 °C are resolved into a high molecular weight (larger peak) and a smaller peak of considerably lower molecular weight to 81 000 g/ mole.

The molecular weight data is useful, but in combination with the FTIR analyses (Section 5.2.2) we can get a good perspective about the distribution of ethylene and propylene amongst the fractions of differing crystallinity.

5.2.2 Size exclusion chromatography coupled with Fourier transform infra-red spectroscopy (SEC-FTIR)

The SEC-FTIR plots for the fractions of the CMR 648 copolymer are shown in Figures 5.3, which indicates the distribution of propylene (left) and ethylene (right) across each of the fractions. It should be noted that in many cases the scatter of data towards the longer elution times (lower molecular weight) is of no importance, this is merely an artefact of the technique.

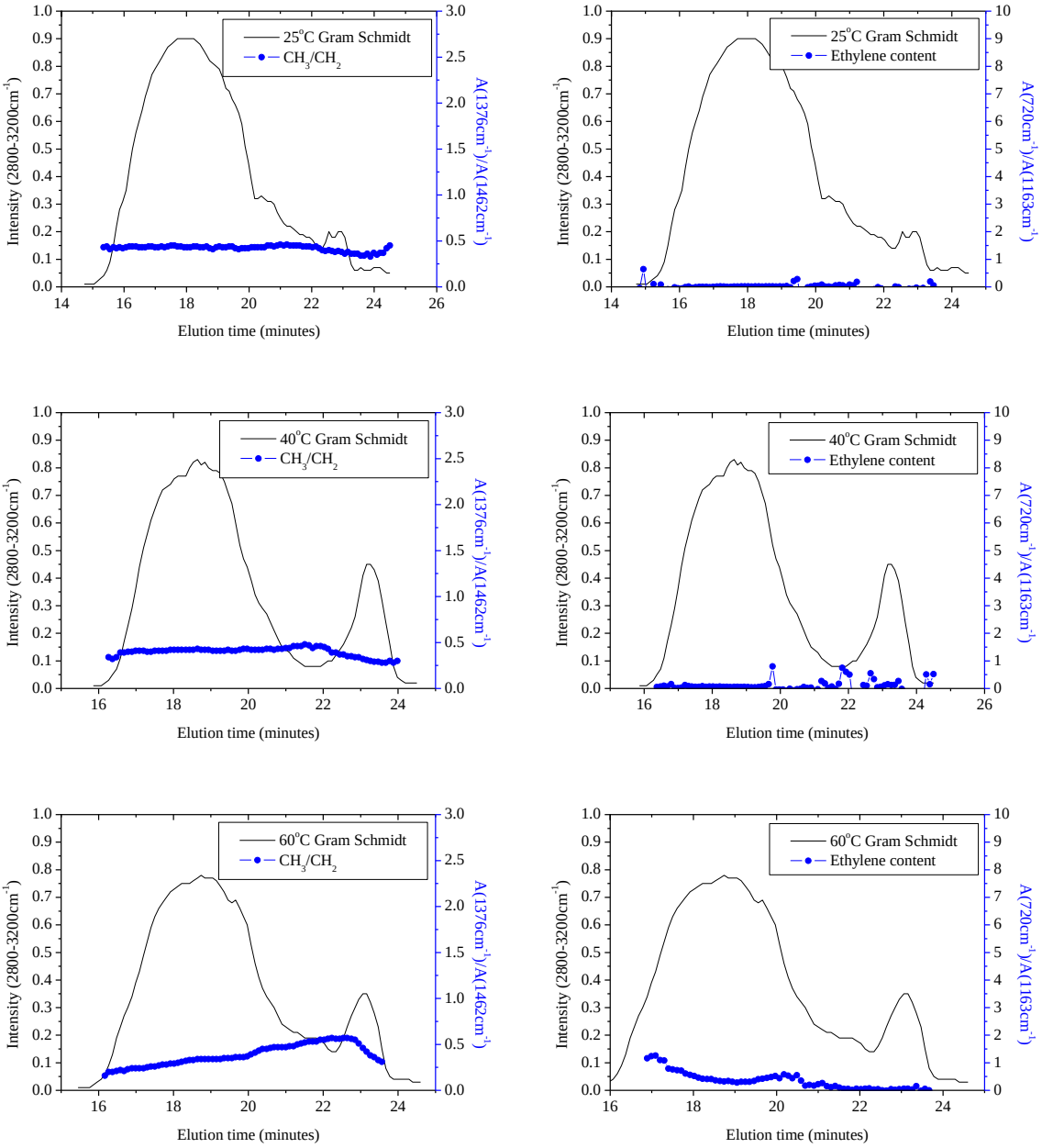

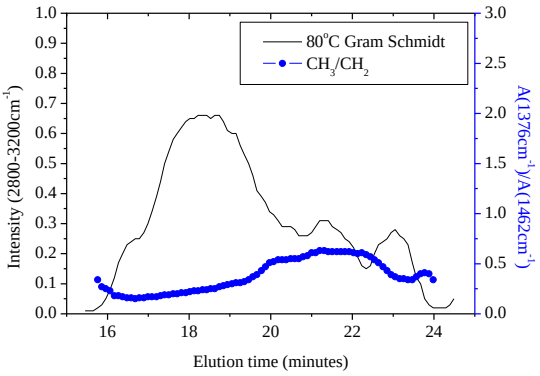

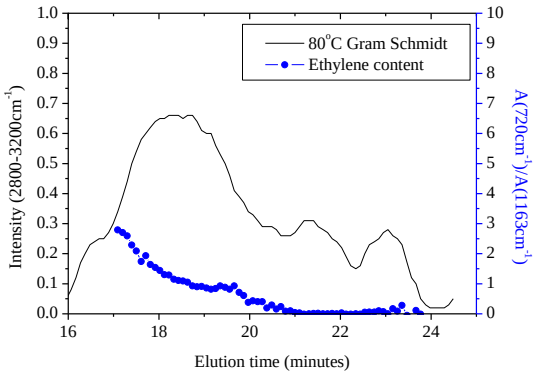

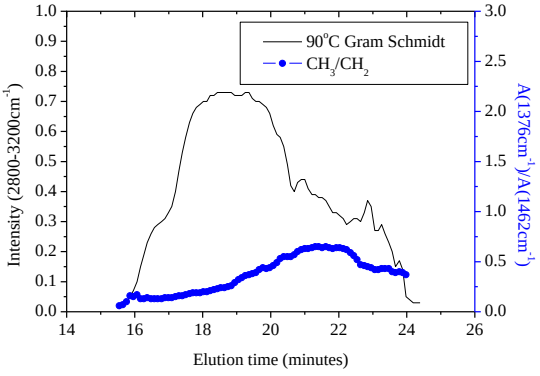

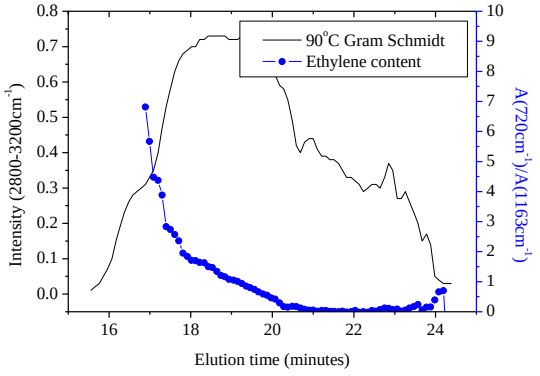

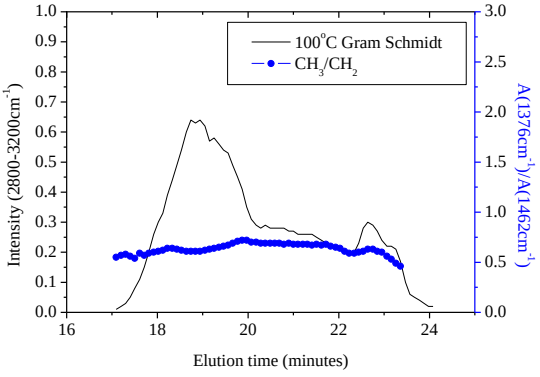

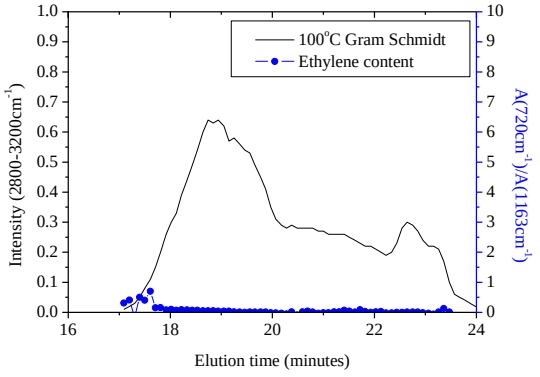

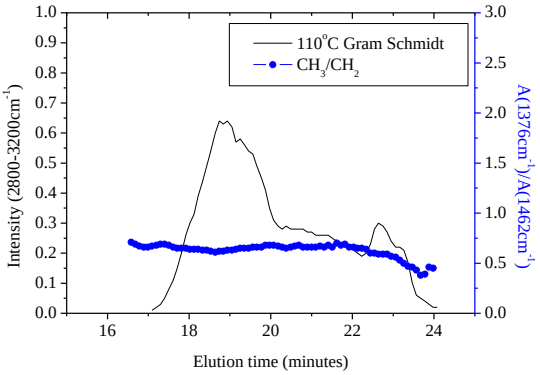

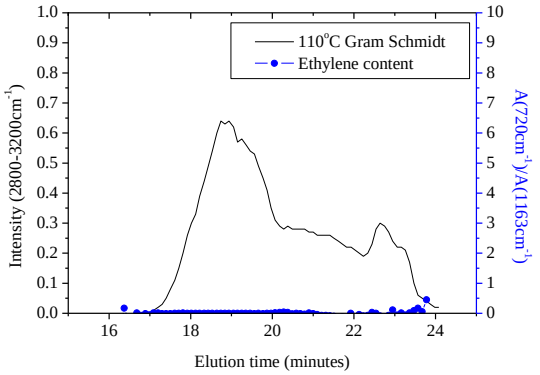

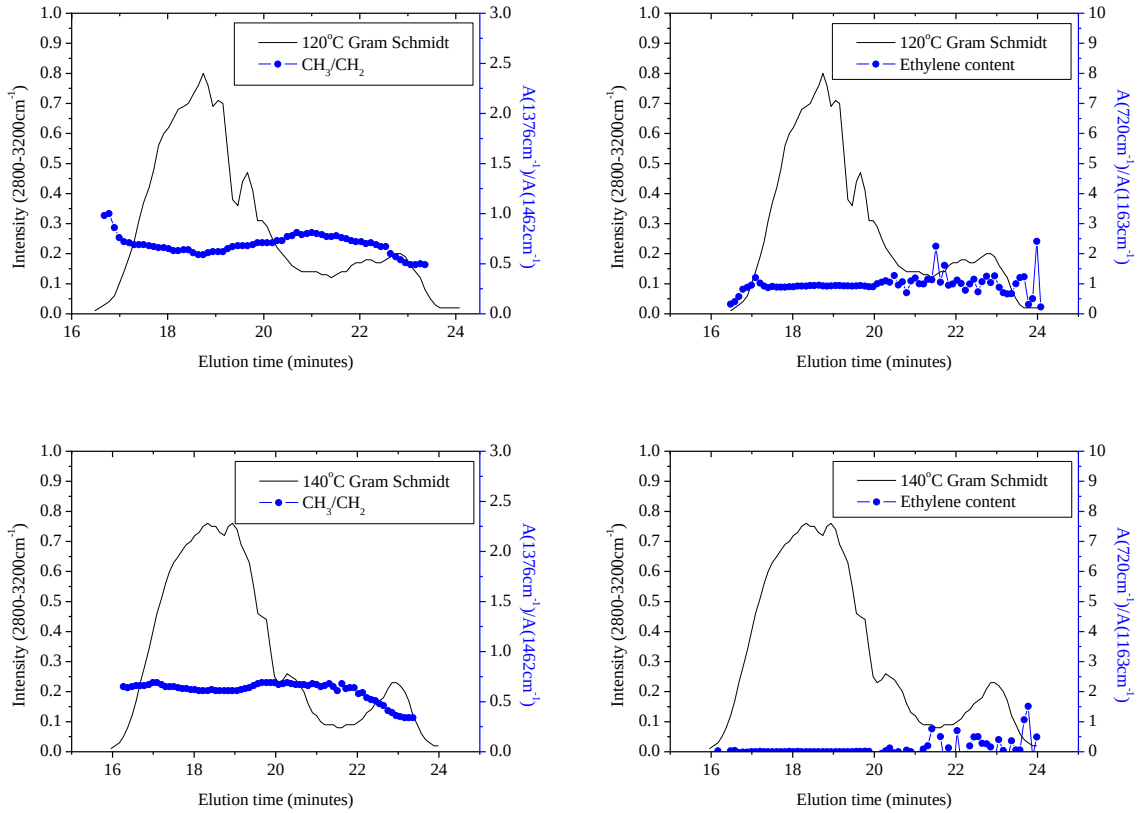

Figure 5.3: SEC-FTIR of the TREF fractions 25 °C to 140 °C for CMR 648, left: propylene distribution, right: ethylene distribution.

If we look at fraction 25 °C, it is clear that both ethylene and propylene is present, and that the ratio of propylene to ethylene is constant across the molecular weight profile. This is similar for the 40 °C fraction.

Significant differences in distribution of ethylene and propylene, is apparent in fractions 60 °C and 80 °C. Here the propylene seems to be distributed with a bias towards the lower molecular weight component, whilst the ethylene content is larger in the higher molecular weight component. These results indicate that these fractions of material are made up of two chemically different components, the higher molecular weight species containing more ethylene and the lower more propylene.

The 90 °C fraction appear to follow a similar trend to the 60 °C and 80 °C fractions, however here the ethylene content in the higher molecular weight fraction is far more pronounced than in the case of the 60 °C and 80 °C fractions. Since this fraction is more crystalline than the 60 °C and 80 °C fractions, we expect long crystallizable ethylene sequences to be present.

Little difference is seen for fractions 100 °C to 140 °C. Here the propylene content remains relatively constant across the molecular weight distribution, with little to no ethylene content present. The only exception seems to be some ethylene in fraction 100 °C and fraction 120

°C, with a very small amount of ethylene content present, and this also appears to remain relatively constant. Since this fraction consists of highly crystalline polymer material; the ethylene presence here is expected to be due to some highly crystalline ethylene homo polymer sequences.

In Figure 5.4, we see the analyses of the “crystalline” portions containing propylene (left) and ethylene (right).

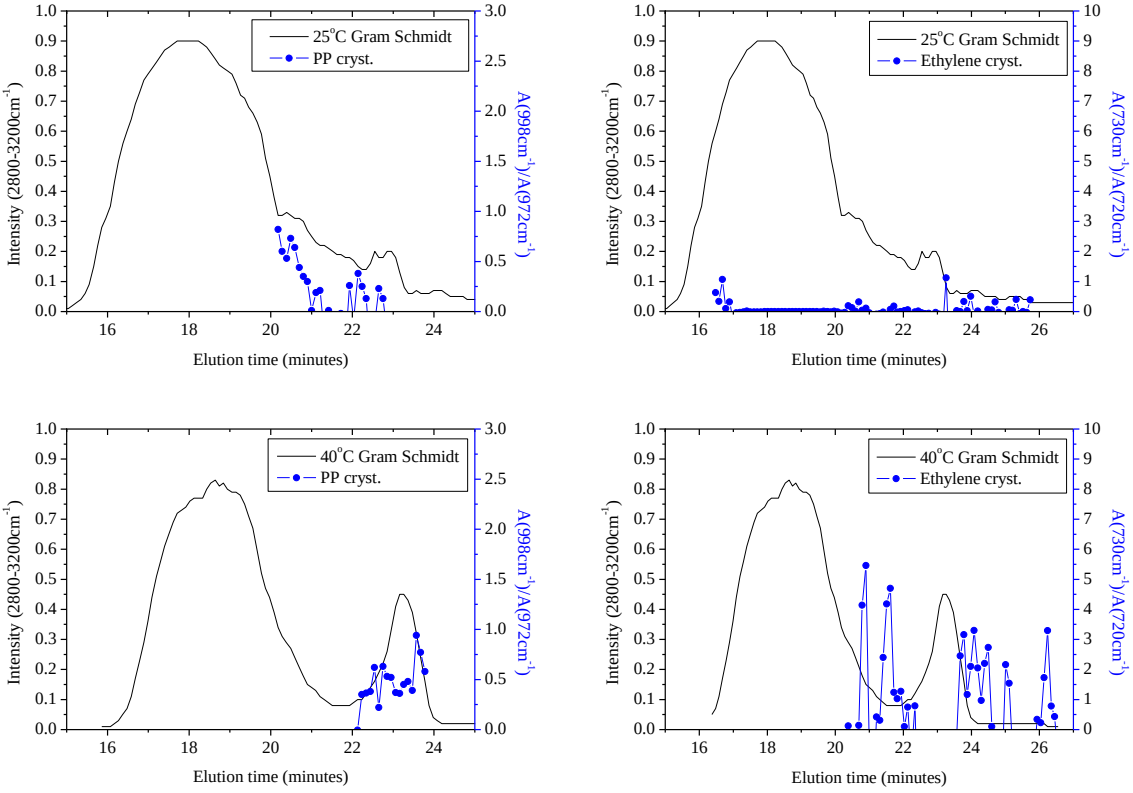

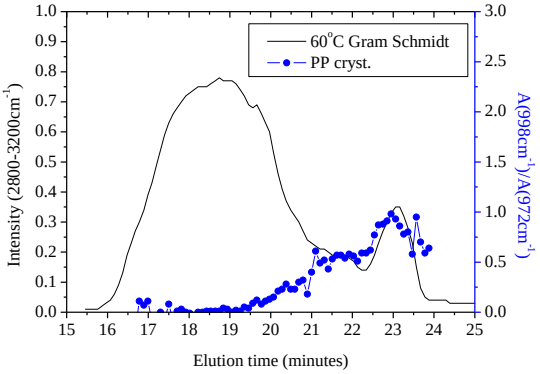

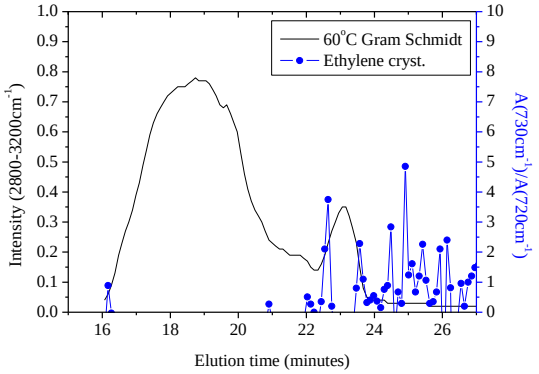

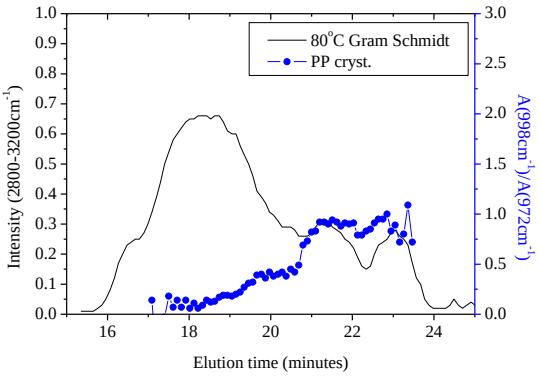

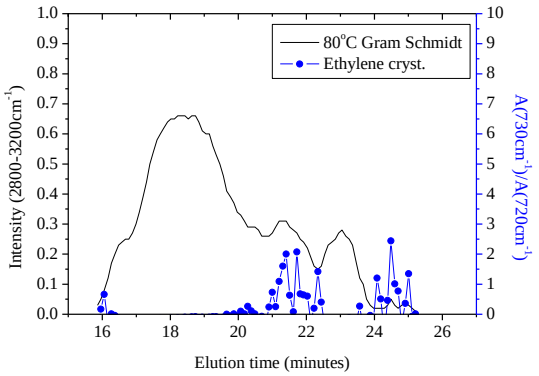

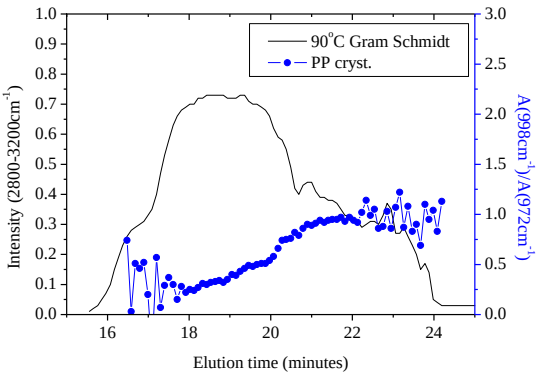

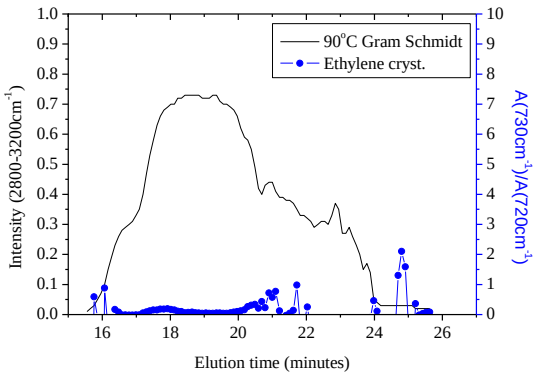

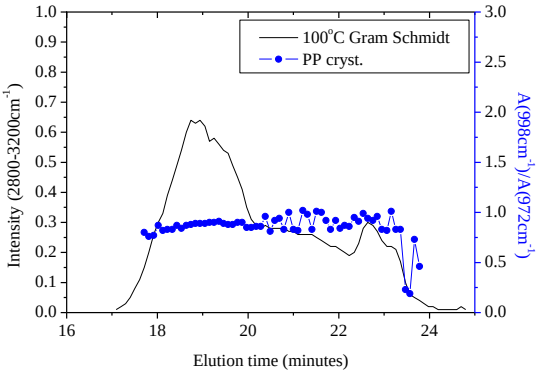

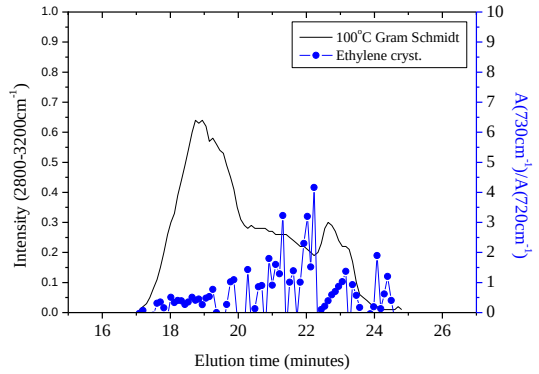

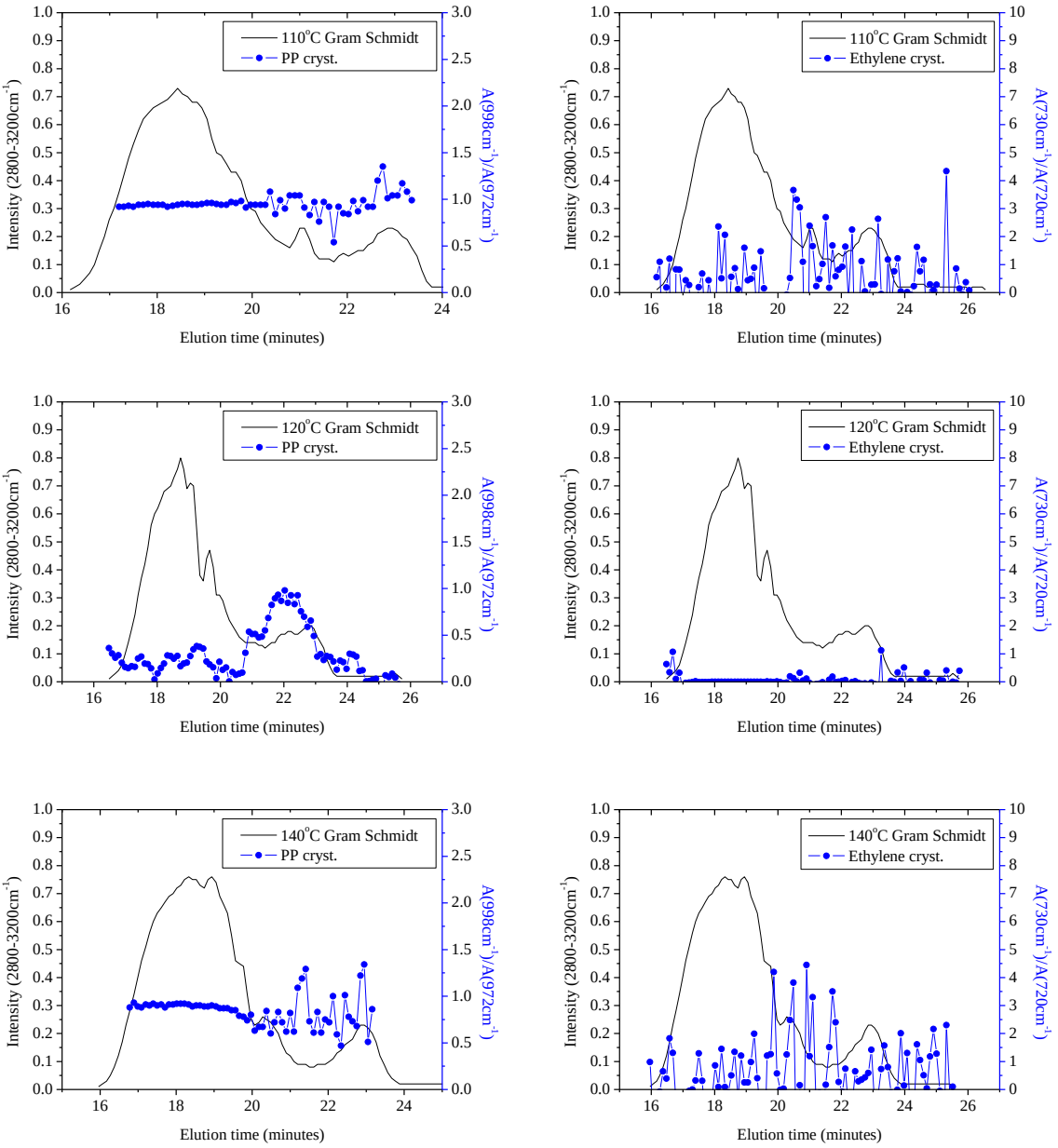

Figures 5.4: SEC-FTIR of the TREF fractions 25 °C to 140 °C for CMR 648, left: PP crystallinity distribution, right: Ethylene crystallinity distribution.

Figure 5.4 shows the crystallinity distribution for ethylene and propylene sequences, across the TREF fractions, ranging from 25 °C to 140 °C. Fraction 25 °C (rubbery fraction) indicates a very small amount of short crystallizable PP sequences (low molecular weight shoulder). This is most likely low molecular weight isotactic polypropylene. There are, no crystallizable ethylene sequences detected.

For the 40 °C fraction we can observe a bimodal molecular weight distribution; with the smaller peak appearing to be made up of both short crystallizable PP and PE sequences. The scatter of the ethylene sequence data makes it impossible to deduce any ethylene crystallinity. Fraction 60 °C also shows a bimodal molecular weight distribution and indicates some

crystalline PP to be present across the entire molecular weight distribution, with a bias to the lower molecular weight side. Fraction 80 °C has a similar profile to the 60 °C fraction. In both 60 °C and 80 °C fractions it is impossible to detect noticeable crystallisable ethylene sequences. This indicates that these fractions comprise sparingly crystalline propylene-rich copolymers.

The 90 °C fraction has PP crystalline material across the whole distribution, increasing towards the lower molecular weight region. Here, for the first time we now see a sustained amount of crystallisable ethylene sequences across the higher molecular weight fraction of the TREF fraction. This appears to indicate that this fraction consists of ethylene rich copolymers (higher molecular weight) and propylene rich copolymers (lower molecular weight).

Data scatter makes it just about impossible to assign any ethylene crystallinity to any of the fractions from 100 °C to 140 °C, with the exception of some crystalline ethylene sequences in the higher molecular weight portion of the 100 °C fraction (ethylene rich copolymer, similar to the 90 °C fraction) and a low amount over the high molecular weight portion of the 120 °C fraction, which is consistent with the assumption that some crystalline polyethylene might be present here.

In conclusion, therefore, it appears that the CMR 648 copolymer comprises a large rubbery fraction consisting primarily of a high molecular weight EPR rubber, and some low molecular weight isotactic polypropylene. The major part of the material is made up of crystalline material, mostly isotactic polypropylene, with a small amount of (high density) polyethylene. The rest of the material comprises mostly propylene-ethylene copolymers of varying crystallinity, with the 40 – 80 °C fractions being mostly propylene-rich, and the 90 °C and some of the 100 °C fraction being mostly ethylene-rich copolymer. Based on these observations, we embarked on a study of the interaction of the compatibilizers with the individual fractions.

5.3 Fluorescence microscopy

A fluorescence technique was developed to study the interaction and dispersion of the different compatibilizers with the polymer matrix and, initially, the wood. The description of the attachment of the Rhodamine B to PPgMA and Fluorescein to EvOH was given in Chapter 3.

Figure 5.5 A shows a wood particle that has auto-fluorescence under the Fluorescein signal analysis conditions (later proved the same in the case of the Rhodamine B analysis conditions). This figure clearly shows that the structure of the wood can be viewed with

fluorescence measurements. It was expected that having dye markers on the compatibilizers, could point out their position on the wood particle structure. The next step would have been to expose the wood particle to the compatibilizer, and the measurement of the extent that the fluorescence signal of the wood particle is "hidden" by the presence of the polymeric compatibilizer, and the detection of the dye signal on the compatibilizer. The interaction of the compatibilizer with the wood particles was difficult to see with this method, and since the wood itself has some degree of auto-fluorescence (relatively strong signal), it interfered with the dye signals on the compatibilizers. This interference signal proved too strong to properly resolve any fluorescence signal differences.

It was observed that upon melting the wood polymer composites, some extractables from the wood particles leaches out, and these extractables were also fluorescent. While nice images could be obtained of the wood particles in a composite, (Figure 5.5 B and C), the study of the interaction of the dye-stained compatibilizer and the wood/ polymer interface proved unsuccessful.

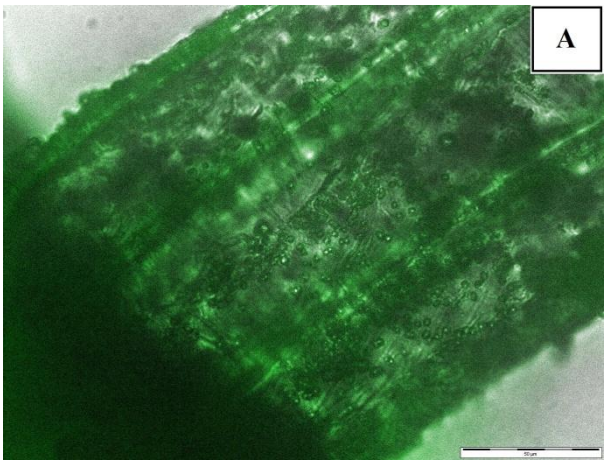

Figure 5.5 A: Fluorescence microscopy image of a single wood particle, Fluorescein signal, scale bar 50 um, at 10 x magnification.

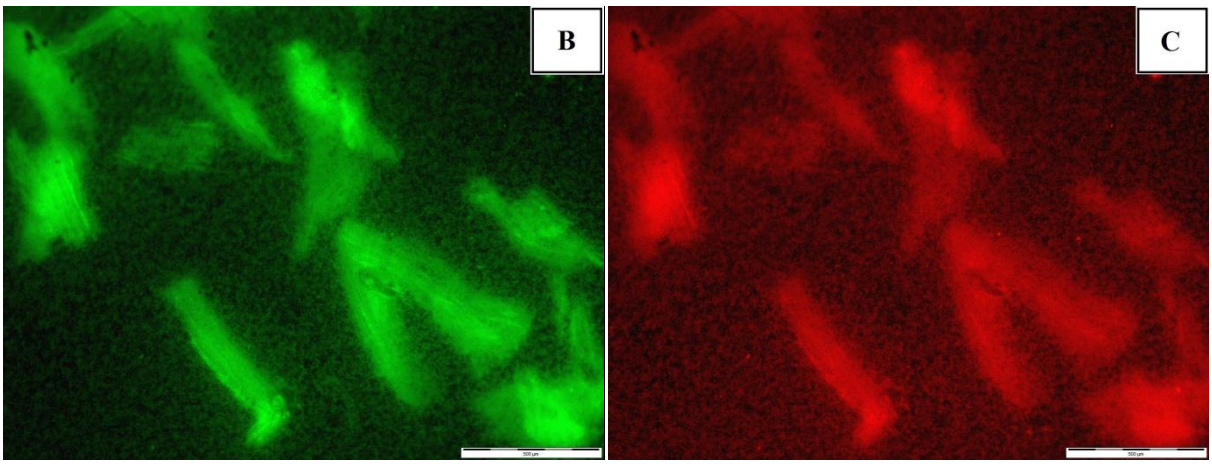

Figure 5.5 B and C: Fluorescence microscopy images of a single wood polymer composite, Fluorescein signal (left) and Rhodamine B signal (right), scale bar 500 um, at 4 x magnification.

On the other hand, however, the interactions of dye-treated compatibilizer in the polymer matrix could be successfully observed. The p-TREF fractions (Section 5.1) of the CMR 648 copolymer were blended with the marked compatibilizer. The images presented in Figure 5.6 (a – p) indicate the interactions of the compatibilizers with each fraction of the polymer matrix. The left-hand images are those of the Rhodamine-B-treated PPgMA mixed with the p-TREF fractions, while those on the right are the corresponding Fluorescein-treated EvOH with the same fraction. The temperature values indicated on the figures themselves represent the temperature at which the fraction eluted.

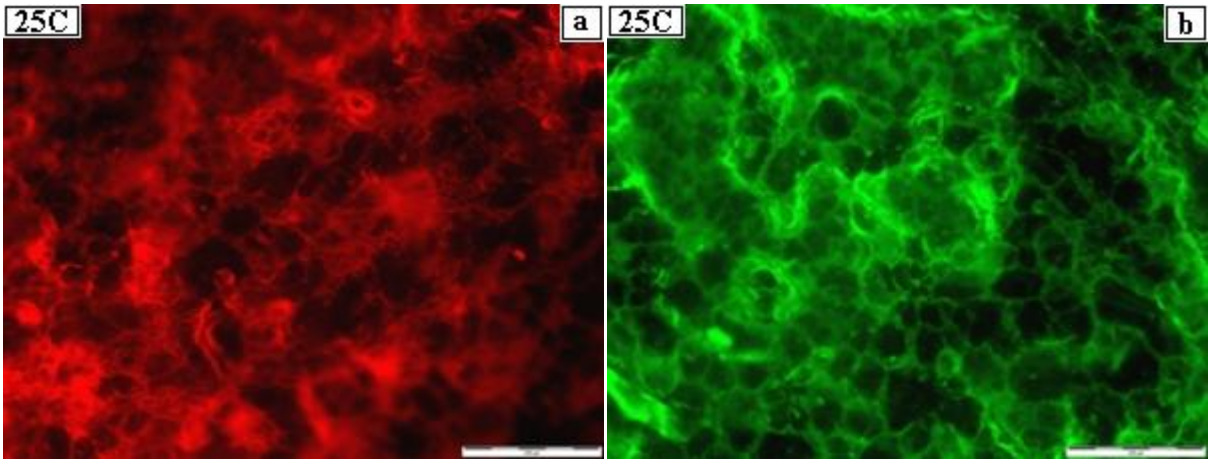

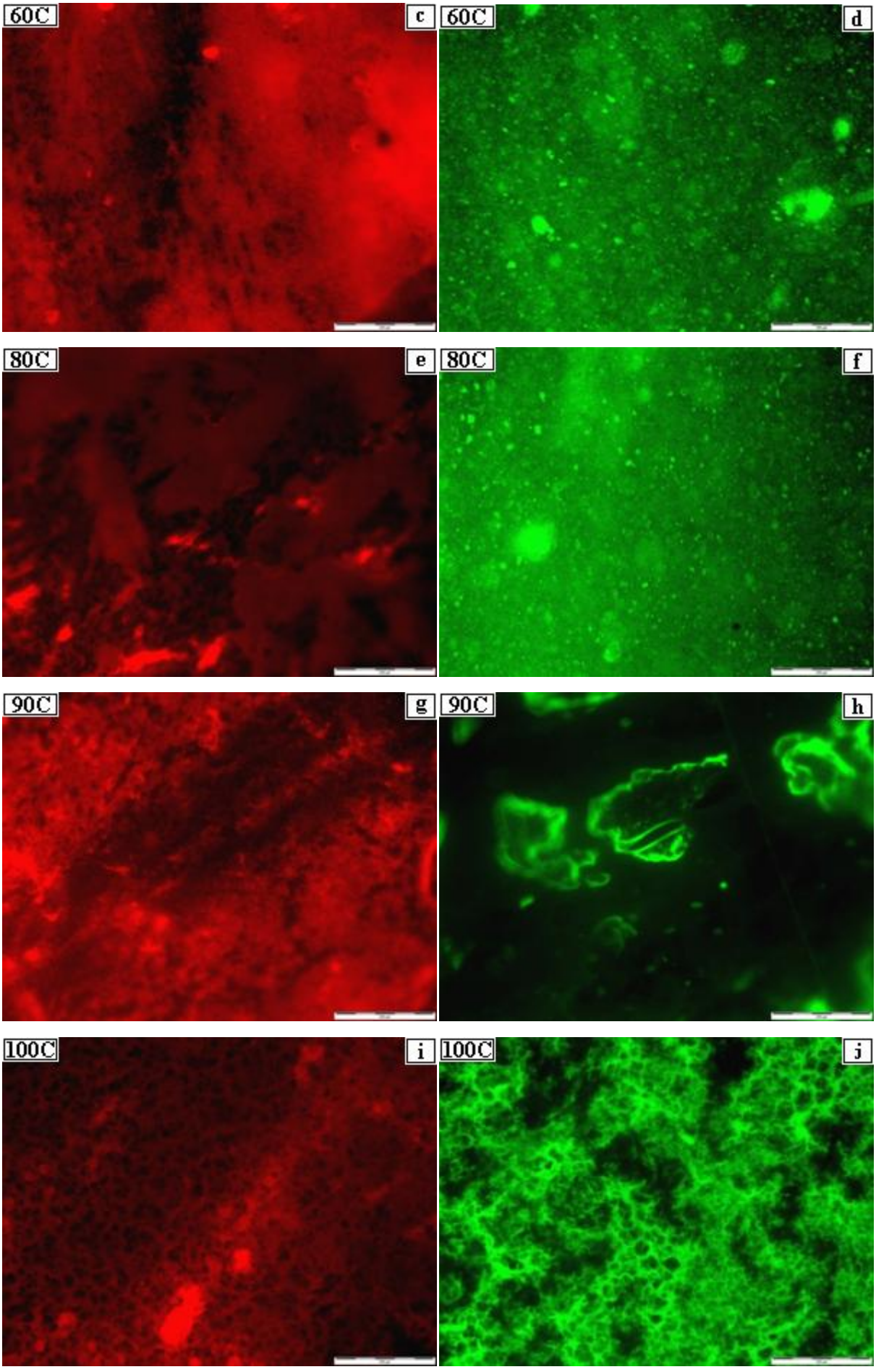

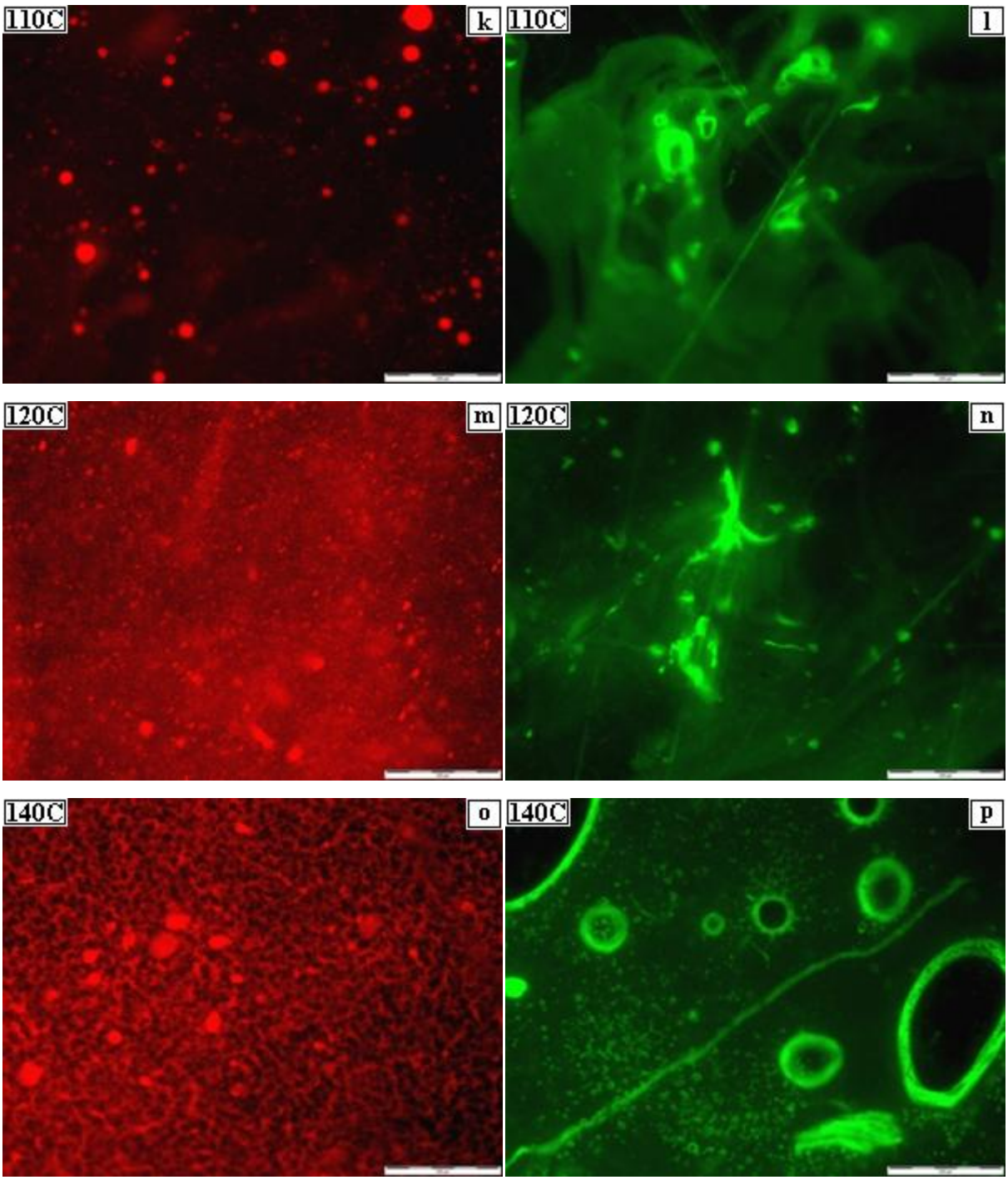

Figure 5.6: Fluorescence microscopy images of dye-treated compatibilizer mixed with the CMR 648 TREF fractions. The PPgMA-Rhodamine B/ fraction mixtures are on the left and the EvOH-Fluorescein mixtures on the right. The scale bar is 200 µm.

Figures 5.6 (a) to (p) show the differences in morphology caused by the compatibilizer polymer interaction for different polymer fractions. The thing to bear in mind here is that an even distribution of the compatibilizer will result in an even spread of the colour in the image, while “phase separation” or clustering will result in bright spots or intensely coloured regions.

In Figures 5.6 (a) and (b) we see little difference in the interaction of PPgMA and EvOH, with the 25 °C polymer fraction, and it appears that both PPgMA and EvOH are homogeneously dispersed. For the 60 °C and 80 °C fractions, which SEC-FTIR shows to consist of propylene-rich semi-crystalline copolymers, we observe distinct differences between the distribution of the PPgMA and the EvOH: In the 60 °C fraction the PPgMA seems evenly dispersed, while with the 80 °C fraction we see some evidence of phase separation, which could be caused by the differences on crystallization behaviour of the PPgMA and the copolymers. EvOH seems to be dispersed relatively well within these fractions, yet the bright spots indicate that we have clustering of the EvOH. We can postulate that this is due to the incompatibility of the EvOH with the propylene-rich copolymers. The unique morphology of the dispersed phases of PPgMA in the 80 °C fraction, do appear strikingly similar to a transmission electron microscopy (TEM) study performed on polymer morphology by Svoboda et al.[2] on polypropylene/ ethylene-octene copolymer blends.

In the 90 °C fraction, which SEC-FTIR show us has longer iPP sequences in the lower molecular weight regions, and some crystalline ethylene sequences in the higher molecular weight portion[6], PPgMA is relatively well dispersed, while EvOH shows a clear phase separation.

For the 100 °C fraction, where analyses indicate that we have significant amounts of ethylene rich copolymers the EvOH appears well dispersed; while the PPgMA appears as bright red regions, yet those regions appear to be continuous. We speculate that we have some phase separation between lower molecular weight propylene rich crystalline material and the aforementioned, dominant ethylene-rich copolymer portion. This is reflected in the way the compatibilizers are dispersed. In the 110 °C fraction, spherical aggregates, like micelles, of PPgMA are visible, which are relatively well dispersed, while EvOH aggregates extensively and is not well dispersed. Similar results can be observed for the 120 °C and 140 °C fractions: PPgMA disperses well, whilst EvOH aggregates.

These results indicate that PPgMA interacts and is dispersed very well in the 25 °C, 60 °C, (to a lesser degree) 80 °C, 90 °C, 120 °C and 140 °C fractions (although the bright spots indicate that the PPgMA is not that compatible with the essentially iPP crystalline material that makes up the 140 °C fraction), but not the 80 °C, 100 °C and 110 °C fractions. This means that it disperses well within the rubbery fraction of the polymer matrix and the highly crystalline iPP fractions of the matrix, but not in the (ethylene rich) copolymer fractions (at 80 – 110 °C).

EvOH disperses well in the 25 °C and 100 °C fractions, but to a lesser degree in the 60 °C, 80 °C and 90 °C fractions, and as expected, in the 110 °C to 140 °C fractions. This indicates that

EvOH preferentially interacts and disperses very well with the rubber and ethylene rich copolymer fractions, but not with the highly crystalline iPP fractions.

These results are quite significant, as they show that since each compatibilizer provides the best results in different fractions of the polymer matrix. When used together, PPgMA will essentially be responsible for interacting with the rubbery and the highly crystalline content of the polymer, which imparts strength, whereas EvOH mainly interacts with the rubbery and copolymer content, which is responsible for the impact resistance and bridging of the crystalline and amorphous regions in the polymer matrix of the composite. We need to point out that where phase separation occurs, it may be either because of incompatibility between the compatibilizer and the polymer matrix, or as a result of interaction with the compatibilizer with a specific molecular species within that fraction, followed by phase separation by the molecular components within the fraction under investigation.

Nevertheless, it is clear that the compatibilizers interact with different parts of the complex copolymer. This extensive study was only conducted with the CMR 648 copolymer, yet we expect similar trends to be observed with the CMR 448 copolymer. Here the difference should lie in the fact that the 100 °C fraction (ethylene-rich copolymer) of the CMR 448 material (see Section 5.1) is not as large. This effectively means that the interaction of EvOH within the more crystalline part of the copolymer will be diminished.

Following on the results obtained with the single compatibilizers, we embarked on a study of the joint compatibilizers. Results are presented in Figure 5.7 (a-p).

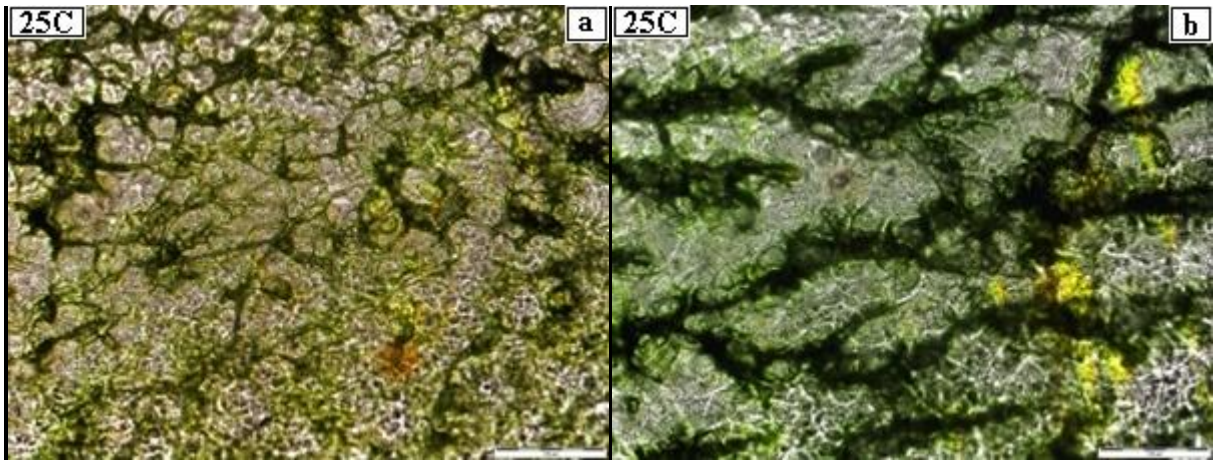

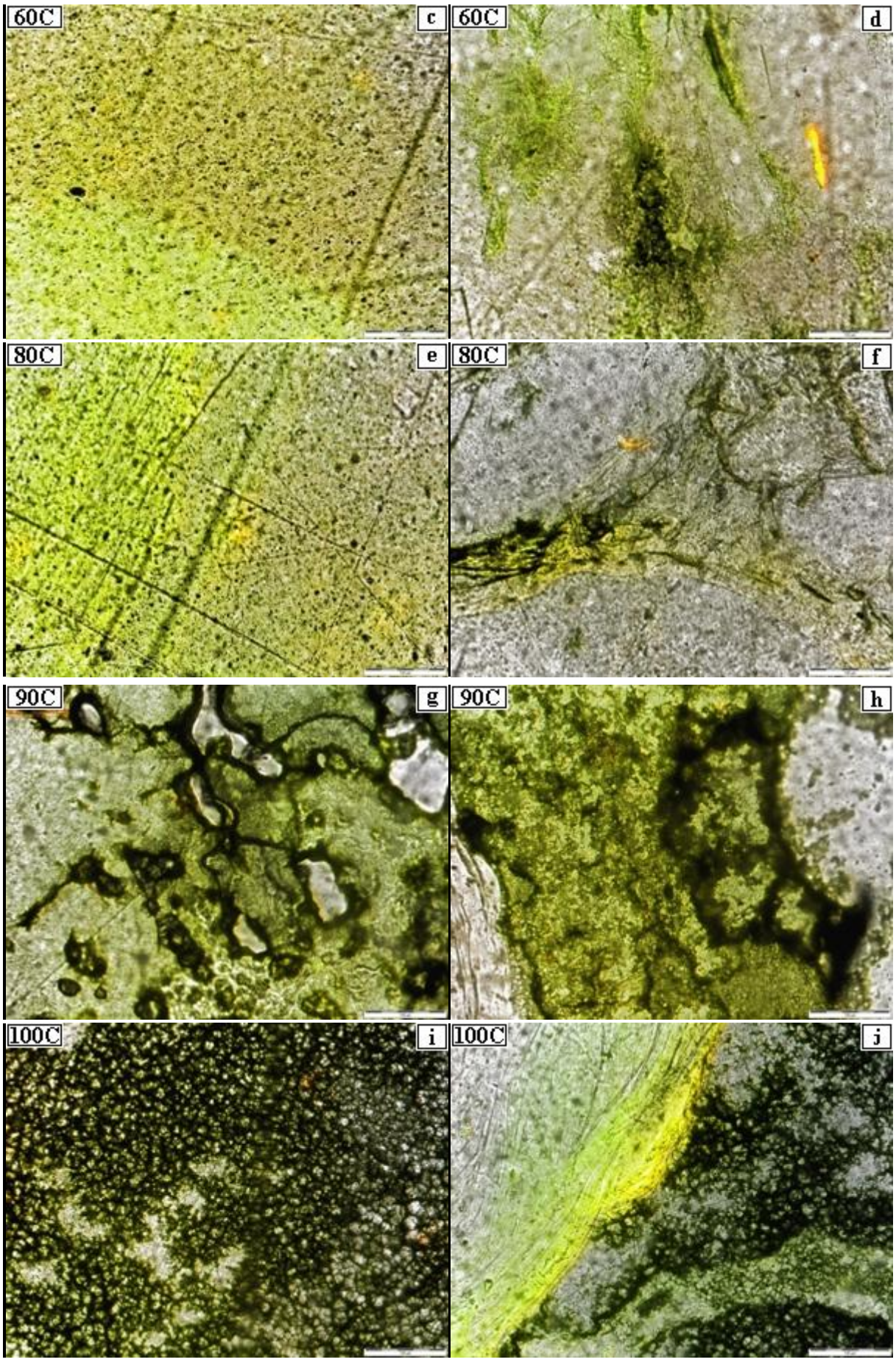

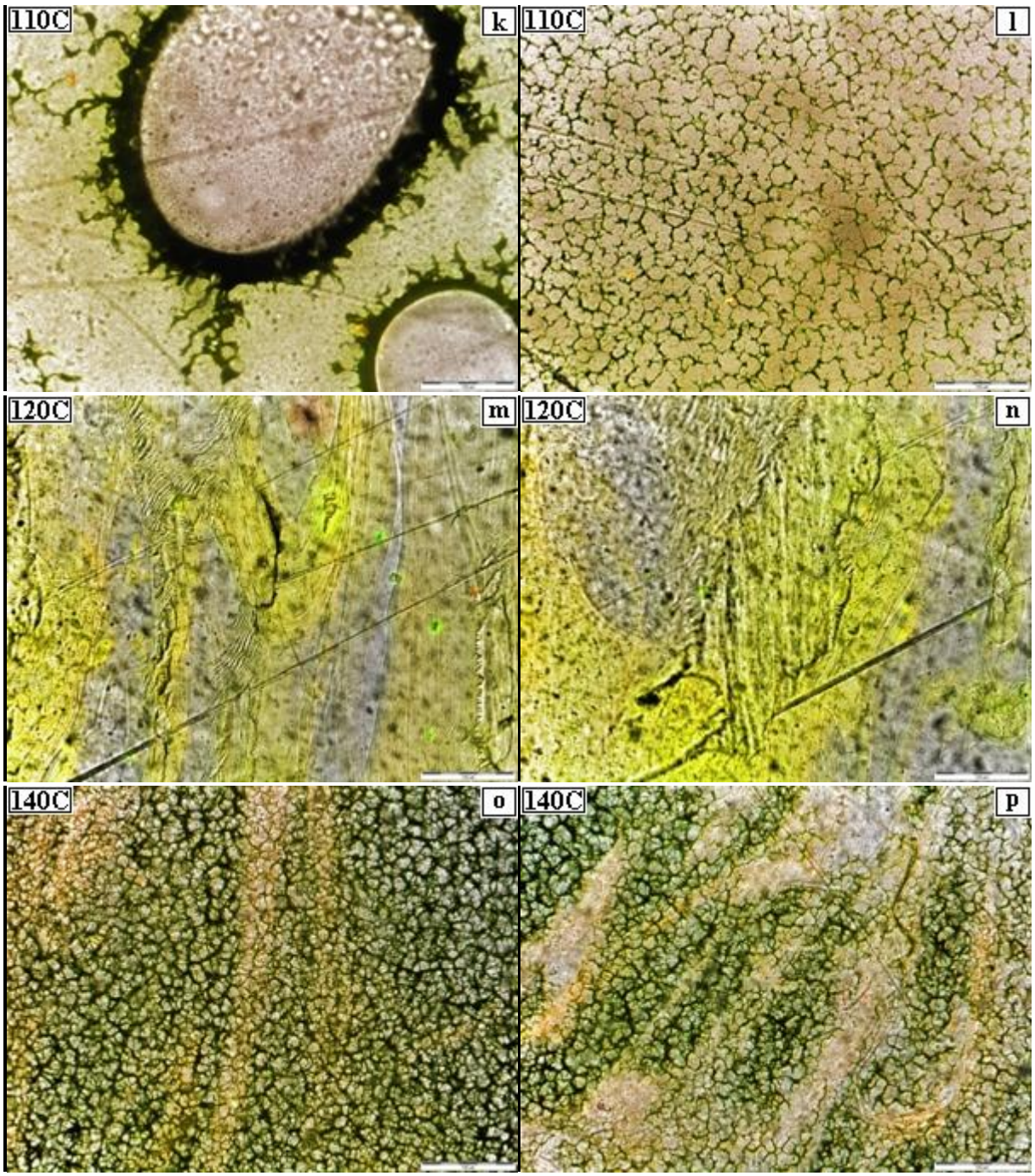

Figure 5.7: Fluorescence microscopy images of CMR 648 polymer TREF fractions, (a) and (b) 25 °C, (c) and (d) 60 °C, (e) and (f) 80 °C, (g) and (h) 90 °C, (i) and (j) 100 °C, (k) and (l) 110°C, (m) and (n) 120°C, (o) and (p) 140 °C. PPgMA-Rhodamine B was pre-reacted with EvOH-Fluorescein in a ratio of 3/ 3, Rhodamine B and Fluorescein signal overlays are shown, and the scale bar is 100 µm.

Figure 5.7 (a) to (p) show how the morphology of the compatibilizer-polymer interactions changes when using a joint compatibilizer system with PPgMA-EvOH ratio of 3/ 3 (total of 6 wt %).

The joint compatibilizer is well dispersed in the (rubbery) 25 °C fraction, but the morphology is somewhat different from the composites with the individual compatibilizers. Larger dispersed areas are visible and arranged in such a way, where they appear to form a type of semi cross-linked morphology within this fraction.

The copolymer fractions at 60 °C and 80 °C show areas of very good dispersion, as well as phase separated areas (Figures 5.7 (c), (d), (e) and (f)). It appears that the joint compatibilizer system does not disperse as well in the copolymer fractions (unlike EvOH), since phase separated areas are clearly present.

The 90 °C fraction shows large phase separated areas with distinct contrast differences within these areas, but generally a good dispersion (Figures 5.7 (g) and (h)).

The 100 °C fraction on the other hand, shows large well dispersed areas with a similar morphology to the 25 °C fraction, but with finer structures. However, these areas also appear to be phase separated into large areas, which appear to comprise well dispersed compatibilizer (within that area). The morphology is similar to that obtained with the 25 °C fraction, when using PPgMA or EvOH alone (Figure 5.6 (a) and (b)).

The 110 °C fraction shows a very fine compatibilizer dispersion (Figure 5.7 (l)), but some large micelle structures, some above 100 µm in diameter, are also visible and are randomly distributed in this polymer fraction. The interior of these micelles is predominately occupied by PPgMA (slight red fluorescence) and polymer, while the rim of the micelles consists of both PPgMA (red) and EvOH(green), with EvOH predominantly on the outside of the micelle. In conjunction with the results obtained by Hironari Sano et al.[3], our results reveal that these micelle structures, could be made up of PP crystalline sequences present in the interior. These results make sense, since PPgMA does disperse relatively well within the polymer matrix, especially where longer propylene sequences are present (higher temperature fractions of the polymer matrix).

Since EvOH did not show any such morphology when used alone (Figure 5.6 (l)), but PPgMA did (Figure 5.6 (k)), it can be assumed that PPgMA is responsible for the formation of these micelle like structures. The 120 °C fraction has an obscure morphology, and the joint compatibilizer is well dispersed, however on a larger scale these areas appear to be phase separated.

The 140 °C fraction shows good dispersion of the joint compatibilizer and only a small degree of phase separation is present (Figures 5.7 (o) and (p)).

From these results (Figures 5.6 and 5.7 (a) to (p)) it becomes clear that PPgMA and EvOH interact in a different manner with the polymer fractions, and when used jointly, they each contribute to improving the dispersion.

5.4 Fluorescence spectroscopy

In order to attempt to make sense of the images that we obtained when using either a single dye-treated compatibilizer or the joint compatibilizer, prepared by pre-reacting two dye-treated compatibilizers, we conducted experiments in order to ascertain the fluorescence intensity of the compatibilizer/polymer fraction mixtures. The results are presented in Figure 5.8.

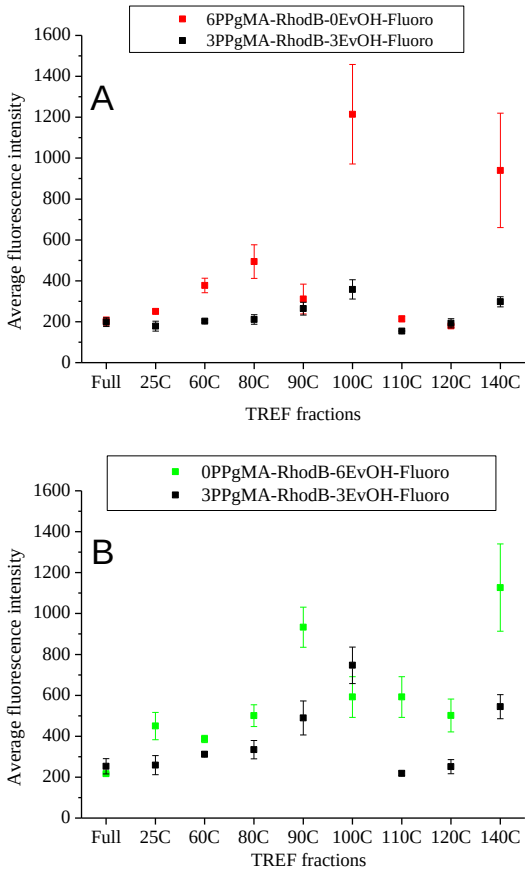

Figure 5.8: Average fluorescence intensity across TREF fractions 25 °C to 140 °C of CMR 648; PPgMA-EvOH 6/ 0, 3/ 3 and 0/ 6 wt % compatibilizer ratios, with dye markers, (A) Rhodamine B signal, and (B) Fluorescein signal.

Fluorescent dyes are used to obtain information on the morphology of samples and can give an enhanced fluorescence signal in the solid state. The differences in morphology between the polymer fractions will strongly influence the change in fluorescence intensity.

In this study (see also Section 5.3), the polymer sample CMR 648, was fractionated according to crystallizability by TREF.

The above Figures 5.8 (A) and (B), give the average fluorescence intensities of the compatibilizers (PPgMA and EvOH) with the attached dyes (Rhodamine B and Fluorescein), mixed and melted with each TREF fraction.

If we look at Figure 5.8 A, the red symbols give the average fluorescence intensity of pure PPgMA-Rhodamine B in each TREF fraction with regards to Rhodamine B. The black symbols give the average fluorescence signal of Rhodamine B when PPgMA and EvOH is jointly reacted and used as compatibilizer in each TREF fraction.

If we observe these two signals closely, we can see that the fluorescence signal drops significantly for the joint compatibilizer at fractions 100 °C and 140 °C, and overall appear lower in the joint compatibilizer system. A drop in the fluorescence signal, especially in the solid state (increased fluorescence detection), would seem to indicate that the dye components are restrained, and unable to come in close contact with one another (in order to excite one another), which would lead to a decrease in fluorescence signal as observed. It was observed (Section 5.3) that the PPgMA was more agglomerated in the 100 °C and (to a lesser degree) in the 80 °C fractions. It appears as if the pre-reaction of the compatibilizer negates this effect to a certain degree. For the 140 °C fraction the decrease in intensity is a little harder to explain. The dispersion of the joint compatibilizer certainly appears to be better, but the reason is hard to see.

The reverse effect is observed for the 100 °C fraction if we look at the Fluorescein signal (Figure 5.8 B). The average intensity is increased, indicating that the joint compatibilizer is less easily dispersed than the EvOH alone. Once again, in the joint compatibilizer the EvOH part appears and is more easily dispersed and less aggregated in the 140 °C fraction than the EvOH alone.

If we study the fluorescence images for either PPgMA or EvOH in the 25 °C fraction as an example, we see that both the compatibilizers appear to be spread relatively well within this fraction. Once these two compatibilizers have been reacted with one another, the morphology has severely changed. In the joint compatibilizer system a larger, more oriented semi-cross-linked structure is visible. This structure is spread relatively well within this fraction, the fluorescence signals also appear to be confined closely to these structures and not spread within the whole sample as is the case when using the compatibilizers individually.

The orientation of the compatibilizers in this fraction when jointly used, is more restrained (in a forced oriented structure), the result is that the dyes do not come in close proximity to one another, as they were in the single compatibilizer systems. The average fluorescence signal is expected to drop, which is the case in Figure 5.8 (A).

Since these samples were fractionated according to crystallizability, one can argue, that the compatibilizer interaction with these samples is affected by their interaction with the polymer fractions based on change in crystallinity. The compatibilizer crystallizes and positions itself within the fraction upon crystallization from the melt. This aspect will be discussed in more detail when the thermal properties of the compatibilizers are shown (Chapter 6). At this stage we can say that the Avrami constants and crystallization rate constant (Table 6.1) indicate that both the PPgMA and the joint compatibilizer will (as the Avrami constant is roughly equal to 1) form crystal domains that have poor dimensional growth and thus appear to be linearly oriented at best (the PPgMA has a fast rate of crystallization). The joint compatibilizer appears to be oriented and spread across the 25 °C fraction as seen in Figure 5.7 (b).

For further explanation, we can once again examine the 100 °C fraction and the 140 °C fraction (Figure 5.8 A); it is clear that the fluorescence signal drops significantly when the joint compatibilizer is used. If we observe Figure 5.6 (i) and Figure 5.7 (i), it certainly appears that while some aggregated domains can be seen when pure PPgMA is used (resulting in increased dye interaction and a stronger signal) when the 3/ 3 wt % joint compatibilizer system is used these domains appear to be absent. Together with the structured morphology observed, this would explain the drop in fluorescence signal. A similar observation can be made for the 140 °C fraction (Figure 5.6 (o) and Figure 5.7 (o)).

Figure 5.8 (B) shows the result with regards to EvOH and only fractions 90 °C and 100 °C will be discussed. If we look at fraction 90 °C, we observe that the fluorescence signal drops, and from Figure 5.6 (h) and Figure 5.7 (h), it is clear that the morphology is quite different. EvOH agglomerates together quite strongly in its pure form with a strong fluorescence signal (highly constrained solid state) due to the presence of phase separation between compatibilizer and polymer material. When the 3/ 3 wt % joint compatibilizer is used, the signal is weaker, and while phase separation is still visible, a rather unique morphology is present, indicating some degree of improvement in compatibilization. A morphological structure that has different domains with good definition can be observed.

The 100 °C fraction has a fluorescence signal that increases slightly (Figure 5.8 B) when the joint compatibilizer is used. If we look at Figure 5.6 (j) and Figure 5.7 (j), we can see that the

EvOH compatibilizer appears to have a good interaction with this fraction in its pure state. Once the 3/ 3 wt % joint compatibilizer is used, there is still a partially structured morphology visible, but also clear phase separated areas and increased fluorescence would be observed at these transition regions and could explain the increased fluorescence signal observed.

5.5 Interactions between chemical functionalities: an AFM study

Chemical force microscopy (CFM), is atomic force microscopy performed with chemically modified silicon tips and was used to study the adhesive forces between different functional groups within the wood polymer composites. In a first step the adhesive force between different functionalized tips (-CH_3, -OH, -C(O)OH groups) and different polymer fractions were compared to that of a gold tip as reference. This was done to determine whether the tips were successfully coated and how much their adhesive forces differed, with regards to their interaction with the polymer matrix. The first results are shown in Figure 5.9.

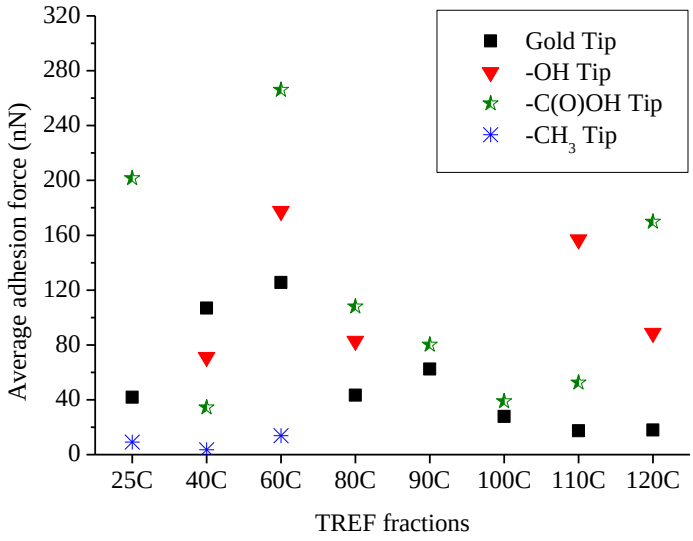

Figure 5.9: Adhesive force between different functionalized tips and p-TREF fractions of CMR 648.

Figure 5.9 clearly shows a difference in adhesive forces between the prepared tips compared to the gold tip. While this might indicate that the functionalization of these tips was successful, it somewhat difficult to explain why the functionalized tips gave the responses that they did. The strong adhesive forces visible for the hydroxyl (–OH) and carboxylic acid (-C(O)OH) tips, compared to the methyl (–CH_3) tips is, difficult to explain. The chemical nature of all of the p-TREF fractions should be essentially similar. Strong adhesive forces are expected between similar chemical groups, for example between the hydrophobic polymer and the methyl tip, however this was not the case and the adhesive force detected with the

methyl tip was much lower than with the other tips. These results also indicate that some fractions of the polymer have better interaction with the functionalized tips than others. This might be due to surface morphology, or even surface chemistry (degradation). The presence of degraded polymer compounds, able to interact with the more hydrophilic tips, could be a possible reason for these strong adhesive forces. This aspect is explored a little later in this chapter.

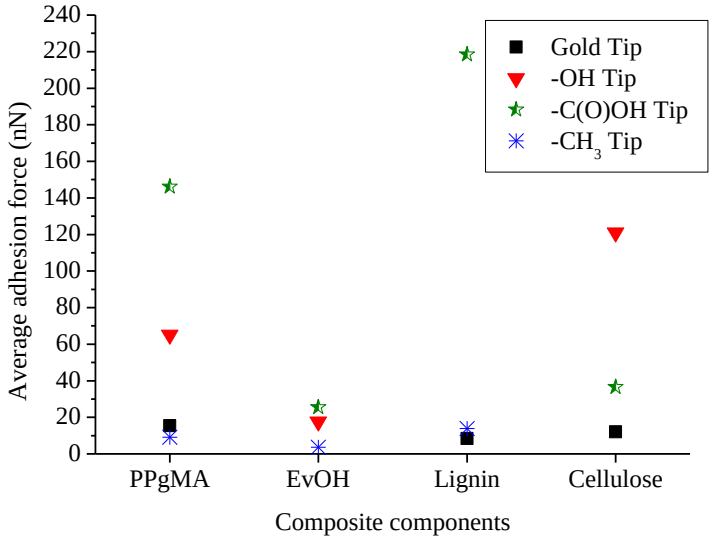

Figure 5.10: Adhesive force between different functionalized tips and the compatibilizer/ wood components.

The second step of this part of the research was to determine the adhesive forces between the same functionalized tips and the compatibilizers, and components that would be present in wood (lignin, α-cellulose). These results are presented in Figure 5.10. The carboxylic acid functionalized tip showed strong adhesive interactions with PPgMA and lignin and much weaker adhesive interaction with EvOH and α-cellulose. Strong adhesive interaction between the maleic anhydride groups present in PPgMA and the acid tip was expected; however, the same is not expected for the acid tip interaction with the lignin. Although lignin contains some hydroxyl and acid functional groups, it is mostly hydrophobic and a weak interaction between lignin and the carboxylic acid functionalized tip was expected. A possible reason for the strong adhesive interaction could be the morphological arrangement of the lignin, with its hydroxyl and acid functional groups arranged in such a way as to be more exposed on the surface than the hydrophobic parts, when a lignin surface was prepared.

A weak interaction between the hydroxyl tip and EvOH is observed, and a stronger interaction with α-cellulose. α-Cellulose has an abundance of hydroxyl groups, therefore the strong interaction with the alcohol tip was expected. The weak interaction with EvOH, which contains about 56 mol % vinyl alcohol, was, however, surprising. Possibly the surface of EvOH was arranged in such a way that the ethylene segments were dominant on the surface, which would result in the poor adhesive interaction with the hydroxyl tip. The methyl tip showed weak interactions on all substrates, even on PPgMA and EvOH, which contains a large amount of hydrophobic segments. Possibly the van der Waals forces for the methyl tip were generally lower, resulting in lower adhesive forces with a maximum around 10 – 20 nN. It could also be possible that the monolayer formed during the methyl tip preparation, was incomplete, and the result, a tip with poor functionality. Overall, though, it is concluded that this method gave inconclusive results with respect to the surfaces monitored.

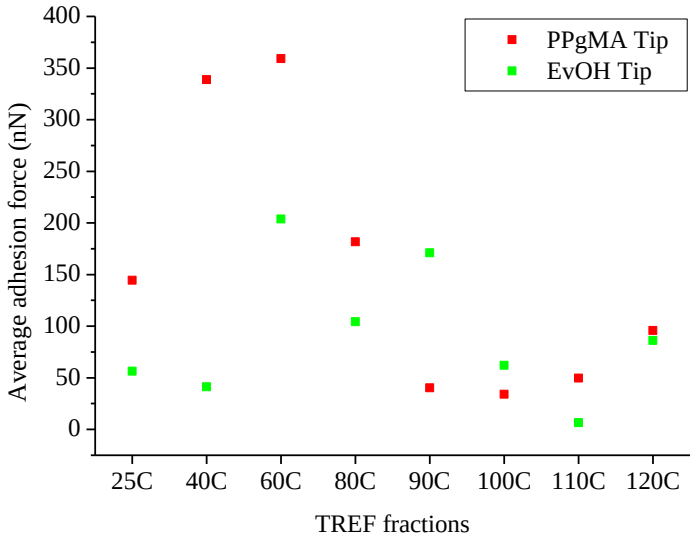

Figure 5.11: Adhesive force between PPgMA and EvOH coated tips and the p-TREF of CMR 648.

The adhesive forces between the PPgMA and EvOH coated tips and the fractionated polymer were used to study the interaction between compatibilizer and different polymer compositions, as displayed in Figure 5.11. PPgMA shows generally larger adhesive forces than EvOH, which indicates a better interaction between compatibilizer and polymer. Of particular interest here is the good interaction between the PPgMA tips and the 40 °C, 60 °C and (to a lesser extent) the 80 °C fractions. These fractions comprise semi-crystalline propylene rich copolymers, and the ethylene content increases in the 80 °C and subsequent fractions. Here the interaction of the PPgMA tip decreases and it remains constant, even at fractions that are essentially isotactic polypropylene. The EvOH tip has fairly poor

interactions, but is better than the PPgMA tip in the 80 °C and 90 °C fractions. We know that these fractions contain semi-crystalline ethylene rich copolymers. It does therefore appear that the interaction between the tips and the fractions are determined by the chemical nature of the fraction as well as the morphology of the particular fraction. It appears as if the more crystalline fractions show a lower adhesive interaction than those fractions with more amorphous content. By the same token, however, the interaction of the tips with the rubbery fractions is poorer than for the partially crystalline fractions. This does indicate that the physical nature of the surface plays a role in determining the adhesive interaction, and that we should be careful in drawing conclusions regarding the interactions observed.

Overall though, it appears that PPgMA and EvOH preferentially interact better with the lower temperature fractions, and the fluorescence results in Chapter 5 (Section 5.3) confirm this.

These AFM results therefore agree reasonably well with the results obtained from the fluorescence study (Section 5.3) where differences in interaction of PPgMA and EvOH with the TREF fractions of the polymer could be observed.

The fluorescence study showed clear phase separated domains for some higher temperature fractions, but still some degree of interction, which the CFM results confirm with a lower (but still existing) adhesive force. These results also highlight the importance to study phase separation and interaction on a micro- and macroscopic scale, in order to acquire a complete representation of the results.

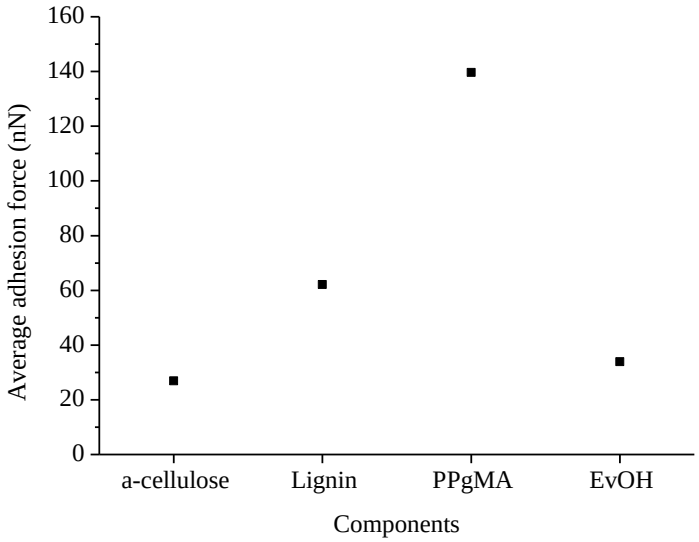

Figure 5.12: Adhesive force between PPgMA coated tips and compatibilizers/ wood components.

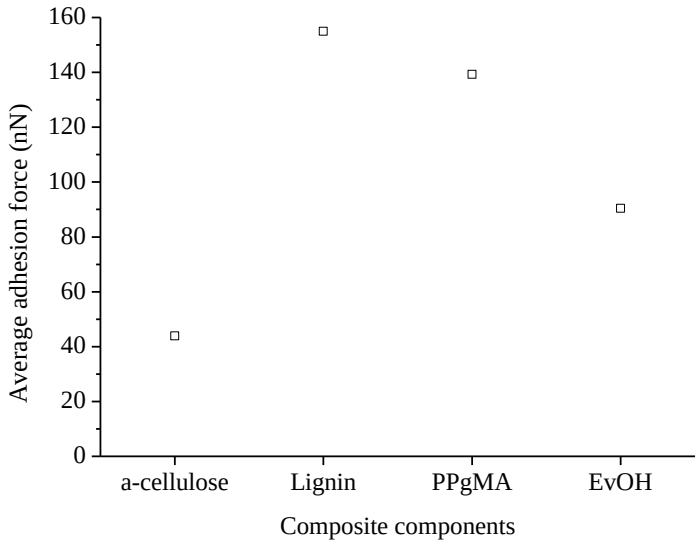

Figure 5.13: Adhesive force between EvOH coated tips and compatibilizer/ wood components.

Figures 5.12 and 5.13 show the adhesive forces determined between PPgMA and EvOH coated tips and compatibilizer, lignin and α-cellulose substrates. The PPgMA tip (Figure 5.12) has, as expected, the strongest interaction with the PPgMA substrate. The adhesive interaction of the PPgMA tip with lignin is weaker, and very poor with EvOH and α-cellulose. Since PPgMA consists of 8-10 wt % MAH groups, the majority of the compatibilizer is made up of PP, which would impart an overall hydrophobic character to the PPgMA tip. Since the α-cellulose and EvOH sample surfaces are hydrophilic in nature (EvOH is also hydrophobic due to ethylene segments), due to the presence of many hydroxyl groups, it is to be expected that PPgMA shows a poorer interaction with these samples. Since the PPgMA tip has a mostly hydrophobic character, which is only partially influenced by the MAH content, it is to be expected that its interaction with lignin (strongly hydrophobic) will be the strongest.

Similar results (Figure 5.13) were observed for the EvOH tip: strong adhesive interaction with lignin (hydrophobic) and PPgMA (hydrophobic), slightly weaker with EvOH (hydrophobic and hydrophilic character) and the poorest interaction with α-cellulose (hydrophilic). The strongest adhesive force was expected with the EvOH substrate, which was, however, not the case. The strongest adhesive interaction was with lignin. The results indicate that the surface chemistry of the functionalized EvOH tip and EvOH substrate is different. These results again cast doubt on the usefulness and applicability of the technique.

We did investigate whether or not surface degradation during the preparation of the substrates for the AFM (CFM) may have occurred. The FTIR (ATR) spectra for the p-TREF factions of CMR 648 are presented in Figure 5.14.

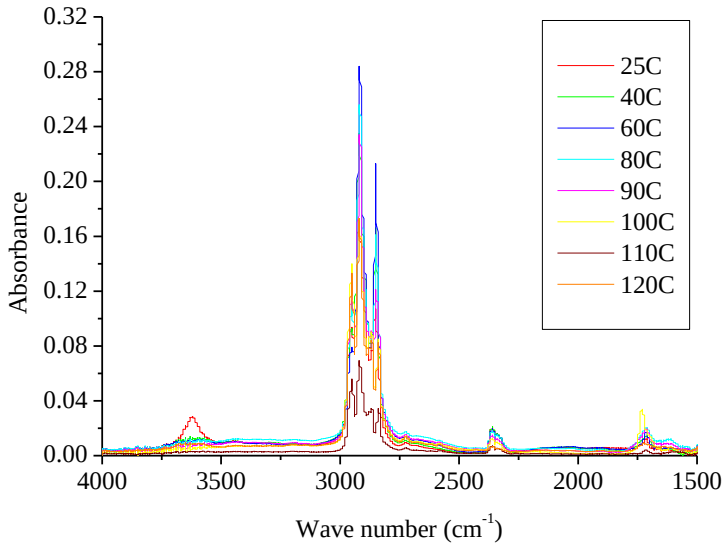

Figure 5.14: FTIR results for the TREF fractions of CMR 648.

In order to try and explain why strong adhesive forces were seen with CFM, for the carboxylic acid and hydroxyl functionalized tips, ATR was performed on the same TREF samples. It was found that although a limited amount of degradation products are present in all of the fractions, specifically carboxylic groups (around 1700 cm-1) hydroxyls and hydroperoxides (3500 to 3750 cm-1) these were too small to cause strong interactions with the functionalized tips. It would seem that the surface morphology of the polymer samples influences the tip responses increased crystallinity at higher temperature fractions leading to a decrease in tip adhesive force response. In conclusion, therefore, although the CFM technique appears to hold some promise, it is very difficult to quantify the interaction of the functionalized tips with substrates that are chemically similar yet morphologically different. This is one area of the research that should be expanded.

5.6 Conclusions

It does appear that the use of fluorescence to observe interactions between the compatibilizers and the polymer fractions is possible. It appears that we may even qualitatively determine the extent of change in morphology of the compatibilizer system among the polymer fractions, and how well the compatibilizer interacts and distributes itself within them. With the combined (pre-reacted) compatibilizers, this is not as readily apparent.

The conclusions that could be drawn from the results presented in this chapter reinforce the observations made with respect to the changes in physical properties of the composites when different compatibilizers are used.

5.7 References

1. N. C. Basson, The effect of molecular architecture on the properties of propylene impact copolymers, MSc thesis, University of Stellenbosch, South Africa, 2010.
2. P. Svobodova, D. Svobodova, P. Slobodian, T. Ougizawa, T. Inoue, Transmission electron microscopy study of phase morphology in polypropylene/ ethylene-octene copolymer blends, European Polymer Journal, 45 (8), p 2434 (2009).
3. H. Sano, T. Usami, H. Nakagawa, Lamellar morphologies of melt crystallized polyethylene, isotactic polypropylene and ethylene-propylene copolymers by the RuO_4 staining technique, Polymer, 27, p 1497 (1986).

CHAPTER 6 THERMAL PROPERTIES

The thermal characteristics of the wood, the compatibilizers and the two matrix polymers (CMR 448 and CMR 648 were determined. The results are presented in the sections that follow.

6.1 Thermogravimetric analysis (TGA)

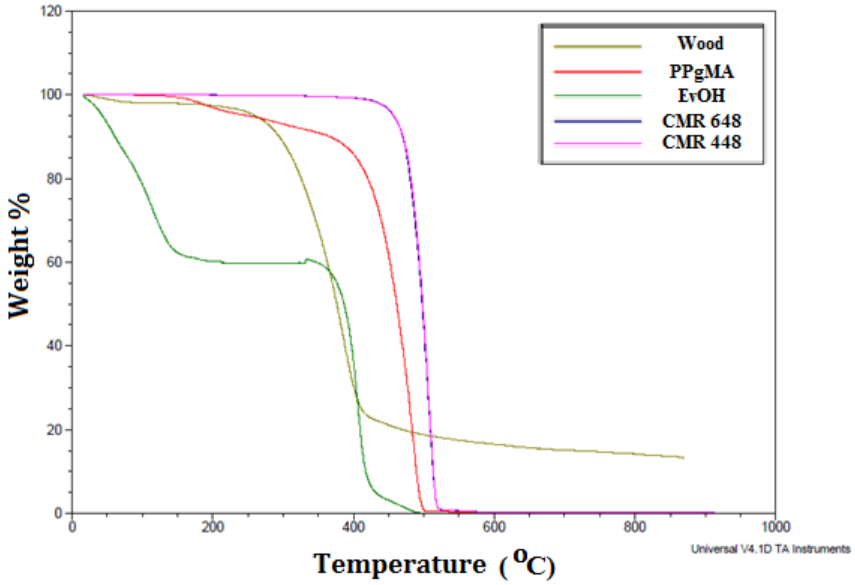

Figure 6.1: TGA thermogram of the individual components used in the preparation of the composites.

Figure 6.1 represents the TGA curves for the individual components used in the preparation of the composites. As can be seen in Figure 6.1, the polymers CMR 648 and CMR 448 both follow the same thermal weight loss pathway, with weight loss commencing at 475 °C and rapidly increasing to 100% at 525 °C. The TGA results show that EvOH has an initial weight loss of 40% between 0 °C and 150 °C, after which the weight remains constant to 275 °C, where after it rapidly, goes to 100 % at 500 °C. The wood particles show an immediate weight loss which continues up to 100 °C (probably moisture) and then show a significant weight loss at about 250 °C which evens out at about, 400 °C, where mostly cellulose remains. PPgMA starts a slow weight loss from 200 °C up to 400 °C, where after it rapidly decomposes.

The derivatives of the TGA curves are shown in Figure 6.2.

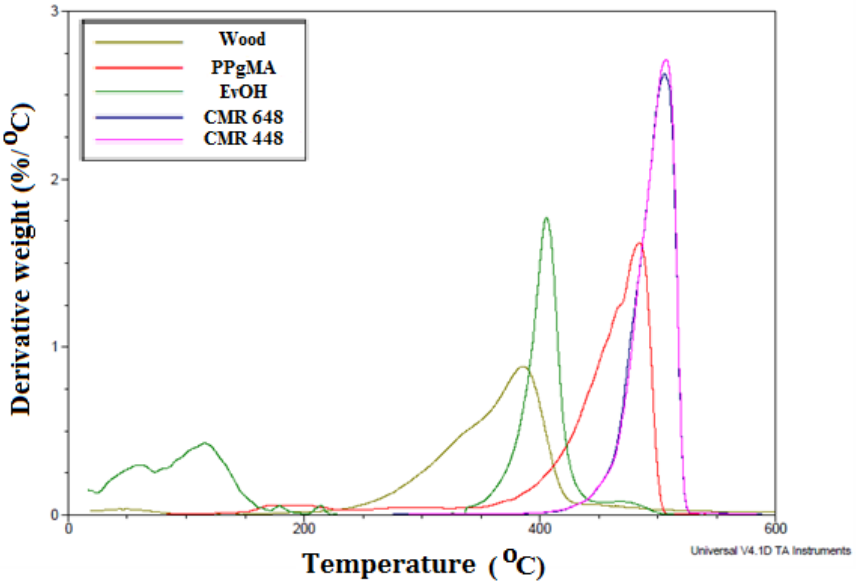

Figure 6.2: The dTGA thermogram of the individual components used in the preparation of the composites.

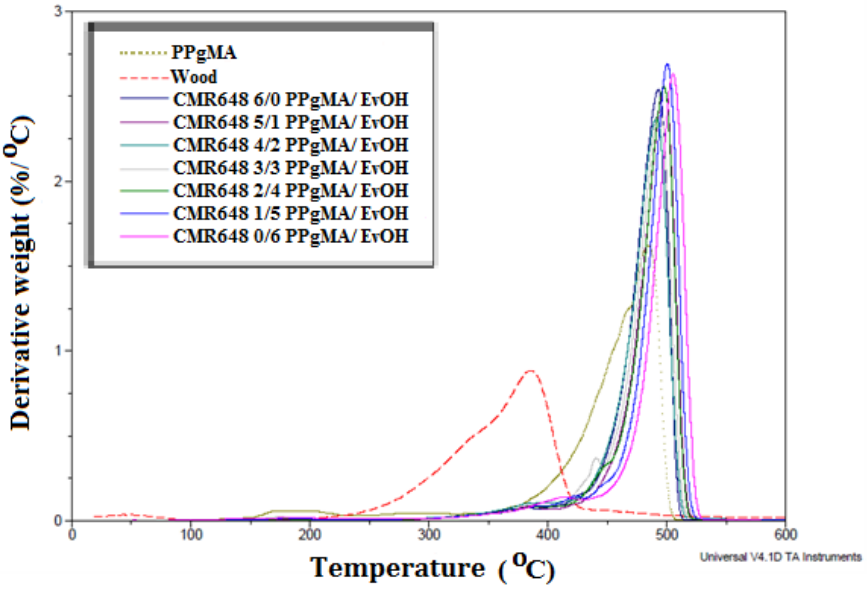

Figure 6.3: dTGA thermograms of the CMR 648 polymer composites (10 wt % wood) prepared with PPgMA-EvOH joint compatibilizer (PPgMA/ EvOH ratios of 6/0 to 0/6).

Figure 6.3 shows the derivative TGA curves for the composites, and it is clear that the composite materials assume the decomposition pathway of the polymer matrix, irrespective of the compatibilizer. The presence of wood in the composite, at the level of 10 wt%, seems to have little effect on the decomposition. As very little difference in the decomposition of the composites can be seen, it seems as if the polymer is the determining component regarding the decomposition pathway followed. The levels of the compatibilizer and wood are probably low enough for the decomposition events associated with these components to be hidden. This indicates two aspects:

first, the individual components are well distributed in the polymer matrix, and, second, the wood and compatibilizer do not have a detrimental effect on the matrix polymer.

6.2 Differential scanning calorimetry (DSC)

In Figures 6.4 and 6.5, the DSC thermograms of the crystallization and melting of the PPgMA-EvOH pre-reacted compatibilizers are shown. Quite obviously, the 6/0 and 0/6 ratios represent the pure PPgMA and pure EvOH, respectively, but it must be remembered that these compatibilizers were also treated with DMAP and heated, as described in Chapter 3.

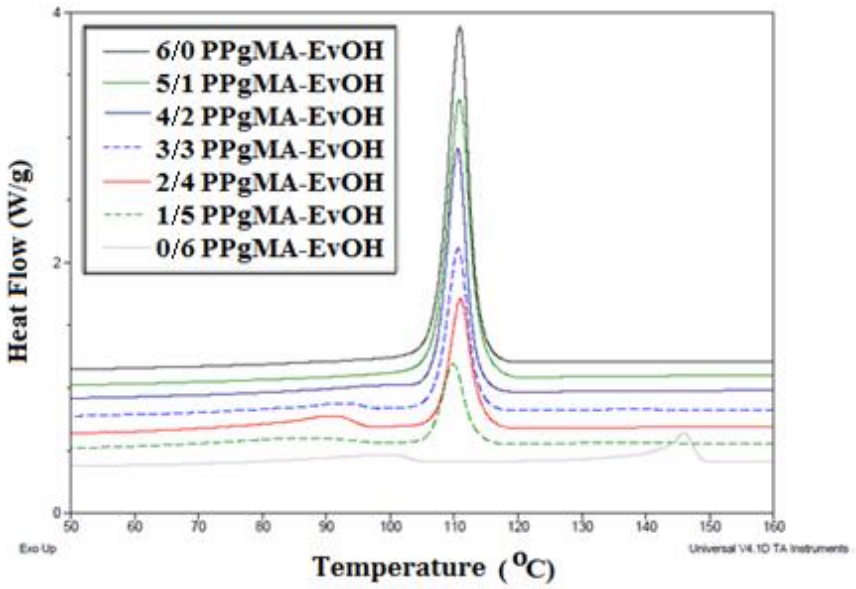

Figure 6.4: Waterfall plot, DSC crystallization of the PPgMA-EvOH pre-reacted compatibilizer series, with wt % ratios 6/0 to 0/6.

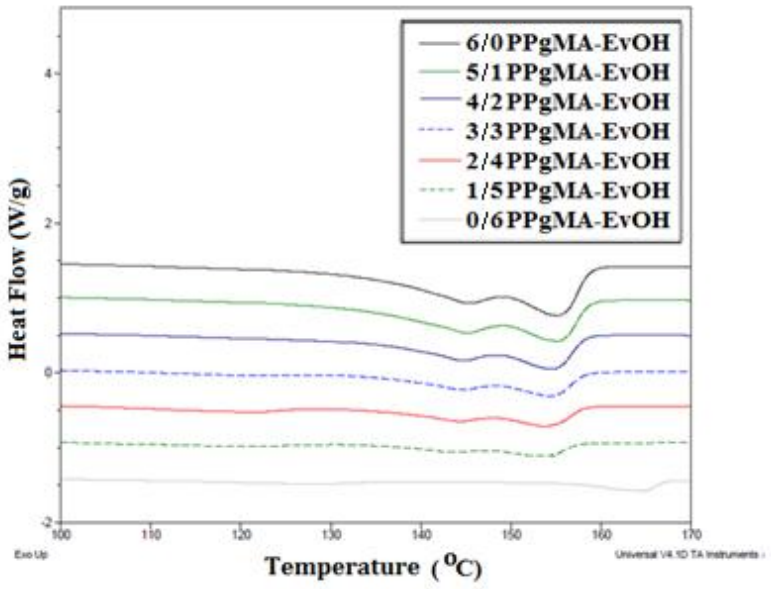

Figure 6.5: Waterfall plot, DSC melting of the PPgMA-EvOH pre-reacted compatibilizer series, with wt % ratios 6/ 0 to 0/ 6.

From Figure 6.4, it is clear that when PPgMA alone crystallizes, a single crystallization event is visible. Once the EvOH content reaches a 3/3 wt % ratio with PPgMA, two crystallization events become visible: one event taking place in the same temperature region as for the PPgMA alone, between 105 °C and 120 °C, and a smaller event between 80 °C and 100 °C, which corresponds to the lower crystallization event of EvOH. The higher crystallization event of EvOH between 155 °C and 170 °C does not occur when PPgMA is present. This is most likely due to the fact that this event is due to the crystallization of hydroxyl-containing units in the copolymer, and these hydroxyls would have been involved in esterification reactions with the maleic anhydride moieties in the PPgMA. The crystallization event in the pure EvOH at around 90 – 100 °C is due to the crystallizable ethylene sequences.

The melting endotherms for the PPgMA-EvOH joint compatibilizers in Figure 6.5 shows two melting peaks in the 145 °C to 155 °C temperature region. This corresponds to the melting peaks of pure PPgMA. The addition of EvOH causes little change, other than an increase in the broadness of the melt peaks.

Once again, the disappearance of the crystallization peak at 145 °C for pure EvOH in the pre-reacted compatibilizers is mirrored by the disappearance of the melting peak for pure EvOH at around 166 °C.

Since it is very difficult to fully explain the crystallization behaviour of the joint PPgMA-EvOH compatibilizers based on the conventional DSC results, it was decided to monitor changes in the crystallization event of the PPgMA with changing EvOH content by isothermal crystallization studies.

These results are presented in Figure 6.6.

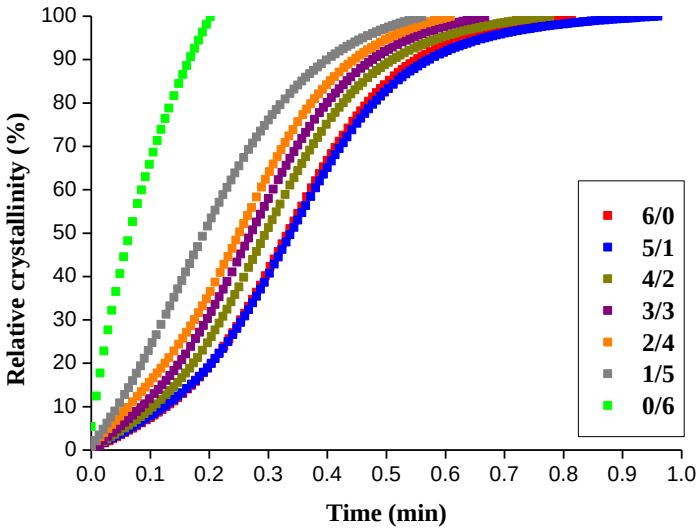

Figure 6.6: The relative crystallinity of the PPgMA-EvOH pre-reacted compatibilizer series as determined by isothermal DSC analysis.

Figure 6.6 shows the relative crystallinity for the different joint compatibilizers. The relative crystallinity for pure EvOH, denoted 0/6, is quite high, as could be expected, since EvOH crystallizes at a much higher temperature than PPgMA.

Looking at the time scale of the isothermal crystallization event, it is obvious that the relative crystallinity increases more rapidly as the EvOH content increases.

A possible explanation for this could be the fact that, as EvOH crystallizes at a higher temperature some of these crystallites may act as crystallization nucleus for PPgMA. This could also explain why the melting endotherm in Figure 6.5 showed such broad melt peaks, indicating a range of different crystallites. It must be remembered that the PPgMA is covalently bound to the EvOH, thus limiting the movement of chains and the ability to phase separate.

Figure 6.7 represents the results of the Avrami-Kolmogorov theory.[1]

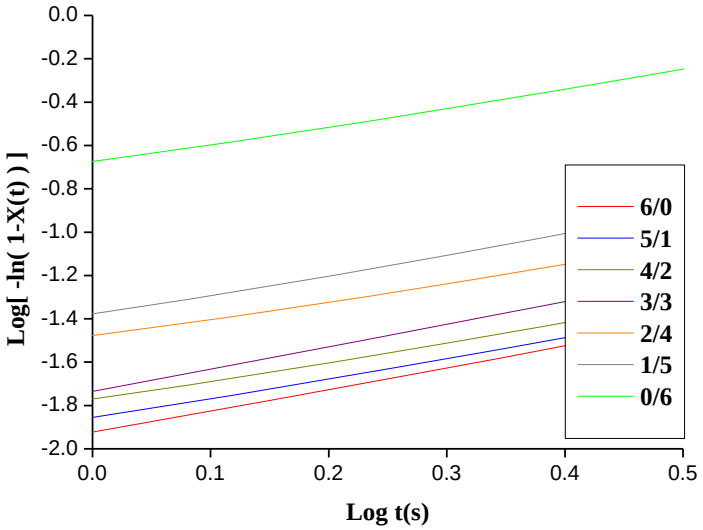

Figure 6.7: Log [-ln(1-X(t))] vs. Log t, of the PPgMA-EvOH series as determined by isothermal DSC treatment.

The isothermal crystallization kinetics of these samples was determined by monitoring the degree of crystalline conversion as a function of time and a constant temperature[1], at the crystallization peak temperature for PPgMA. We first determined the relative amount of crystallization of the joint compatibilizer system as the EvOH content increases (Figure 6.6), at a constant temperature. Then we use the Avrami equation to monitor the development of the relative crystallinity, plotted in Figure 6.7 with the equation as reported by Li et al.[1].

$$log\ -ln\ 1-X\ t\ \ = nlogt + logK \qquad (1)$$

From Figure 6.7 the rate constant K (Log K values are obtained from the y-axis intercept for each line) and the Avrami exponent n (the slope of each line plot); n is a constant that relates to the mechanism of nucleation and type of crystal growth, whereas K is a rate constant containing the nucleation and growth parameters.[1] K and n can thus be used to determine information on nucleation, growth and dimension of crystallites formed during the crystallization process of this joint compatibilizer system. The crystallization time at half life $t_{1/2}$, when the amount of crystallization is at 50 %, can be used to correlate the K values determined.

It can be seen that the crystallization event takes place in a linear fashion, as seen by the slope of the lines (Figure 6.7), indicating that there is no secondary crystallization event at the isothermal crystallization temperature of 110 °C. The values obtained for K and n are listed in Table 6.1.

Table 6.1: Rate constant K and the Avrami exponent n for the PPgMA-EvOH pre-reacted compatibilizer series.

Sample ID	**Rate constant K**	**Avrami exponent n**	**$t_{1/2}$ (min)**
6/0	0.012	1.012	0.910
5/1	0.014	0.977	0.933
4/2	0.016	0.962	0.814
3/3	0.018	1.051	0.529
2/4	0.034	0.798	0.717
1/5	0.042	0.945	0.327
0/6	0.218	0.824	0.068

The results show that as the EvOH content increases, the time at half life decreases, which is an indication that the rate of crystallization increases, as confirmed by the rate constant K that increases slightly. The Avrami exponent is close to (or less than) 1, which means that there is no preferential dimensional growth mechanism.[1]

The reason for this could be the PPgMA, with a low average molecular weight of (Mn = 8 100 g/ mole) which simply lacks long stereo regular chains necessary for proper crystal growth. The time at which crystallization takes place is simply too fast for proper dimensional crystal growth.[1]

The poor crystalline growth mechanism can explain to some degree why the physical properties at the interface region (Chapter 5) do not appear to differ a lot. Improved stiffness of the composite material, although small, also lies in the small presence of esterification between the compatibilizers PPgMA and EvOH and its improved interaction with the polymer matrix and wood components (see section 4.5).

6.3 References

1. J. Li, C. Zhou, G. Wang, Y. Tao, Q. Liu, Y. Li, Isothermal and non-isothermal crystallization kinetics of elastomeric polypropylene, Polymer Testing, 21, p 583 (2002).

CHAPTER 7 MORPHOLOGY OF THE COMPOSITES

7.1 Scanning electron microscopy

In order to observe the effect of the presence of the compatibilizers, we used both SEM and FE-SEM to study the fracture surfaces of the samples subjected to high speed tensile impact tests. This would allow us to observe the interface between the wood particles and the polymer matrix, and to better understand the interaction between wood and polymer.

7.1.1 Wood-polymer composites with no compatibilizer

In Figure 7.1 the SEM micrographs of fracture surfaces of both CMR 448 and CMR 648 composites are shown. These composites contained no compatibilizer.

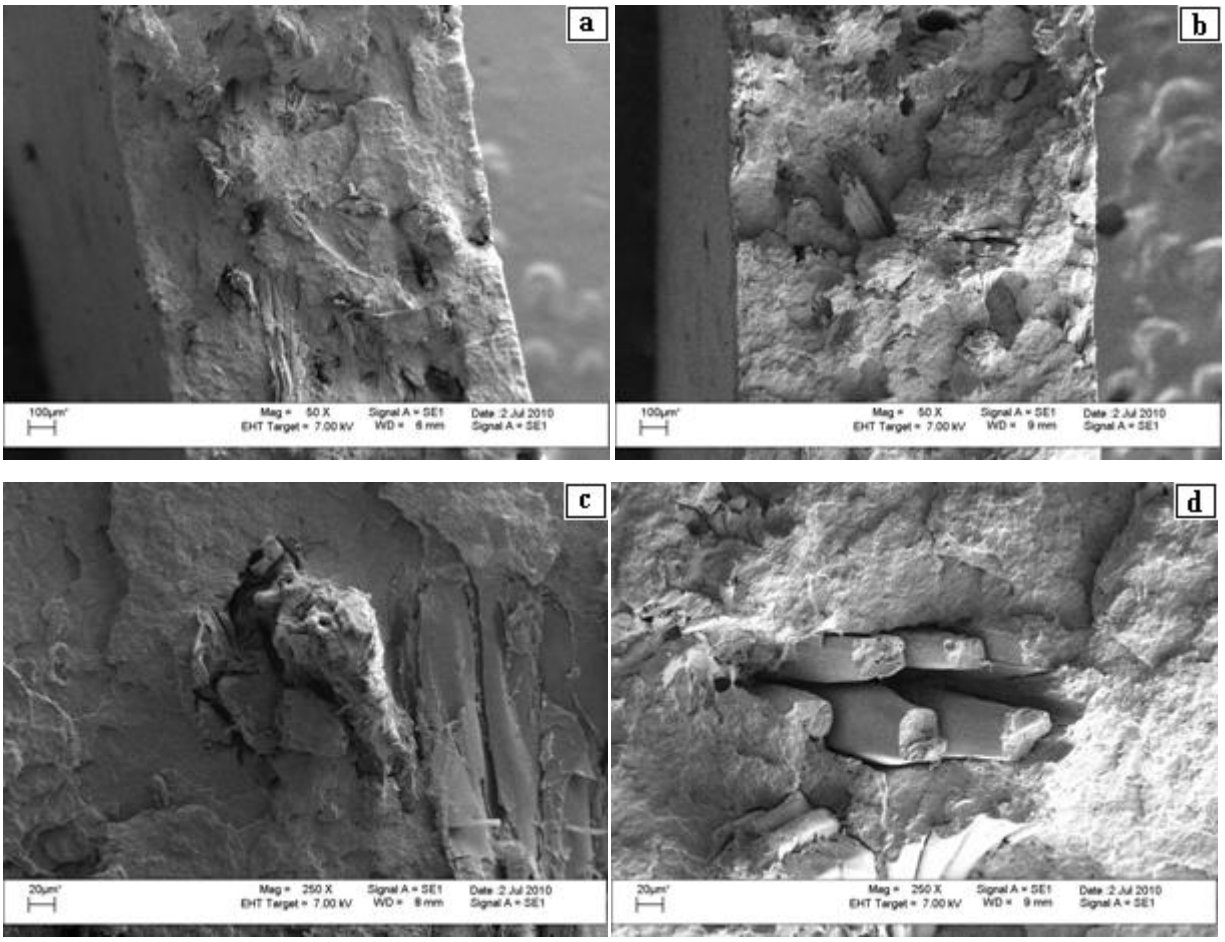

Figure 7.1: Images of high speed tensile impact fractured surfaces. CMR 648 composite, (a) 50 x mag., scale bar100 μm (c) 250 x mag., scale bar 20 μm, CMR448 composite, (b) 50 x mag., scale bar 100 μm (d) 250 x mag., scale bar 20 μm. Wood content 10 wt % for all composites.

Figures 7.1 (a) and (b) show the fracture surfaces of both polymer matrices at 50 x magnification. The wood particles are clearly protruding, with little or no polymer covering them and voids are clearly visible in the fractured surfaces (the same was observed at 20 and 30 wt% wood content). This is indicative of fibre pullout.[1-2] At 250 x magnification (Figure 7.1 (c) and (d)) it can be seen that the wood particles are exposed and not connected to the polymer matrix.

These images explain why the polymer composite has such weak impact properties, as described in Chapter 4. A significant decrease in the impact properties was clearly visible after addition of wood. The narrow standard deviations of the impact values indicate that the fracture of these composites happen fast and effortlessly, as no adhesion between polymer and wood is present that would affect the impact properties. Instead of breaking, the fibres are pulled out, as there is a clear separation between the polymer matrix and wood particles.

7.1.2 Wood-polymer composites containing compatibilizer

7.1.2.1 PPgMA

Figure 7.2 shows the fracture surfaces for CMR 448 and CMR 648 composites with 6 wt % PPgMA as compatibilizer.

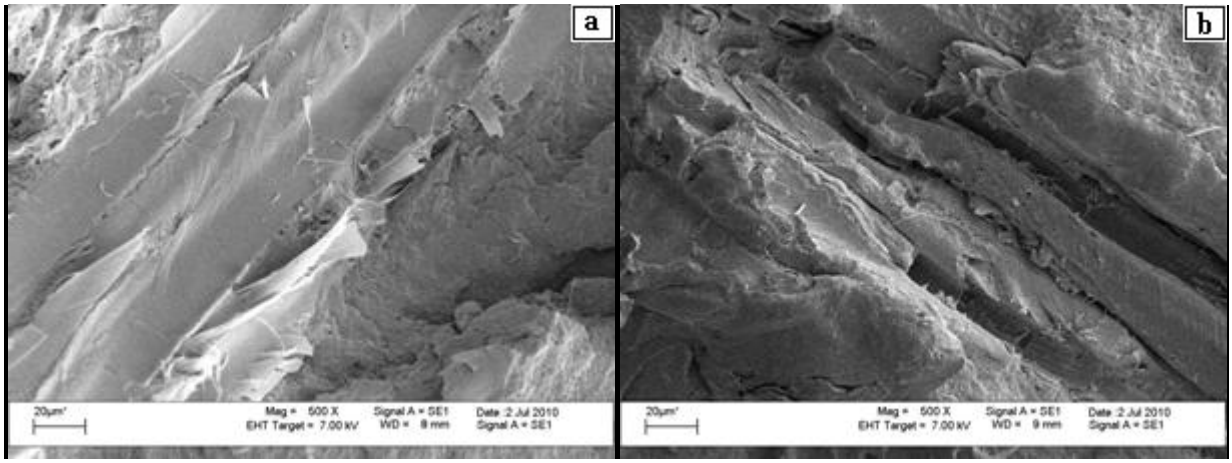

Figure 7.2: CMR 648 polymer composite (a) 500 x mag., CMR 448 polymer composite (b) 500 x mag. The PPgMA content was 6 wt %, the wood content 10 wt %. The images are of high speed tensile impact fractured surfaces, scale bar 20 µm.

Figures 7.2 (a) and (b) shows a wood particle inside the polymer matrix. No clear boundaries of the interface are visible and the wood particle is firmly embedded into the polymer matrix, for both the CMR 648 and CMR 448 composites. This indicates PPgMA provided a bridge between the wood and polymer, and fibre fracture instead of fibre pullout occurred during fracture.

SEM images were taken for composites with compatibilizer contents ranging from 2 to 10 wt % PPgMA, but since 6 wt % resulted in the best physical properties, only these samples are shown here. Similar results were found by Bledzki et al.[3], who found 5 % MAH-PP content to be optimal.

7.1.2.2 EvOH

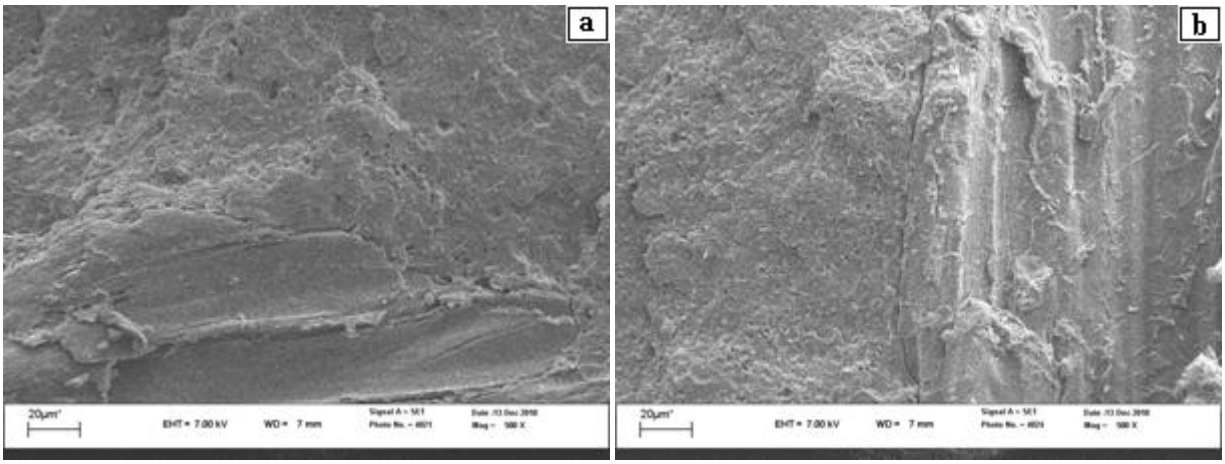

Figure 7.3: CMR 648 polymer composite (a) 500 x mag., CMR 448 polymer composite (b) 500 x mag. The EvOH content was 2 wt %, the wood content 10 wt %. Images are of high speed tensile impact fractured surfaces, scale bar 20 µm.

Figures 7.3 (a) and (b) shows a thin boundary at the polymer and wood interface. It appears that the EvOH promotes interactions between wood and polymer and although it improves the interface, it does not bridge this interface as successfully as PPgMA does. This was observed for EvOH contents between 2 and 10 wt %. The SEM images do, however, not provide enough information as to why the stiffness of the polymer was improved, as indicated in Chapter 4. DSC analysis (Chapter 6) provides some answers to this question, as changes in the crystallization kinetics of PPgMA with changing EvOH content, and their interaction with the polymer matrix could explain the improved stiffness.

7.1.2.3 PPgMA-EvOH joint compatibilizer

Figure 7.4 shows a few SEM micrographs of the fracture surfaces (see Chapter 4 for results) of CMR 648 composites prepared with pre-reacted compatibilizers (heat treatment). Similarly, Figure 7.5 presents fracture surfaces for the CMR 448 composites.

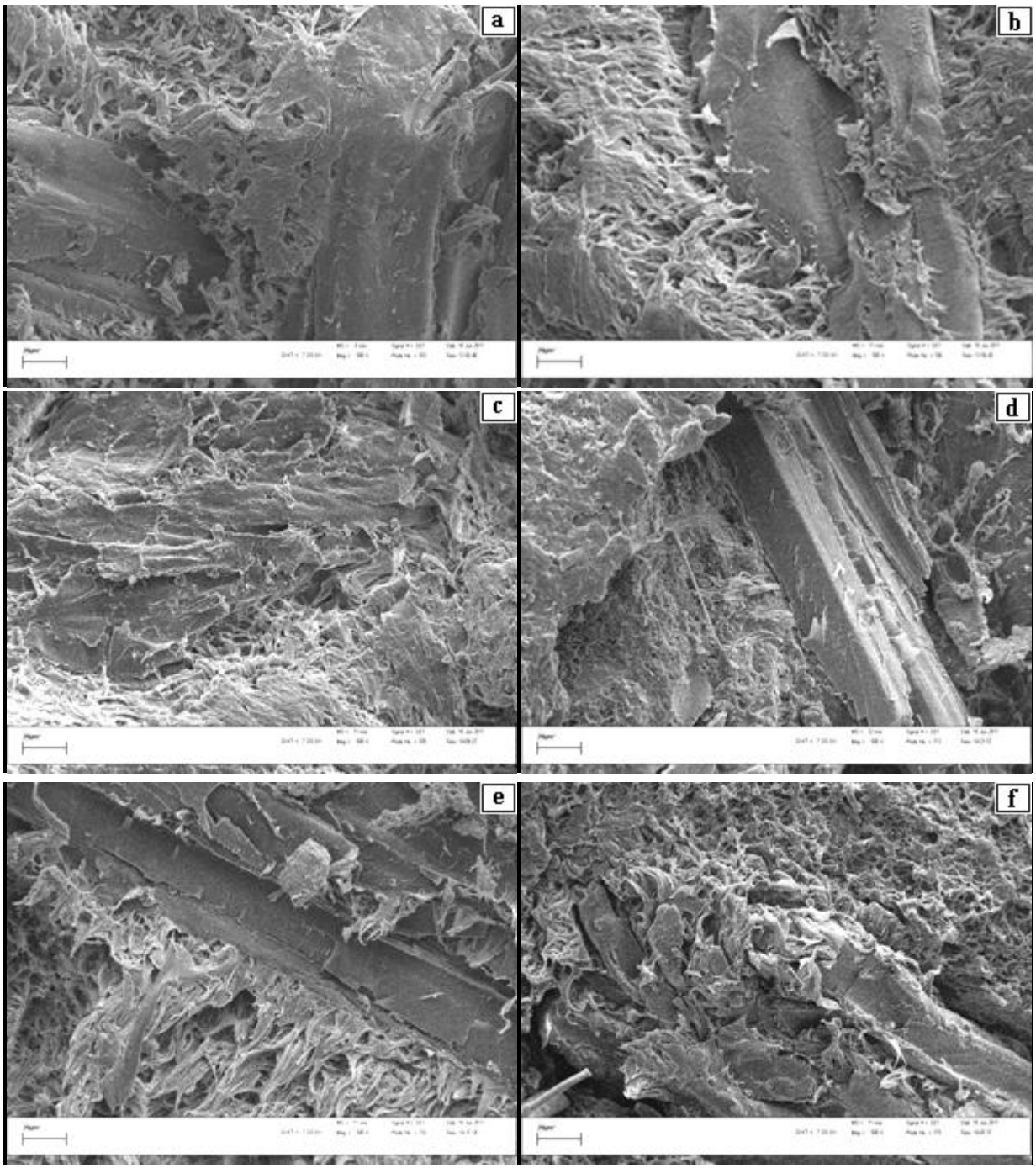

Figure 7.4: CMR 648 polymer composites, (10 wt % wood) PPgMA/ EvOH ratios (a) 5/1, (b) 4/2, (c) 3/3, (d) 2/4, (e) 1/ 5, (f) 0/ 6, at 500 x mag., compatibilizers were pre-reacted (heat assisted). Images are of tensile bar fractured surfaces, scale bar 20 μm.

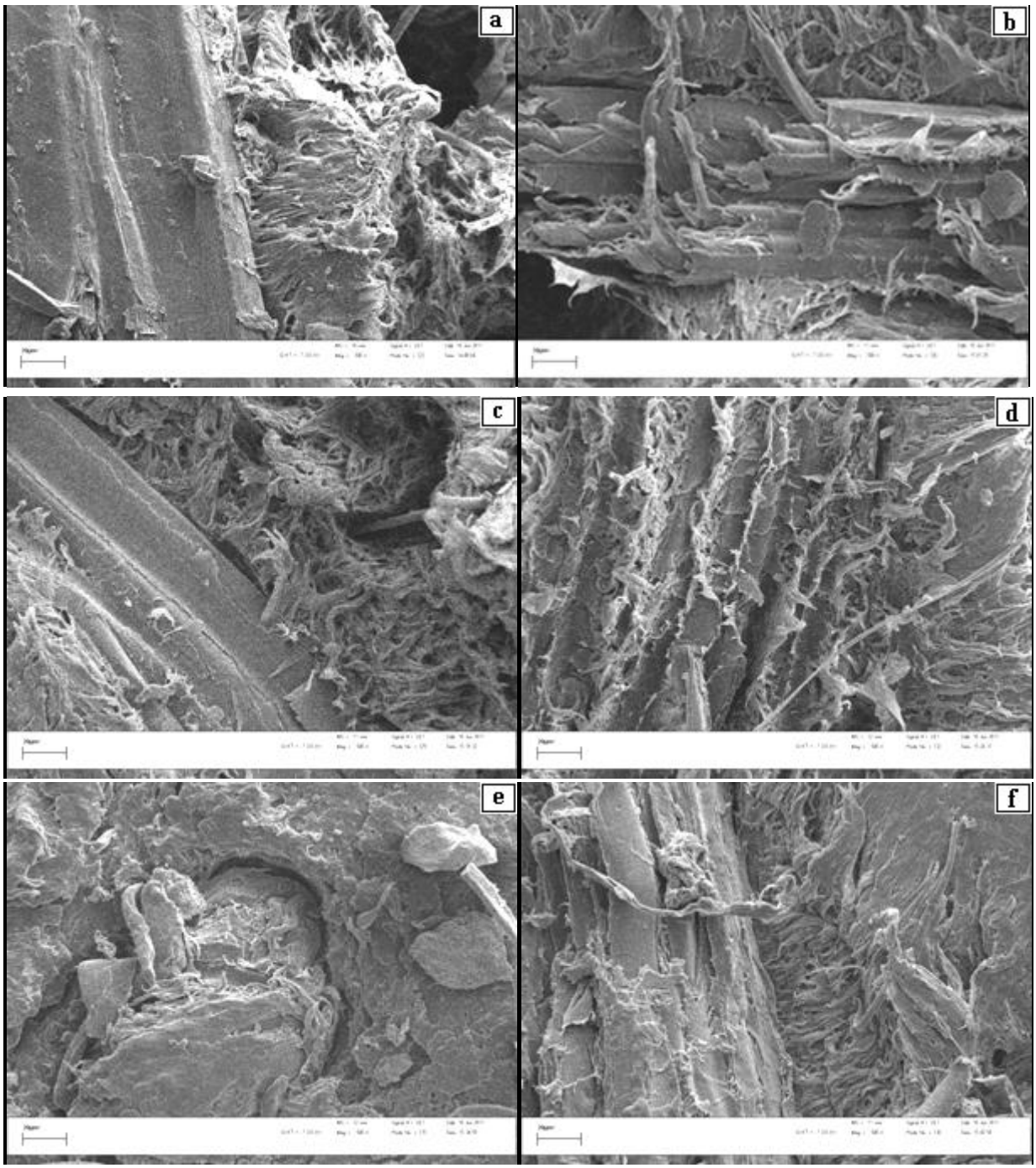

Figure 7.5: CMR 448 polymer composite, (10 wt % wood content) PPgMA/ EvOH ratios (a) 5/ 1, (b) 4/ 2, (c) 3/ 3, (d) 2/ 4, (e) 1/ 5, (f) 0/ 6, at 500 x mag., compatibilizers were pre-reacted (heat assisted with DMAP). Images are of tensile bar fractured surfaces, scale bar 20 µm.

Observing Figures 7.4 and 7.5 closely, it becomes clear that the morphology of the fractured composites are very different for the different polymer matrices and also changes with the PPgMA/ EvOH wt % ratio.

Figures 7.4 (a) and 7.5 (a) shows the composites with the 5/1 PPgMA/ EvOH joint compatibilizer. In the case of the CMR 648 polymer web-like or fibre-like structures are visible at the wood-polymer interface. This appears to be firmly connected to the wood particle and covers most of the

wood particle. In the case of the CMR 448 polymer there appears to be less of the fibre-like structures, and the matrix appears smoother. This is interesting; as the one major difference between the two polymers (see Chapter 5) is that the CMR 648 polymer has a significantly larger proportion of ethylene rich crystalline copolymer (100 °C TREF fraction). Nevertheless, the polymer appears to be firmly connected to the wood particle in places, but the fractured surface reveals the uncovered wood particle and a much cleaner fracture surface.

In the CMR 648 polymer composite (Figures 7.4 (a), (c) and (e)) the morphology at the interface changes to a finer structure with increasing EvOH content, and at the same time we observe more clean, uncovered wood surface as the EvOH content in the compatibilizer is increased. For the highest EvOH content (Figure 7.4 (f)) the wood particle is only partially covered, and a clear interface boundary is visible, which indicates weak interaction.

Figures 7.5 shows good interaction between the CMR 448 polymer and wood as well, however, the wood particles appear more exposed than in the CMR 648 matrix, which indicates that the polymer composition plays a significant role with regards to the interface and interaction of the compatibilizer with the wood particles. The images presented in Figures 7.4 and 7.5 suggest that the ability of the polymer matrix to flow under stress, together with the compatibilizer composition affect the interface between wood and polymer to a significant extent.

If the polymer matrix and the compatibilizer interact well, the interface will undergo deformation together with the rest of the polymer matrix while still covering the wood particles. However, if the interaction is weak, the polymer matrix will slip, leaving the compatibilizer wood interface and the surface of the wood particles exposed.

7.2 Field emission scanning electron microscopy

Since field emission scanning electron microscopy (FE-SEM) has improved resolution compared to conventional SEM, it was decided to use this technique to observe the morphology of the tensile fractured polymer wood composites, at the wood polymer interface region.

Figure 7.6 shows the FE-SEM images for unfractured and fractured tensile bar samples of CMR 648 composites containing 10 wt % wood and 6 wt % pre-reacted compatibilizer.

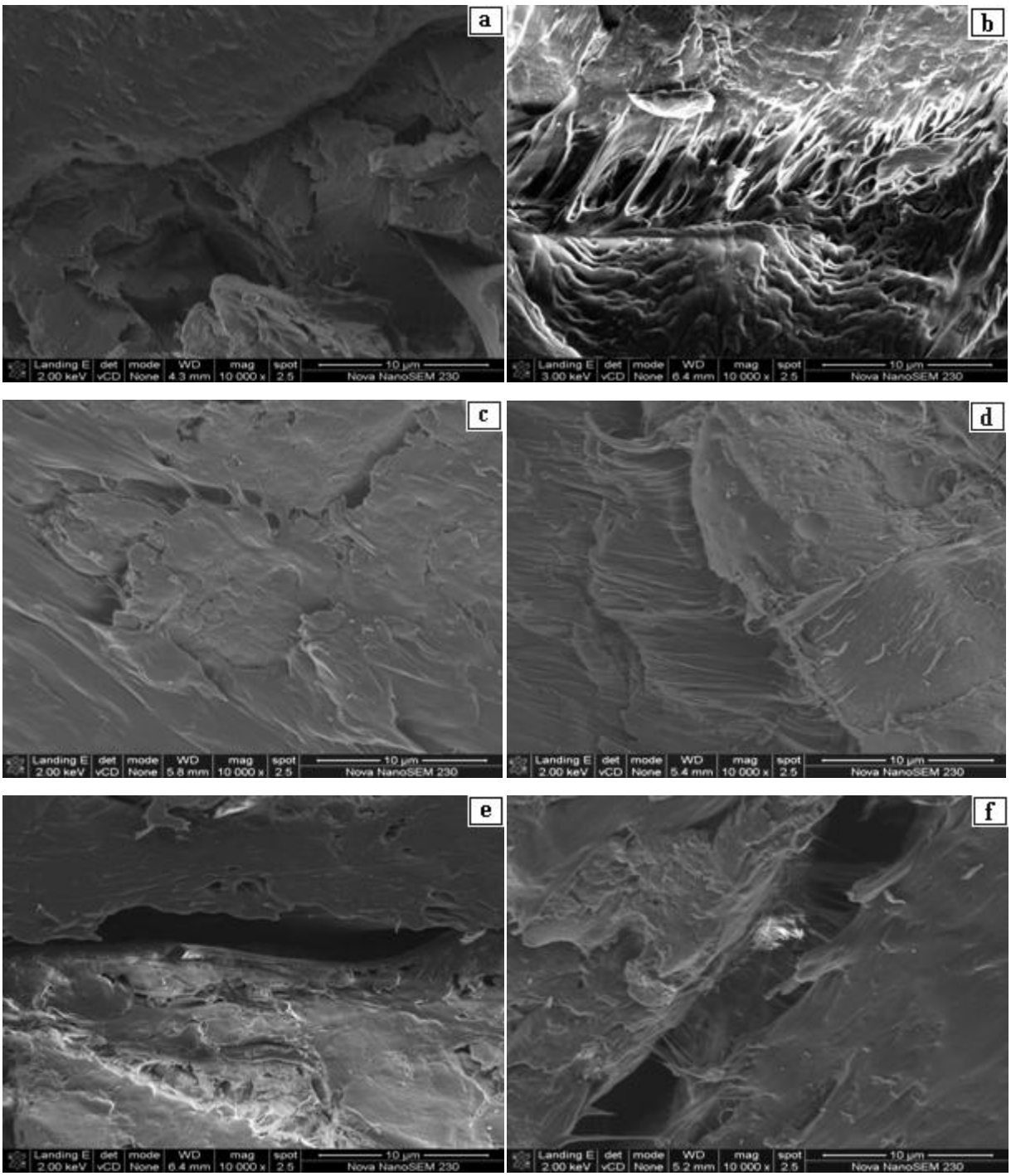

Figure 7.6: FE-SEM images for CMR 648 polymer composites, (10 wt % wood), unfractured (U) and fractured (F) tensile samples. The ratios indicated are for PPgMA/ EvOH in the pre-reacted compatibilizer. (a) 5/ 1 U, (b) 5/1 F, (c) 3/3 U, (d) 3/3 F, (e) 1/5 U, (f) 1/5 F. Scale bar 10 μm.

Figure 7.6 (a), (c), and (e) show the unfractured tensile samples and Figure 7.6 (b), (d), and (f) the fractured tensile samples.

At a PPgMA/ EvOH ratio of 5/1 (Figure 7.6 (b)), good adhesion at the polymer-wood interface can be seen, indicating that the compatibilizer promotes good interaction at this interface, similarly found by Mamunya et al.[4] In Figure 7.6 (d) the wood polymer interface is not clearly visible, which

indicates that the interaction between polymer and wood is improved with a 3/ 3 PPgMA/ EvOH ratio.

With a higher EvOH content (Figure 7.6 (f)) these interfaces are not continuous and seem to be randomly connected. This indicates that although there is interaction between wood and polymer, it is not as strong as for the 3/ 3 PPgMA/ EvOH ratio, and weaker physical properties can be expected.

The observations of the fracture surfaces of compatibilized and non-compatibilized wood-polymer composites clearly indicate that the compatibilizer improves interaction between the wood particle and the polymer matrix. It is also clear that the interaction between the compatibilizer and the polymer-wood interface is dependent on both the compatibilizer (PPgMA or EvOH) and the polymeric matrix. It appears that as single compatibilizer, the PPgMA functions better than the EvOH, particularly in the case of the CMR 648 composites. It is when the joint compatibilizers are used that some interesting results are seen. The morphology of the polymer at the wood-polymer interface of tensile impact fractured samples appears to be dependent on both the composition of the pre-reacted compatibilizer and the composition of the polymeric matrix. Overall it appears that the addition of EvOH might be beneficial, but that a dominant presence of EvOH in the joint compatibilizer results in a weak interface between the polymer and the wood.

7.3 References

1. Q. Yuan, D.Wu, J. Gotama, S. Bateman,Wood fiber reinforced polyethylene and polypropylene composites with high modulus and impact strength, Journal of Thermoplastic Composite Materials, 21, p 195 (2008).
2. B.-D. Park, J. J. Balatinecz, Mechanical properties of wood-fiber/ toughened isotactic polypropylene composites, Polymer Composites, 18 (1), p 79 (1997).
3. A. K. Bledzki, O.Faruk, Wood Fiber reinforced polypropylene composites: effect of fibre geometry and coupling agent on physic-mechanical properties, Applied Composite Materials, 10, p 365 (2003).
4. Y. Mamunya, M. Zanoaga, V. Myshak, F. Tanasa, E. Lebedev, C. Grigoras, V. Semynog, Structure and properties of polymer-wood composites based on an aliphatic copolyamide and secondary polyethylenes, Journal of Applied Polymer Science, 101, p 1700 (2006).

CHAPTER 8 CONCLUSIONS AND RECOMMENDATIONS

8.1 Conclusions

The conclusions can be summarized as follows:

The use of compatibilizers influences the properties of wood-polyolefin composites. This held true for the case where Pinus radiata was used as nominally 180 μm particles at a level of 10 wt % to prepare composites with impact PP as the matrix. From this general observation a more detailed investigation into the effect of different compatibilizers also lead to the conclusion that the interaction of the compatibilizer(s) with the polyolefin is complicated, and is influenced by the chemical composition distribution of the specific impact PP.

It was also clear that the two compatibilizers used, PPgMA and EvOH, interacted with the impact PP copolymers in different ways. This led to an attempt to use the compatibilizers jointly. This attempt led to the realization that the compatibilizers would, through their functional groups, react during the preparation of the composites, and that pre-reacting these compatibilizers would lead to a more homogeneous product and more reproducible results.

It was seen that a study of the interaction of the compatibilizers with the components of the impact PP copolymers would be necessary. To accomplish this, the two impact PP copolymers were fractionated by p-TREF and the differences in the TREF profiles noted. Interaction studies were concentrated on just one of the two impact copolymers, the CMR 648. This was the copolymer with the highest ethylene content, and the highest impact strength.

Interaction studies were conducted by making use of fluorescence microscopy and spectroscopy. An AFM (CFM mode) study was also attempted to see if interaction between the various wood components and the compatibilizers could be quantified.

Morphology of the composites were also studied, specifically the fracture morphology of composites with and without compatibilizers.

Specific conclusions are presented as a bulleted list below.

- The two compatibilizers PPgMA and EvOH proved to successfully compatibilize the wood particles with the polymer matrix, and the reproducible physical properties were found to be at about 6 wt % compatibilizer.
- A simple admixture of the two compatibilizers influenced the properties of the composites, but large standard deviations were seen. More reproducible results could be obtained if the two compatibilizers were first heated in the presence of DMAP in order facilitate the

esterification reaction between them. The joint compatibilizer of PPgMA and EvOH gave the best improvement of the physical properties at a compatibilizer ratio of 3/ 3 wt %.

- A fluorescence microscopy and fluorescence spectroscopy method was developed to study the compatibilizer interactions with the copolymer fractions prepared by TREF. This method proved to be successful, and the melt morphology could be related to the macroscopic properties of the composites.
- This method proved that the PPgMA and EvOH interacted differently with different parts of the impact PP. These results are quite significant, as this is the first time that this type of interaction could be studied in this fashion.
- Fluorescence could not be used to probe the wood/ polyolefin or wood/ compatibilizer interaction, as wood fluorescence in the same spectral range as the dyes that was chemically attached to certain species were present.
- AFM tips were prepared with PPgMA and EvOH coatings. The interaction of these tips with the fractions of the impact PP prepared by p-TREF was measured, and while some conclusions could be drawn, it does appear as if both the physical state (amorphous or crystalline) as well as the chemical composition distribution influences the measure of the adhesion between each polymer fraction and compatibilizer. This makes drawing of definite conclusions very difficult.
- Information obtained from SEC-FTIR, such as molecular weight and chemical composition of the pTREF fractionated copolymer, complimented the fluorescence study and the interaction of compatibilizer with the polymer components could be correlated with the composition of the polymer matrix.
- Compatibilizer interactions with the main constituents of wood were determined with AFM and both compatibilizers appear to have better adhesion to lignin than α-cellulose. Once again, this is thought to be a result of artifacts such as surface morphology rather than chemical composition distribution.
- The morphology of the wood-polyolefin interfaces studied by FE-SEM and SEM could be explained in terms of the interaction studies that were conducted. In addition to this, the morphology studies correlated well with the measurement of physical properties.

8.2 Recommendations for future work

- Further development of the fluorescence method needs to be done. This method could be expanded to include the interaction with, and dispersion of chemically well defined/ characterized wood species (with high cellulose or high lignin content). In addition, it appears as if the presence or movement of extractables in wood during the processing of

these composites could be investigated with fluorescence studies. Preliminary results showed that the fluorescence of the wood species is largely due to the presence of extractable materials.

- Improving the fluorescence method used even further, by using time resolved fluorescence to obtain quantitative information of the compatibilizer polymer interactions.
- Further study of AFM tip modifications with model compatibilizers, specifically with regards to EvOH, can be beneficial. Here we could study the effect of molecular weight and hydroxyl content on the adhesive forces.
- This study concentrated on the interaction of two compatibilizers on one type of impact PP. This study should be expanded to investigate (in depth) the interactions with a chemically different impact PP. While two impact PPs were used in this study, the interaction studies focused only one type.

APPENDIX STANDARD DEVIATION DATA

Table A 1: Figure 4.9 Tensile strength, max stress standard deviation data, polymer matrix CMR 648.

Sample ID	Maximum stress: standard deviation (MPa)		
	Wt % compatibilizer content		
	2	**4**	**6**
CMR 648 PPgMA	0.69	0.28	1.04
CMR 448 PPgMA	1.77	1.69	1.86
CMR 648 EvOH	0.50	0.67	0.35
CMR 448 EvOH	1.85	0.81	0.46

Table A 2: Figure 4.10 Tensile strength, max % strain standard deviation data, polymer matrix CMR 648.

Sample ID	Maximum % strain: standard deviation		
	Wt % compatibilizer content		
	2	**4**	**6**
CMR 648 PPgMA	0.97	0.61	0.11
CMR 448 PPgMA	0.03	0.03	0.03
CMR 648 EvOH	0.30	1.76	1.02
CMR 448 EvOH	0.89	1.09	0.41

Table A 3: Figure 4.24 Micro hardness standard deviation data, polymer matrix CMR 648.

Sample ID	Standard deviation of the hardness (HV)				
Wood content and size	Wt % ratio PPgMA/ EvOH content				
	6/0	**5/1**	**3/3**	**1/5**	**0/6**
30 % 180 um	0.88	0.51	0.46	0.56	0.52
10 % 180 um	0.56	0.52	0.26	0.49	0.26
30 % Less 180 um	0.93	1.11	1.12	0.77	0.46
10 % Less 180 um	0.35	0.46	0.59	0.82	0.64

Table A 4: Figure 4.25 High speed tensile impact resistance standard deviation data, polymer matrix CMR 648.

Sample ID	Standard deviation of the impact resistance (KJ/ m^2)				
Wood content and size	Wt % ratio PPgMA/ EvOH content				
	6/0	**5/1**	**3/3**	**1/5**	**0/6**
30 % 180 um	0.05	0.05	0.05	0.08	0.04
10 % 180 um	0.06	0.10	0.17	0.11	0.10
30 % Less 180 um	0.08	0.05	0.06	0.04	0.05
10 % Less 180 um	0.10	0.15	0.09	0.05	0.03

Table A 5: Figure 4.26 Tensile strength, max stress standard deviation data, polymer matrix CMR 648.

Sample ID	Standard deviation of the max stress (MPa)				
Wood content and size	Wt % ratio PPgMA/ EvOH content				
	6/0	**5/1**	**3/3**	**1/5**	**0/6**
30 % 180 um	0.88	0.85	0.92	0.43	0.51
10 % 180 um	1.17	0.56	0.33	1.23	0.37
30 % Less 180 um	4.12	0.69	0.98	0.68	0.90
10 % Less 180 um	0.53	1.24	0.84	0.31	0.37

Table A 6: Figure 4.27 Tensile strength, max % strain standard deviation data, polymer matrix CMR 648.

Sample ID	Standard deviation of the max % strain				
Wood content and size	Wt % ratio PPgMA/ EvOH content				
	6/0	**5/1**	**3/3**	**1/5**	**0/6**
30 % 180 um	0.19	0.56	1.28	0.51	0.71
10 % 180 um	0.49	1.22	1.38	1.43	1.53
30 % Less 180 um	1.50	0.44	0.47	0.25	0.19
10 % Less 180 um	1.55	1.02	1.07	0.59	1.71